Assessing Ecosystem Productivity Through the Integration of Micrometeorology and Optical Remote Sensing

by

Saulo Manuel Castro

A thesis submitted in partial fulfillment of the requirements for the degree of

Doctor of Philosophy

Department of Earth and Atmospheric Sciences
University of Alberta

Abstract

The main goal of this thesis is to contribute to the growing body of scientific work by exploring mechanisms of ecosystem productivity through the integration of remote sensing and micrometeorological data. This was done throughout by (i) identifying the environmental mechanisms affecting productivity in tropical dry forest during normal and drought conditions; (ii) assessing the use of proximal PRI sensors as a proxy of photosynthetic efficiency and use towards a complete remote sensing derived measure of ecosystem productivity; and (iii) evaluating the impact of temporal aggregation and phenology on LUE model parametrization and ecosystem productivity in two deciduous forests.

Chapter 2 uses information on seasonal phenology and carbon fluxes derived from optical remote sensors and eddy covariance to identify key mechanisms of ecosystem productivity under normal and drought seasonal precipitation regimes. Precipitation was identified as the trigger for the initiation of the phenological cycle. Results also showed a substantial decrease in productivity, net ecosystem exchange, and respiration due to drought, but the Tropical Dry Forest remained a net carbon sink over the season. Relative importance analysis identified latent heat as the principal controlling factor of TDF productivity. However, during drought, soil moisture became the limiting variable of productivity.

Chapter 3 evaluates continuous data collected from recently available autonomous PRI sensors as a proxy of light use efficiency (LUE) in an aspen (*Populus tremuloides*) forest. Quantum yield values were calculated from eddy covariance data and used to assess the ability for PRI measurements to track changes in canopy light use efficiency. Spectrometer measurements were also used to validate and calibrate the sensor's PRI signal. Uncalibrated PRI data was unable to resolve diurnal patterns and resulted in an overestimation of LUE and productivity. An offline diurnal calibration procedure

was proposed to resolve diurnal and seasonal LUE trends. Calibrated PRI data was then used to derive productivity through a LUE model parameterized solely by remote sensing data. Modeled productivity significantly correlated with measured GPP values from an eddy covariance system. Chapter 4 explores the effect of temporal aggregation and phenology on LUE model variables and productivity in a tropical dry forest (TDF) and deciduous boreal forest (DBF). This was done as part of developing data management protocols for remote sensing data integration. Results showed the different impacts of aggregation in seasonal analysis than when data was divided by phenological cycle, for some variables (e.g. fAPAR). Results suggest that temporal aggregation can significantly impact LUE model accuracy and should be considered as we explore the proper protocols for optical and flux data integration. Relative importance results showed differences in dominant variables of productivity between seasonal and phenological analysis. Findings confirm that physiological and structural contributions of the *LUE* model change between vegetation, environmental condition and phenology.

Preface

This thesis is an original work by Saulo Castro. Chapter 2 was published in *Environmental Research Letters* as "Castro, S. M., G. A. Sanchez-Azofeifa, and H. Sato. 2018. "Effect of Drought on Productivity in a Costa Rican Tropical Dry Forest." Environmental Research Letters 13(4) and Chapter 3 was published in MDPI's *Sensors* as " Castro, S., & Sanchez-Azofeifa, A. (2018)". Testing of Automated Photochemical Reflectance Index Sensors as Proxy Measurements of Light Use Efficiency in an Aspen Forest. Sensors, 18(10), 3302". Chapter 4 has not been submitted for publication.

This dissertation was completed with the guidance of Dr. A. Sanchez-Azofeifa. Research and analysis conducted in Chapter 2, 3, and 4 are my original work. Chapter 2 was developed in collaboration with Hiro Sato from the University of Toronto, who contributed to the data analysis and manuscript writing. I contributed to project formation, data collection, analysis, and writing of the final manuscript.

Acknowledgements

I would like to thank my supervisory committee, including Dr. Benoit Rivard and Dr. John Wilson. I am indebted to my supervisor Dr. Arturo Sanchez-Azofeifa who provided me with guided me through my program. I thank you for all the challenges, encouragement, and opportunities. But most of all, I thank you for your patience through this long process and the support you gave my family and me throughout. Gracias Don! I would also like to gratefully acknowledge my co-workers and very hard-working field assistant, including Peter Carlson, Mei Mei Chong, Kayla Stan, Sofia Calvo, Cassidy Rankine, and Iain Sharp. Additional acknowledgements and funding sources for the individual projects are provided in each published chapter.

Thank you too my loving God who has been so faithful in all ways. To Him be the glory for ever and ever! Thank you to my incredible family for all their support and encouragement. Thank you to my Mateo and little jumping bean for bringing me so much joy after hard days. But most of all, I would like to thank and dedicate this thesis to my amazing wife, Amy, who did a Ph.D. with me. Your kindness, patience, and prayers made this possible. I love you and your beautiful heart.

Psalm 8:3-9

Table of Contents

List of Tables

List of Figures

about GPP for (a) 2013, (b) 2014, (c) 2015, and (d) 2016 growing seasons. Four relative importance models were used including LMG, First, Genizi, and CAR. GLM accounted for 80.01%, 89.91%, 84.34%, and 72.65% of 2013, 2014, 2015, and 2016 GPP variability, respectively.

Figure 2.10 Relative importance analysis of GLM GPP = PAR + VWC + VPD + LE for drought event in (a) 2014 and (b) 2015. Four relative importance models were used including LMG, First, Genizi, and CAR. GLM accounted for 93.42% and 94.29% of 2014 and 2015 GPP variability, respectively.

Figure 3.1 Location of the Peace River Environmental Monitoring Super Site (red star). Red triangle shows the location of the flux tower at the edge of an old growth deciduous boreal forest. The tower contains eddy covariance system, meteorological sensors, and proximal remote sensing sensors. A Wireless Sensor Network (WSN) composing of 36 nodes is located east of the eddy covariance tower, within the flux footprint.

Figure 3.2 (**a**) Example of midday and diurnal cross-calibration functions for the 532 nm SRS-PRI fore-optic. Cross-calibration ratios are shown as a function of sun elevation (binned every 3°). Illumination of 100% represents clear and sunny sky conditions. (**b**) Example of the observed signal difference (radiance – irradiance), in machine units, as a function of illumination percentage for the 41°–43° solar elevation bin. Radiance and irradiance measurements were collected from the 532 nm SRS-PRI sensor pair.

Figure 3.3 Boxplot distribution of diurnal cross-calibration ratios for the 532 nm SRS-PRI fore-optic. Each boxplot represents a 3° solar elevation bin. Red points represent outliers and were observed more often in low solar elevation bins.

Figure 3.4. (**a**) Comparison of uncorrected and corrected (diurnal and midday) PRI diurnal patterns. (**b**) Comparison of spectrometer PRI measurements with uncorrected and corrected SRS-PRI measurements. The diurnal cross-calibration procedure shows the strongest and closest correlation to spectrometer readings and 1:1 (gray) line.

Figure 3.5. Mean diurnal monthly pattern of gross primary productivity (GPP) (black dotted line)

Figure 4.2- Coefficient of determination as a function of aggregation period (hours) for PAR during the a) 2013 TDF, b) 2014 TDF, c) 2015 DBF, and d) 2016 DBF seasons.

Figure 4.3 - Coefficient of determination as a function of aggregation period (hours) for $APAR_{green}$ during the a) 2013 TDF, b) 2014 TDF, c) 2015 DBF, and d) 2016 DBF seasons.

Figure 4.4 - Coefficient of determination as a function of aggregation period (hours) for LUE_{green} during the a) 2013 TDF, b) 2014 TDF, c) 2015 DBF, and d) 2016 DBF seasons.

Figure 4.5 - PCA biplot displaying the two first components (Dim 1 and Dim 2) and explained variance (%) derived from PAC analysis of gross primary productivity (GPP), fraction of available photosynthetically active radiation (*fAPAR*), photosynthetically active radiation (*PAR*), and light use efficiency (*LUE*). Vectors show the contribution of single variables to the principal component. Color bar shows the day of the year (for DBF) or day of season (for TDF) for season a) 2013, b) 2014, c) 2015, and d) 2016.

Figure 4.6 - Relative importance analysis of 2013 LUE model variables PAR, fAPAR, and LUE about GPP for (a) combined season, (b) green-up, (c) maturity, and (d) senescence. An LMG relative importance models was used. Combined variables accounted for 90.03%, 90.77%, 87.21%, and 96.13% of seasonal, green-up, maturity, and senescence GPP variability, respectively.

Figure 4.7 - Relative importance analysis of 2014 LUE model variables PAR, fAPAR, and LUE about GPP for (a) combined season, (b) green-up, (c) maturity, and (d) senescence. An LMG relative importance models was used. Combined variables accounted for 83.59%, 95.88%, 77.95%, and 97.12% of seasonal, green-up, maturity, and senescence GPP variability, respectively.

Figure 4.8 - Relative importance analysis of 2015 LUE model variables PAR, fAPAR, and LUE about GPP for (a) combined season, (b) green-up, (c) maturity, and (d) senescence. An LMG relative importance models was used. Combined variables accounted for 87.33%, 88.62%, 89.68%, and 97.06% of seasonal, green-up, maturity, and senescence GPP variability, respectively.

Figure 4.9 - Relative importance analysis of 2016 LUE model variables PAR, fAPAR, and LUE about GPP for (a) combined season, (b) green-up, (c) maturity, and (d) senescence. An LMG relative importance models was used. Combined variables accounted for 86.80%, 86.34%, 88.25%, and 87.34% of seasonal, green-up, maturity, and senescence GPP variability, respectively.

Figure A1.1 Relative importance analysis of GLM NDVI = PAR + VWC + VPD + LE during green-up of the (a) 2013, (b) 2014, (c) 2015, and (d) 2016 seasons. Four relative importance models were used including LMG, First, Genizi, and CAR. GLM accounted for 16.12%, 22.92%, 66.96%, and 36.81% of 2013, 2014, 2015 and 2016 GPP variability, respectively.

Figure A1.1 Relative importance analysis of GLM NDVI = PAR + VWC + VPD + LE during green-up of the (a) 2013, (b) 2014, (c) 2015, and (d) 2016 seasons. Four relative importance models were used including LMG, First, Genizi, and CAR. GLM accounted for 16.12%, 22.92%, 66.96%, and 36.81% of 2013, 2014, 2015 and 2016 GPP variability, respectively.

Figure A1.3: Relative importance analysis of GLM NDVI = PAR + VWC + VPD + LE during senescence of the (a) 2013, (b) 2014, (c) 2015, and (d) 2016 seasons. Four relative importance models were used including LMG, First, Genizi, and CAR. GLM accounted for 89.93%, 95.64%, 96.00%, and 90.15% of 2013, 2014, 2015 and 2016 GPP variability, respectively.

Figure A2.1. Gross primary productivity (GPP) and seasonal meteorological parameters for the 2015 growing season at the Peace River Environmental Monitoring Super Site. From top to bottom: (**a**) daily average net ecosystem exchange and ecosystem respiration, (**b**) photosynthetic photon flux density (PPFD), (**c**) temperature, (**d**) relative humidity (RH), and (**e**) vapor pressure deficit (VPD).

Figure A2.2. Time series of apparent quantum yield and (**a**) temperature, (**b**) relative humidity (RH), and (**c**) soil volumetric water moisture (VWC). Apparent quantum yield values were derived from eddy covariance measurements.

Figure A3.1 Conceptual diagram of temporal aggregation workflows for each of the LUE model variables: (a) PAR, (b) fAPAR, (c) APAR, and (d) LUE. Aggregation was done sequentially increasing the period by 1 hour, centered on midday, until the maximum diurnal hours were reached. This procedure was applied for datasets from both TDF and DBF sites.

List of Abbreviations

α – Photochemical efficiency (mol CO_2 mol^{-1} PPFD).

APAR – Absorbed photosynthetically active radiation (μmol m^{-2} s^{-1}).

A_{max} – GPP at maximum PPFD (μmol m^{-2} s^{-1}).

ε – Light use efficiency (mol CO_2 mol^{-1} PPFD).

EMEND –Ecosystem Management Emulating Natural Disturbance.

fAPAR – Fraction of absorbed photosynthetically active radiation.

FOV – Field of View.

FWHM – Full width half maximum.

GPP – Gross primary productivity (μmol m^{-2} s^{-1}).

H – Sensible heat flux (W m^{-2}).

IRGA – Infra-red gas analyzer.

LE – Latent heat flux (W m^{-2}).

LUE – Light use efficiency (mol CO_2 mol^{-1} PPFD).

MODIS – Moderate Resolution Imaging Spectroradiometer.

NDVI – Normalized Differential Vegetation Index

NEE – Net ecosystem exchange (mol CO_2 mol^{-1} PPFD).

ρ_a – The density of dry air (mol m^{-3}).

ρ_{PAR} – Total reflectance of photosynthetically active radiation.

$\rho_{corrected}$ – Corrected reflectance normalized with 99% reflective white standard.

ρ_{PYR} – Total reflectance of solar radiation.

PAR – Photo synthetically active radiation. Remote sensing synonym for PPFD.

PPFD – Photosynthetically-active photon flux density (µmol m^{-2} s^{-1}).

PR-EMSS – Peace River Environmental Monitoring Super Site.

PRI – Photochemically Reflectance Index.

sPRI – Scaled Photochemically Reflected Index.

Q_{10} – Temperature sensitivity coefficient for TER (dimensionless).

R_{10} – The rate of TER at 10°C (µmol m^{-2} s^{-1}).

RH – Relative humidity (%).

s' – Molar mixing ratio fluctuation (mol mol^{-1} dry air).

SRNP- EMSS – Santa Rosa National Park Environmental Monitoring Super Site.

T – Air temperature (°C).

TER – Total ecosystem respiration (µmol m^{-2} s^{-1}).

VPD – Vapor pressure deficit (KPa).

VWC – Volumetric Soil Water Content (%).

w' – Vertical wind velocity fluctuation (m s^{-1}).

WSN – Wireless Sensor Network.

CHAPTER 1 – Introduction

1.1 Introduction

Uncertainty in the quantification of terrestrial carbon sequestration has limited our understanding of carbon cycle dynamics and our ability to predict future photosynthetic activity and risk within climate models. However, with the onset of remote sensing, a number of semi-empirical upscaling methods have emerged with the goal of transforming local CO_2 fluxes into ecosystem-scale productivity. Remote sensing provides the ability to gather a wide range of data from locations that were previously inaccessible and do so in a non-destructive way. To better understand ecosystem functions, systematic studies looking at temporal patterns within individual ecosystems need to be conducted. Characterizing ecosystem processes, which in turn are linked to its functioning, allow us to create regional models that characterize the challenges, limitations, and feasibility of global-scale models (Field et al., 1995). As such, we can think of ecosystem studies as being a key to correctly informing global models (Schimel, 1995; Braswell et al., 1997; Reich et al., 1999; Running et al., 2004; Turner et al. 2005).

Two vulnerable ecosystems with important influence on global climate are tropical dry forests (TDFs) and boreal forests. As such, the affect and significance of these two ecosystems in the context of global climate makes these important ecosystems to study. Their shared deciduous responses, caused by different limiting resources, make for interesting ecosystem comparisons. However, the study of these two ecosystems does represent significant challenges including their remote location and spatial extent, which perhaps has contributed to our limited understanding of these ecosystems.

Our limited knowledge of variability and controls on fluxes in tropical ecosystems limits our ability to predict CO_2 and H_2O cycling and future climatic changes due to natural and anthropogenic disturbances predictions (Schimel et al., 2001). Over the last 20 years, there has been a greater effort from the scientific community to characterize the mechanisms that control carbon exchange within the various tropical ecosystems. However, even though tropical dry forests (TDFs) account for over 40% of tropical forest worldwide, they have remained considerably understudied. The lack of available data has prevented the full characterization of carbon flux dynamics in this ecosystem. Furthermore, to date, there has been very limited information published on the effect of drought and resilience on ecosystem productivity within tropical dry forests. As climate change effects are predicted to lead to decrease water availability in many tropical dry forested areas (Enquist, 2002;

IPCC, 2013), it has become increasingly important to understand tropical dry forest's vulnerability to drought. The quantification of net carbon balance in topical systems is critical for understanding ecosystem respiration and photosynthesis components, as well as to establish the response of topical systems in a changing global climate

The boreal forest plays the most important regulatory influence on global climate by affecting the overall carbon, energy, and water balance (Walter 1979; Kasischke and Stocks 2000; Dale et al. 2001; French, 2002; Balzter et al. 2005). Carbon sequestration and release, changes in energy budgets driven by albedo changes, and modification of moisture balance are examples of processes by which borel forests have been shown to affect global climate conditions (French, 2002; Pan et al. 2011). Furthermore, climate change is projected to have an amplified impact on northern latitudes, with reports suggest climatic warming in the Arctic exceeding 1.9 times the global average (Brock and Xepapadeas, 2017; Winton 2006). As large extents of the boreal forests occupy northern latitudes, they provide the opportunity to explore the impact of climate change and volatility in this ecosystems.

Modern remote sensing techniques can provide continuous measurements that help characterize and identify rapid changes in vulnerable ecosystems. Additionally, integration of optical with eddy covariance flux measurements can provide further insight into ecosystem functioning than would be possible with either method independently (Gamon, 2015). Remote sensing driven Light Use Efficiency (LUE) models (Monteith, 1977) offer the ability to sample sites with high heterogeneity, complex topography, and other non-ideal sites for the eddy covariance technique. In turn, eddy covariance can provide direct physiological validation to remote sensing empirical observations. One of the challenges of integrating optical and flux data arises from the different time and space scales of optical and flux measurements. To achieve meaningful integration of remote sensing with flux data, an in-depth assessment exploring the temporal aggregation requirements needed to build relationships that properly represent the physiological status of plant canopies is necessary.

Integrated National Aeronautics and Space Administration (NASA) field campaigns, First International Satellite Land Surface Climatology Project Field Experiment (FIFE) (Sellers et al., 1992) and Boreal Ecosystem-Atmosphere Study (BOREAS) (Sellers et al., 1997), were the first large scale success studies of remote sensing and flux integration towards a greater understanding of ecosystem physiology and ecology. The integration of remote sensing and micrometeorological data can be done using the light-use efficiency model as the unifying concept. The LUE model, conventionally expressed in terms of Gross Primary Productivity (GPP), is expressed as follows:

$$GPP = \Sigma A_{PAR} \times \varepsilon \quad (1)$$

where ΣAPAR refers to the integration of Absorbed Photosynthetic Available Radiation over a time frame, and ε represents the LUE (Monteith, 1977; Asrar et al., 1984; Sellers 1985). Conceptually, the LUE model can be separated into a structural component, described by changes in A_{PAR}, and a physiological component portrayed through the LUE term. Much work has been done in displaying a direct link between optical remote sensing and the APAR term (Sellers, 1985; Sellers et al., 1987; Myneni and Williams, 1994). However, addressing the efficiency term of the LUE model from remote sensing has been more challenging. Advances in the spectral resolution of remote sensing tools have provided some new opportunities for estimating LUE. One possible method involves the Photochemical Reflectance Index (PRI), typically derived from narrow-band reflectance at 531 and 570 nm (Gamon et al., 1990; 1992; 1993; Peñuelas et al., 1995; Filella et al., 1996). PRI interpretation becomes particularly problematic over large time scales (e.g. seasonal change) or spatial scales (e.g. regional or global satellite measurements), where many confounding factors including canopy structure, view and illumination angles can affect PRI (Barton & North, 2001). To understand the mechanism of PRI response, it is important to determine what the index is truly representing, taking into account the irradiance and the spatial and temporal dimension of PRI measurements within a specific ecosystem. The recent availability of continuous PRI sensors provides the opportunity to expand the current understanding of PRI responses to physiological changes in vegetation as well as provide additional tools for the integration of optical and flux data.

In this context, the main goal of my Ph.D. dissertation is to contribute to the growing body of scientific work by exploring mechanisms of ecosystem productivity through the integration of remote sensing and micrometeorological data. The evaluation of ecosystem productivity has traditionally been done within the framework of a single scientific discipline. However, contemporary development in the field of remote sensing has proved a powerful tool allowing continuous and enhance monitoring of ecosystem status. Interdisciplinary studies, combining flux measurements with proximal remote sensing, represent novel approaches that help to systematically explore ecosystem processes. My research looks to continue in this path and explore some of the mechanisms of productivity in a tropical dry forest in Costa Rica and a deciduous boreal forest in Canada.

In order to support my main goal, the specific objectives of this thesis are:

1) To identify the environmental mechanisms affecting productivity in a tropical dry forest before and after a severe drought period.
2) To determine if new continuous sampling PRI sensors can be used as a proxy of light use efficiency and calculate ecosystem productivity of an aspen forest.
3) To evaluate the impact of temporal aggregation and phenology on LUE model parametrization and ecosystem productivity.

Each objective was explored by a chapter in this thesis and can be summarized as follows:

Chapter 2 **- Effect of Drought on Productivity in a Costa Rican Tropical Dry Forest** (Castro, Sanchez-Azofeifa, and Sato; 2018) – Tropical dry forests (TDF) are substantially understudied and represent a small fraction of the total research on tropical ecosystems (Sanchez-Azofeifa et al. 2005). This has contributed to the current poor understanding of TDF productivity. Precipitation regimes in tropical regions are projected to change by global climate models (Feng et al., 2013). However, limited research is available on the driving mechanisms of productivity at ecosystem scale or how productivity may respond to changing precipitation and water availability regime. In this study, I used information on seasonal phenology and carbon fluxes derived from optical remote sensors and eddy covariance collected over four growing seasons (2013-2016). Through the analysis of the integrated time series, I was able to identify key mechanisms of ecosystem productivity under normal seasonal precipitation regimes (2013 and 2016 seasons). The 2014 and 2015 growing seasons recieved a 30% and 63% reduction in precipitation, respectively, and were designated as drought seasons. These datasets were used to identify the effect of drought on optical phenology and carbon dynamics of a secondary TDF. Normal and drought conditions were compared and contrasted through eddy covariance accumulation curves and relative importance analysis. Optical and flux collections and analysis of TDF are uncommon, and these datasets represent unique and valuable additions to the scientific literature, specifically in tropical environments. Results of this study can be used to understand secondary TDF productivity and help parametrize and validate productivity models.

Chapter 3 **- Testing of Automated Photochemical Reflectance Index Sensors as Proxy Measurements of Light Use Efficiency in an Aspen Forest** (Castro and Sanchez-Azofeifa; 2018) – Advances in the spectral resolution of remote sensing instrumentation has provided new opportunities for estimating LUE through optical tools like the Photochemical Reflectance Index (PRI) (Gamon et al., 1990; 1992; 1993; Peñuelas et al., 1995; Filella et al., 1996). However, as this index is derived from narrow spectral bands (531 and 570 nm), its response can be affected by several individual and

combined confounding variables, making PRI interpretation difficult over large temporal and spatial scales (Sims & Gamon, 2002; Stylinski et al., 2002; Filella et al., 2009; Garrity et al., 2011; Gamon & Berry, 2012). Until recently, the lack of readily available continuous measurements made it difficult to assess PRI as a proxy of LUE over time and space. In this study, we evaluated the reliability of data collected from recently available autonomous PRI sensors as a proxy of light use efficiency (LUE) in an aspen (*Populus tremuloides*) forest stand. Midday and diurnal calibration procedures were used to determine how to most accurately resolve diurnal and seasonal PRI patterns. Quantum yield was derived from eddy covariance measurements, through the use of light response curves, and used to validate the response of PRI measurements. Modelled productivity from light use efficiency models using PRI and quantum yield were derived and compared to eddy covariance Gross Primary Productivity (GPP). Protocols described in this study can be used as a framework for calibrating and validating spectral indices from automated sensors. Also, results contribute towards a better understanding of PRI as a proxy of LUE and a deeper understanding of diurnal and seasonal changes of vegetation physiology that can be explored through continuous measurements. A deeper understanding of the proper use of PRI as a proxy of LUE is necessary for integration with flux measurements and vegetation productivity modelling.

***Chapter 4* - Effect of temporal aggregation and phenology on LUE model variables and productivity in two deciduous forests** – The integration of remote sensing and flux measurements represents an important development in multidisciplinary science and can provide significant insight into ecosystem functioning (Gamon, 2015)**.** Remote sensing provides the ability to continuously monitor any ecosystem at a variety of spatial and temporal scales, while eddy-covariance data provides the physiological validation to empirical remote sensing observations. As such, the combined optical and flux data can provide a deeper exploration of the underlying controls on ecosystem-atmosphere interactions than would be possible independently from one another (Gamon, 2015). As part of developing data management protocols for remote sensing data integration, the effect of temporal integration of data must be explored. In this study, a multisite and multi-season temporal aggregation analysis on each LUE model variable (PAR, fAPAR, APAR, and LUE) was done. Study sites included Tropical Dry Forest (TDF) (2013 and 2014 growing seasons) and a Deciduous Broadleaf Forest (DBF) (2015 and 2016 growing seasons). Aggregation analysis was also done within each phenological stage (green-up, maturity, and senescence) and effects were compared to growing seasonal patterns. Relative importance analysis for seasonal and phenology divided data helped explore the changing contributions by LUE model components on productivity. The study

findings have significant relevance towards the parametrization of LUE models, as well as tests Garbulsky et al. (2007) theory suggesting that the contribution to the LUE model can change between vegetation and environmental conditions.

1.2 References

Asrar, G., Fuchus, M., Kanemasu, E. T., and Hatfield, J. L. (1984). Estimating absorbed photosynthetic radiation and leaf area index from spectral reflectance in wheat. Agronomy Journal 76:300-306.

Barton, C. V. M., & North, P. R. J. (2001). Remote Sensing of canopy light use efficiency using the Photochemical Reflectance Index. Model and analysis. Remote Sensing of Environment, 78(264), 273.

Braswell, B.H., Schimel, D.S., Linder, E., and Moore III, B. (1997). The response of global terrestrial ecosystems to interannual temperature variability. Science 278:870-873.

Brock, W., & Xepapadeas, A. (2017). Climate change policy under polar amplification. European Economic Review 99: 91–112.

Balzter, H., Gerard, F.F., George, C.T., Rowland, C.S., Jupp, T.E., McCallum, I., Shvidenko, A., Nilsson, S., Sukhinin, A., Onuchin, A. and Schmullius, C., (2005). Impact of the Arctic Oscillation pattern on interannual forest fire variability in Central Siberia. Geophysical Research Letters. 32(14).

Dale, V.H., Joyce, L.A., McNulty, S., Neilson, R.P., Ayres, M.P., Flannigan, M.D., Hanson, P.J., Irland, L.C., Lugo, A.E., Peterson, C.J., Simberloff, D., Swanson, F.J., Stocks, B.J. and Wotton, B.M., (2001). Climate change and forest disturbances. Bioscience. 51(9), 723- 734.

Enquist, C.A.F., (2002). Predicted regional impacts of climate change on the geographical distribution and diversity of tropical forests in Costa Rica. Journal of Biogeography, 29:519-534.

Feng, X., Porporato, A., & Rodriguez-Iturbe, I. (2013). Changes in rainfall seasonality in the tropics. Nature Climate Change, 3(9), 811.

Field C.B., Randerson J.T., and Malmastrom C.M. (1995) Global net primary production: combining ecology and remote sensing. Remote Sensing of Environment, 51:74-88.

Filella. I., Amaro, T., Araus, J., L., and Peñuelas, J. (1996) Relationship between photosynthetic radiation-use efficiency of barley canopies and the photochemical reflectance index (PRI). Physiol Plant 96: 211–216.

Filella, I., Porcar-Castell, A., Munné-Bosch, S., Bäck, J., Garbulsky, M. F., & Peñuelas, J. (2009). PRI assessment of long-term changes in carotenoids/chlorophyll ratio and short-term changes in de-epoxidation state of the xanthophyll cycle. International Journal of Remote Sensing, 30(17), 4443-4455.

French, N.N.F., (2002). The Impact of Fire Disturbance on Carbon and Energy Exchange in the Alaskan Boreal Region: A Geospatial Data Analysis. Ph.D. dissertation Thesis, University of Michigan, Ann Arbor, 105.

Gamon, J.A., Field, C.B., Bilger, W., Björkman, O., Fredeen, A.L., and Peñuelas, J. (1990) Remote sensing of the xanthophyll cycle and chlorophyll fluorescence in sunflower leaves and canopies. Oecologia 85: 1–7.

Gamon, J.A., Peñuelas J., and Field C.B. (1992). A narrow-waveband spectral index that tracks diurnal changes in photosynthetic efficiency. Remote Sensing of Environment 41: 35–44.

Gamon, J.A., Filella, I., Peñuelas, J. (1993) The dynamic 531-nanometer Δ reflectance signal: a survey of twenty angiosperm species. Yamamoto HY , Smith CM (Eds). Photosynthetic Responses to the Environment. American Society of Plant Physiologists, Rockville. pp. 172-177.

Gamon, J. A., & Berry, J. A. (2012). Facultative and constitutive pigment effects on the Photochemical Reflectance Index (PRI) in sun and shade conifer needles. Israel Journal of Plant Sciences, 60(1-2), 85-95.

Gamon, J. A. (2015). Reviews and syntheses: Optical sampling of the flux tower footprint.

Garbulsky, M. F., Peñuelas, J., Gamon, J., Inoue, Y., & Filella, I. (2011). The photochemical reflectance index (PRI) and the remote sensing of leaf, canopy and ecosystem radiation use efficiencies: A review and meta-analysis. Remote Sensing of Environment, 115(2), 281-297.

Garrity, S. R., Eitel, J. U., & Vierling, L. A. (2011). Disentangling the relationships between plant pigments and the photochemical reflectance index reveals a new approach for remote estimation of carotenoid content. Remote Sensing of Environment, 115(2), 628-635.

IPCC (2013). Climate Change 2013: The Physical Scientific Basis. Contribution of Working Group I to the Fifth Assessment Report of the Intergovernmental Panel on Climate Change. Cambridge University Press, New York, USA.

Kasischke, E.S. and Stocks, B.J., (2000). Fire, Climate Change, and Carbon Cycling in the Boreal Forest. Ecological Studies 138. Springer-Verlag, New York, pp. 461.

Pan, Y., Birdsey, R.A., Fang, J., Houghton, R., Kauppi, P.E., Kurz, W.A., Phillips, O.L., Shvidenko, A., Lewis, S.L., Canadell, J.G. and Ciais, P. (2011). A large and persistent carbon sink in the world's forests. Science, 333(6045), 988-993.

Penuelas, J., Filella, I., & Gamon, J. A. (1995). Assessment of photosynthetic radiation-use efficiency with spectral reflectance. New Phytologist, 131(3), 291-296.

Monteith, J.L. (1977). Climate and the efficiency of cop production in Britain. Phil. Trans. R. Soc. Lond. B. 281: 277-294.

Myneni, R.B., & Williams, D.L., (1994). On the relationship between FAPAR and NDVI. Remote Sensing of Environment, 49:200-211.

Reich, P.B., Turner, D.P., Bolstad, P. (1999). An approach to spatially distributed modeling of net primary production (NPP) at the landscape scale and its application in validation of EOS NPP products. Remote Sensing of Environment, 70: 69−81.

Running S.W. et al. (2004). A continuous satellite-derived measure of global terrestrial primary production. Bioscience, 54(6): 547-560.

Sánchez-Azofeifa, G.A., Quesada, M., Rodriguez, J.P., Nassar, J.M., Stoner, K.E., Castillo, A., Garvin, T., Zent, E.L., Calvo-Alvarado, J.C., Kalacska, M.E. and Fajardo, L., (2005). Research priorities for neotropical dry forests. Biotropica, 37(4), pp.477-485.

Sims, D. A., & Gamon, J. A. (2002). Relationships between leaf pigment content and spectral reflectance across a wide range of species, leaf structures and developmental stages. Remote sensing of environment, 81(2-3), 337-354.

Schimel D.S. (1995). Terrestrial biogeochemical cycles: global estimates with remote sensing. Remote Sensing of Environment, 51: 49−56.

Schimel, D.S., House, J.I., Hibbard, K.A., Bousquet, P., Ciais, P., Peylin, P., Braswell, B.H., Apps, M.J., Baker, D., Bondeau, A. and Canadell, J., (2001). Recent patterns and mechanisms of carbon exchange by terrestrial ecosystems. Nature, 414:169-172.

Sellers, P.J. (1985). Canopy reflectance, photosynthesis, and transpiration. International Journal of Remote Sensing, 6(8):1335-1372.

Sellers, P.J. (1987). Canopy reflectance, photosynthesis, and transpiration II. The role of biophysics in the linearity of their interdependence. Remote Sensing of Environment, 21: 143−183.

Sellers, P. J., Hall, F. G., Asrar, G., Strebel, D. E., & Murphy, R. E. (1992). An overview of the first international satellite land surface climatology project (ISLSCP) field experiment (FIFE). Journal of Geophysical Research: Atmospheres, 97(D17), 18345-18371.

Sellers, Piers J., et al. "BOREAS in 1997 (1997). Experiment overview, scientific results, and future directions." Journal of Geophysical Research: Atmospheres 102.D24: 28731-28769.

Stylinski, C., Gamon, J., & Oechel, W. (2002). Seasonal patterns of reflectance indices, carotenoid pigments and photosynthesis of evergreen chaparral species. Oecologia, 131(3), 366-374.

Turner, D. P., et al., (2005). Site-level evaluation of satellite-based global terrestrial GPP and NPP monitoring, Global Change Biol., 11(4), 666–684.

Walter, H., (1979). Vegetation of the Earth and Ecological Systems of the Geo-biosphere. Springer-Verlag, New York, pp. 274.

Winton, M. (2006). Amplified Arctic climate change: What does surface albedo feedback have to do with it? Geophysical Research Letters, 33(3).

CHAPTER 2 – Effect of Drought on Productivity in a Costa Rican Tropical Dry Forest

Abstract

Climate models predict that precipitation patterns in tropical dry forests (TDFs) will change, with an overall reduction in rainfall amount and intensification of dry intervals, leading to greater susceptibility to drought. In this paper, we explore the effect of drought on phenology and carbon dynamics of a secondary TDF located in the Santa Rosa National Park (SRNP), Costa Rica. Through the use of optical sensors and an eddy covariance flux tower, seasonal phenology and carbon fluxes were monitored over a four-year period (2013-2016). Over this time frame, annual precipitation varied considerably. Total precipitation amounts for the 2013-2016 seasons equaled 1591.8 mm (+14.4mm SD), 1112.9 mm (+9.9mm SD), 600.8 mm (+7.6mm SD), and 1762.2 mm (+13.9mm SD), respectively. The 2014 and 2015 (ENSO) seasonal precipitation amounts represent a 30% and 63% reduction in precipitation, respectively, and were designated as drought seasons. Phenology was affected by precipitation patterns and availability. The onset of green-up was closely associated with pre-seasonal rains. Drought events lead to seasonal NDVI minimums and changes in phenologic cycle length. Carbon fluxes, assimilation, and photosynthetic light use efficiency were negatively affected by drought. Seasonal minimums in photosynthetic rates and light use efficiency were observed during drought events, and gross primary productivity was reduced by 13% and 42% during drought seasons 2014 and 2015, respectively. However, all four growth seasons were net carbon sinks. Results from this study contribute towards a deeper understanding of the impact of drought on TDF phenology and carbon dynamics.

2.1 Introduction:

Tropical dry forests (TDFs) hold a strong economic and cultural connection to human development in the Neotropics (Maass et al., 2005). TDFs not only provide a source of agricultural and urban land but also an important source of goods and ecosystem services for the communities that live around them (Balvanera et al., 2011; Castillo et al., 2005; Fajardo et al., 2005;). Such is the close connection of TDFs to human activity that they are considered the most heavily utilized and disturbed ecosystem in the world (Janzen, 1998; Sanchez-Azofeifa et al., 2005). Tropical forests have been estimated to account for a third of global metabolic activity (Malhi, 2012), and TDF may account for

roughly 42% of all tropical ecosystems (Quesada et al. 2009; Murphy and Lugo, 1986). However, TDFs are surprisingly understudied and currently represents only a fraction of research on tropical ecosystem (Sanchez-Azofeifa et al. 2005). The former has contributed to the fact that we still have a poor understanding of TDF response to climatic factors, including moisture dynamics, which are needed to understand ecosystem responses to climate change.

The eddy covariance technique has become the backbone for regional and continental carbon balance modeling efforts (Papale & Valentini, 2002; Reichstein et al., 2003) as well as validation and calibration of ecosystem models (Baldocchi, 1997; Hanan et al., 2002; Hanson et al., 2004; Reichstein et al., 2002, 2003). However, as global modeling has progressed, there remains an underrepresentation of tropical ecosystems. Fluxnet-Multi-Tree Ensemble (MTE) upscaling efforts in detecting global variability in terrestrial carbon and water cycles indicated a high index of extrapolation in tropical areas (Jung et al., 2009). A more recent Fluxnet (2015) summary report on global fluxes, reported insufficient flux measurements in the tropical ecosystems (Kumar et al., 2016), leading to an underestimate of gross primary productivity (GPP) in these regions.

Global climate models project precipitation regimes in tropical regions to change (Feng et al., 2013) with increasing in seasonality and variability as main outcomes. Rainfall patterns are predicted to move towards more extreme events and lead to an overall reduction in the amount and an extension of the dry intervals (Chadwick et al., 2015; Malhi et al., 2008; Zelazowski et al. 2011). Changes in precipitation regimes are of particular importance to tropical dry forests as water dynamics determine the alternating seasonality between wet and dry seasons. As such, the issue of how TDFs will respond to the predicted drier conditions has become important to consider. A recent synthesis by Allen et al. (2017) reviewed multiple data sources including seedling, dendrochronology and modeling data to suggest changes in structure and functionality, including a reduction in carbon storage, as drought frequency increases and precipitation becomes more variable.

In this context, the objective of this study is to contribute to the discussion of how TDFs will respond to changes in rainfall regimes, specifically in the context of phenology and ecosystem carbon exchange. Through the use of eddy covariance measurements, optical phenology, and meteorological data collected through four growing seasons (2013-2016), including a drought (2014) and an ENSO severe drought season (2015), we explored the following questions: 1) How are phenology and carbon exchange in a TDF impacted by drought? 2) What drives seasonal variations of GPP and respiration under ‘normal’ and drought conditions? This analysis will contribute towards a deeper

understanding of the mechanisms controlling ecosystem productivity and explores TDFs sensitivity and resilience to drought in the face of changing climate.

2.2 Methods:

2.2.1 Site description

The study was conducted within the Santa Rosa National Park Environmental Monitoring Super Site (SRNP-EMSS), Guanacaste, Costa Rica. The SRNP-EMSS is located in the northwest of Costa Rica, near the border with Nicaragua and is part of a broader conservation area called Area de Conservacion Guanacaste (ACG) (Fig. 2.1). The park area consists of a series of plateaus ranging from 300 masl to sea level and covered by a mosaic of pasture and tropical dry forest in various stages of regeneration (Janzen, 2000; Sen & Sanchez-Azofeifa, 2017). The study plot is located at 10°44.206' N, 85°37.034 W with an altitude of 290 masl, and is characterized as an intermediate successional stage tropical dry forest with average tree height of 13m (Li et al. 2017) (Fig. 2.1). Its topography is slightly sloping (<2%) in the north direction, and the predominant wind direction is from the north-west. The mean annual air temperature for the area is 25ºC and mean annual precipitation over the past 26 years is 1575mm, with 85-97 % of precipitation falling between May and November. The natural phenologic cycle initiates during the onset of rains (May) and extends, through a prolonged senescence, into late February of the following calendar year.

2.2.2 General Instrumentation

The study site has been monitored with an eddy covariance system and meteorological station installed on a 35m 0.70m x 2.0 m-section triangular steel tower located within the forest stand. The eddy covariance (EC) method (Aubinet et al., 1999; Baldocchi et al., 1988, Moncrieff et al., 1997) provided measurements of net ecosystem CO2 exchange (NEE) (mg m-2 s-1), latent heat flux (LE) (W m-2), and sensible heat (H) (W m-2) fluxes continuously from 2013 – 2016. Further detail on the eddy covariance instrumentation and data processing can be found in the supplementary methods section.

Proximal remote sensing sensors mounted on south-facing arms extending from the steel tower allow the tracking of forest stand phenology progression. A broadband NDVI was derived from the two-band spot radiometers following a revised method of the Huemmrich et al. (1999) method. NDVI seasonal changes were used to calculate the phenological cycle and its stages, green-up, maturity, and senescence. Dates for the start of the season, end of season, as well as transitions

between stages were determined by analyzing the rate of change throughout the time series, using second derivative functions. Additionally, a meteorological station provided ancillary climate variables including temperature (T), vapor pressure deficit (VPD), relative humidity (RH) measurements and volumetric soil water content (VWC). More detailed information on sensor deployment can be found in the supplementary methods section.

2.2.3 Eddy Covariance Partitioning

Measurements of NEE was partitioned into its two components: Gross Primary Productivity (GPP) (mg m-2 s-1) and total ecosystem respiration (Reco) (mg m-2 s-1). Reco was estimated using night-time fluxes based on the approach suggested by Reichstein et al. (2005). Additionally, a light-response curve model, independent of temperature by relying solely on characterizing carbon assimilation as a function of light, was used as an independent method for estimating Reco and GPP. A series of hyperbolic functions were used to assess the response of photosynthesis to incident radiation, following the methods outlined by Hutyra et al. (2007) used in tropical forests (equations and detailed explanation found in supplementary material section).

2.2.4 Analysis of Relative Importance

A stepwise multiple regression model was used to identify the environmental drivers most affecting the temporal variability in GPP. The identified regression and predictors are expressed by the following formula:

$$GLM = GPP \sim PAR + VWC + VPD + LE \quad (1)$$

where gross primary productivity (GPP) is a product of photosynthetically active radiation (PAR), volumetric soil water content (VWC), vapor pressure deficit (VPD), relative humidity (RH), temperature (T), and latent heat flux (LE).

A relative importance analysis based on the multiple regression framework of these combined variables provided the strength of each predictor in relation to seasonal GPP (2013-2016). Four different relative importance techniques were used including the LMG (Chevan and Sutherland, 1991; Lindeman et al., 1980), First, Genizi (Genizi, 1993), and CAR (Zuber and Strimmer, 2010) models. All models were bootstrapped using 1000 replicates producing 95% confidence intervals. The LMG model has been described as the most robust method as it takes into account the direct and adjusted

effects of each regressor allowing more effective R2 decomposition. Further details on the stepwise multiple regression and relative importance model can be found within the supplementary material section.

2.3. Results

2.3.1 Comparison of Meteorological Conditions

Total seasonal precipitation during the four monitored growing seasons was 1591.8mm (+14.4mm SD), 1112.9 mm (+9.9mm SD), 600.8 mm (+7.6mm SD), and 1762.2 mm (+13.9mm SD) during 2013, 2014, 2015, and 2016, respectively. Precipitation accumulation for the 2013 and 2016 years was comparable to published seasonal totals (Gillespie, Grijalva & Farris 2000), and therefore, these seasons were treated as receiving 'normal' precipitation amounts. In contrast, accumulation amounts during the 2014 drought and 2015 ENSO drought represented 30%, and 62% declines, respectively, from 2013 'normal' levels (Fig. 2.2). Interseasonal variability in precipitation patterns was also observed; results can be found in the supplementary results section. Precipitation amounts were also totaled for each phenological stage (Table 2.1): green-up, maturity, and senescence. Rainfall during green-up accounted for 24%, 8.4%, 23%, and 12% of total for 2013, 2014, 2015, and 2016, respectively. The bulk of the added rainfall occurred during maturity, and senescence only accounted for <1% of total. Before the start of each of the 2013, 2014, 2015, and 2016 seasons, precipitation events were observed totaling 20.5mm, 18.2 mm, 74.0mm, and 72.6mm, respectively (Fig. 2.3).

Main temporal changes in PAR, T, RH, and VPD were driven by seasonality (Fig. 2.4). PAR, T and VPD maximums occur during the dry season and minimums during the wet season, when cloud cover and precipitation are common, and RH values reach maximums. Temporal patterns of VWC were connected to precipitation frequencies. VWC spiked with precipitation events and plateaued during dry periods. Interannual variability associated with drought was observed in all meteorological parameters (Table 2.2). Average seasonal values of PAR (1082.64 μmol m-2 s-1), T (28.05 oC), VPD (11.79 hPa), and VWC (15.12 %) were highest during the 2015 severe drought season, compared to 2013, 2014, and 2016 season values. The 2013 season had the lowest VPD and RH quantities and spanned the greatest range (Table 2.2). During each season, minimum values of VPD approached zero during peak precipitation periods (common in September and October months).

2.3.2 Changes in Phenology

Seasonal phenology was monitored by tracking changes in canopy NDVI and phonologic stages, green-up, maturity, and senescence, were identified (Fig. 2.5). Phenologic stages represented consistent time periods. Greenup, Maturity, and Senescence accounted for approximately 7% (+3%), 65% (+4%), and 27% (+4%) of the total phenologic cycle, respectively. The duration of phenologic stages varied from year to year. Drought seasons 2014 and 2015 were 34 days longer and 22 days shorter, respectively, than the 2013 season; while the 2016 season was 51 days longer (Table 2.3). Comparison of seasonal NDVI showed maximum values during 2013 (0.85) and consistently decreased during 2014 (0.82) and 2015 (0.80) drought years, before stabilizing during 2016 (0.80).

The start of season date also varied interannually, with green-up initiating shortly after the start of seasonal rains (Fig. 2.5). Following green-up, a rapid transition from green-up to maturity was observed, lasting between 18-36 days. Proportionally, the majority of the growing season was spent within maturity and comparison between the four years showed this period as having the most variability between these seasons. Using the 2013 season as a standard for comparison, the 2014 and 2016 phenologic cycles were longer (332 and 358 total days, respectively), while the 2015 phenologic cycle was shorter (150 total days) (Table 2.4).

Seasons with longer maturity periods coincided with late-season rain events (Fig. 2.2). Intra-seasonal NDVI variability was also greatest during maturity due to droughts occurring during this stage. Large decreases in NDVI, amounting to approximately 0.1, were observed during July and August months in drought years 2014 and 2015, indicating marked losses of canopy greenness. Drought months were characterized by low variability in daily NDVI values, showing consistency in depressed quantities. During the second half of the 2013 maturity, instrument error affected data quality and is likely the cause for the sudden observed decrease in NDVI and high spike in measurement variability.

2.3.3 Ecosystem Carbon Fluxes

Common patterns emerged from the evaluation of carbon fluxes of ‘normal’ precipitation years (2013 and 2016). GPP increased consistently from green-up to maturity, plateaued during peak precipitation months (September and October). This is followed by steady GPP declines into senescence and the dry season (Fig. 2.6b). Drought years 2014 and 2015 deviated from this pattern by displaying GPP reductions during drought months (July and August). Following the return of rainfall events, GPP increased to pre-drought levels. Total accumulated GPP was greatest during the 2016

season, amounting to 1453.53 g C m^{-2} $season^{-1}$, a 29% increase from 2013 (1125.30 g C m^{-2} $season^{-1}$) (Fig. 2.7b). GPP levels were significantly reduced during drought years, totaling 949.97 g C m^{-2} $season^{-1}$ in 2014 and 636.41 g CO_2 m^{-2} $season^{-1}$ in 2015, a 16% and 43% decrease, respectively (Fig. 2.7b). Accumulated NEE quantities for both 'normal' precipitation and drought seasons showed net carbon sequestration to the amounts of -659.20 g C m^{-2} $season^{-1}$, -577.97 g C m^{-2} $season^{-1}$, -361.69 g C m^{-2} $season^{-1}$, and -581.84 g C m^{-2} $season^{-1}$, for 2013-2016 seasons respectively (Fig. 2.7a).

High levels of respiration were observed at the onset of the 2013, 2014, and 2015 seasons (0.41 $\pm$ 0.02, 0.22 $\pm$ 0.03, and 0.31 $\pm$ 0.13 mg m^{-2} s^{-1}, respectively) (Fig. 2.8b). Following the initial burst of respiration in 2013, levels decreased steadily until dormancy. During 2016, respiration initiated at a low 0.08 $\pm$ 0.04 mg m^{-2} s^{-1}, then increased and plateaued at elevated levels (0.33 $\pm$ 0.02 mg m^{-2} s^{-1}) for much of the reminder of the season. Drought months (July and August) of 2014 and 2015 seasons showed sharp declines in respiration rates. 2015 drought levels (0.050 $\pm$ 0.01 mg m^{-2} s^{-1}) were comparable to dry season rates (0.052 $\pm$ 0.02 mg m^{-2} s^{-1}). Following droughts, respiration rates recovered, followed by steady decreases into dry season (Fig. 2.6a).

2.3.4 Controls on Carbon Fluxes

Relative importance analysis showed strong agreement in importance ranking of predictors using the LMG, Genizi, and CAR models, across all growth seasons. In 2013, the set of environmental drivers within the multiple linear regression accounted for 80.1% of GPP variance. LE and VPD combined for over 69% of the LMG, Genizi, and CAR models' R^2, with LE having the highest relative importance (37-39%) (Fig. 2.9a). The "First" method showed slightly different results, showing VPD as the variable of highest importance followed by LE. Differences in results should be interpreted in the context of the model. The "First" metric is derived by adding correlations by a regressor individual, ignoring adjustments based on the combined weight of other regressors within the model, thus producing less robust sets of results. Notwithstanding, atmospheric evaporative power (represented by LE and VPD) still remains the main driving mechanism affecting GPP. Analysis of the 2016 data showed similar patterns to the 2013 season, with LE and VPD, as the main driving variables accounting for over 76% of the models correlation to GPP. Latent heat flux displayed the largest relative importance metric of 43-58% (Fig. 2.9d). The combined set of predictors accounted a total of 72.65% of GPP variability. Drought seasons 2014 and 2015 displayed an increase in predictive power by VWC compared to the 2013 and 2016 seasons, especially during the 2015 severe drought year (Fig 2.9b, c). Closer analysis of the relative importance of parameters

solely during the drought months (Fig. 2.10) in 2014 and 2015 seasons show VWC as the main predictor metric. During the 2014 season, VWC had a relative importance contribution of 56-76% to the models' predictive power. The second ranked predictor was LE with 20-36%. Combined variables accounted for 93.42% of GPP variability. In the 2015 ENSO year, we also see VWC as the main predictor, accounting for 60-83% model predictive power. Latent heat flux represented the second highest relative importance and represented 11-28% of models R^2. All combined variables accounted 94.29% of GPP variability observed during the 2015 drought months.

2.4. Discussion

2.4.1 Water Relations and Phenology

Preseason precipitation appears to play a significant role in the initiation of the phenologic cycle of this secondary tropical dry forest. However, since tree water status was not monitored for this study, we cannot conclusively identify the ecophysiological mechanism by which trees respond to the onset of water availability. Nevertheless, results (shown in supplementary section) from relative importance analysis comparing various environmental drivers (PAR, VWC, VPD, and LE) to NDVI changes during green-up can be used to indicate some of the processes at hand. Throughout all seasons, volumetric soil water was consistently ranked with the most important variable during green-up. The correlation between the onset of precipitation events and VWC (Fig. A1.1, Table A1.1 of supplementary results), as well the importance of VWC during the start of the season would complement observations by Borchert (1994) where irrigation experiments led to stem recharge and leaf flush within one week of application. Reich and Borchert (1984) also reported rapid girth growth but only in response to heavy rains, suggesting a presence of a minimum rehydration threshold for bud break; the threshold varying with the degree of previous dehydration of soil and trees. This threshold variability would in part explain the different pre-season precipitation amounts observed during the 4-year study. During the 2013 and 2014 seasons, 18-21mm of rainfall was observed before bud break. However, pre-season amounts increased to +70 mm for both the 2015 and 2016 seasons. During the 2015 dry season, a series of small rainfall events of less than 9mm were observed before a heavy rainfall event of 49mm, which appeared to trigger the start of the growing season. It is unclear if a higher threshold was required to achieve complete stem recharge or if the smaller precipitation events were not sufficient to reach total rehydration. In contrast, the 2016 season did see a pre-season heavy precipitation event of 26mm that did not trigger bud break. This seeming higher threshold may suggest a strongly water-stressed ecosystem as consequence of the 2015 severe drought conditions.

Similar reported results (Daubenmire, 1972; Liebermann, 1982; Reich and Borchert, 1982) indicate rainfalls of 20-40mm caused bud break in moderately but not strongly water-stressed trees, and rainfall greater than 50-60mm trigger most trees. Our results are in line with the concept that pre-season precipitation serves as a primer for bud-break and the threshold required to trigger stem recharge varies as a result of prior dehydration of soil and trees (Eamus and Prior, 2001).

Analysis of the NDVI time series showed the effect of drought on phenology. During the 2014 and 2015 drought months' seasonal minimums were observed during periods where maximums are the norm. Drought decreases in NDVI are likely associated with decreases in nitrogen and chlorophyll contents. Personal correspondence with members of the Area de Conservacion Guanacaste (ACG) confirmed, through visual inspection, the yellowing of canopy leaves during the extended drought periods. And, although a qualitative observation, this would confirm changes in leaf greenness observed during drought. The initiation of senescence showed by the decline in NDVI, coincided with low precipitation and high evaporative demand (Fig. A1.3 of supplementary results). Leaf fall would then be associated with depleting water levels stored in trees as observed in previous studies (Borchert, 1994; Reich and Borchert, 1984). Substantial rainfall events were observed during the latter part of the 2016 growing seasons. These events lead to high soil water moisture levels and likely delayed leaf drop (Whigham et al. 1990).

2.4.2 Seasonal Carbon Balance Patterns

The impact of drought on carbon fluxes was substantial. Decreases in precipitation during the 2014 and 2015 drought months were accompanied reductions in GPP, NEE, and Reco. Low drought productivity suggests that precipitation accumulated before intra-seasonal drought events did not provide sufficient moisture (soil or atmospheric) to maintain peak productivity levels over the drought periods. Late dry-season periods following drought years acted as mean carbon sources. These episodes may demarcate the limits of drought-adapted vegetation, perhaps due to depletion of moisture reserves in plant tissue and soil layers. However, it's important to note that this ecosystem still acted as a mean carbon sink, even when confronted with severe drought (Fig. 2.7a). Our study suggests that this secondary tropical dry forest was sensitive to precipitation anomalies, particularly during El Niño severe drought events.

The first precipitation events that marked the end of the dry season were followed by a sudden emission of carbon dioxide through the four-year period (Fig. 2.8b), indicating that the onset of respiration is dependent on water dynamics. The wetting of dry soils and the subsequent pulse of CO2

release and nitrogen mineralization is known as the 'Birch Effect' (Birch, 1958), which was observed interannually at the ecosystem level through eddy covariance methods in this study. The magnitude of the precipitation-induced carbon pulse is dependent on the amount of stored carbon in the forest soils as well as the severity of the dry season (Jarvis, 2007). The observed pulse sizes could indicate a potential reduction in carbon pool size over drought years (2014-2015) relative to a 'normal' year (2013), possibly due to reduced litterfall for decomposition through the previous drought-afflicted growing season (Fig. 2.6a). The 'Birch Effect' has been recently observed in another tropical dry forest site in Guanacaste, however on a smaller spatial scale using simulated precipitation and chamber-based measurements (Waring, 2016).

The results of our study fit well into the body of research on how drought affects the carbon fluxes of other tropical ecosystems. Hutyra et al. (2007) performed a similar four-year study in tropical rainforest (Tapajos National Forest, Para, Brazil), examining the controls of CO2 exchange and the possible effects of water limitation. Tapajos National Forest is classified as primary rain forest, with distinct seasonal meteorology including an approximate five-month dry season (July to September). However, dry season in the Tapajos rainforest still receives an order of magnitude more seasonal precipitation than our study site (~300-400 mm vs. ~20-30 mm).

The seasonal patterns and magnitudes of carbon fluxes from tropical dry and rainforest overlap and diverge in some aspects. The severity TDF dry season is reflected in our site by the progressive decline of respiration and GPP throughout the dry season (Fig. 2.6). NEE remained negative during the dry season for non-drought years and acted as a carbon sink, possibly due to the presence of evergreen trees with deep root systems. However, NEE tapers off with progress into the end of the dry season, switching to a carbon source at the end of the season. In contrast, rainforests have been shown to sustain high levels of productivity during its dry season with highest uptake values occurring during its driest period, coinciding with peak levels of PAR (Goulden et al., 2004; Huete et al., 2006). Light has been shown to be a consistent control of rainforest fluxes, resulting in increases in carbon sequestration during seasonal drought (Bonal et al., 2016). This is a notable difference from tropical dry forest productivity, which is largely controlled by seasonally dictated water availability. Our studied TDF was also found to have higher peak rates of GPP (> 13 μmol m-2s-1) than the Tapajos rain forest (~ 8 μmol m-2s-1) during its wet season (Hutyra et al. 2007).

Respiration rates of rainforest have been found to decrease during the dry season, attributed to the drying of surface litter. Thus, the aridity of the dry season in rainforest may be sufficient to suppress respiration, but insufficient to inhibit productivity. The net effect is a negative NEE through

the dry season, implying that it is a carbon sink during this phenologic period (Hutyra et al., 2007). During the wet season, both rain and dry forest (for non-drought years) follow a similar hill-shaped pattern of productivity where GPP increases at the onset of the rains, peaks in mid-season, then declines for the rest of the season. This pattern and magnitudes of respiration agree with a study of similar timescale on a tropical dry forest site in northwest Mexico, where pulses of CO2 were observed at the onset of the growing seasons (Verduzco et al., 2015). Tropical savanna, while much less dense in woody plants, has shown similar responses of ecosystem respiration to drought (Kutsch et al., 2008).

2.4.3 Controls on Gross Primary Production

The relative importance analysis was used to discern primary factors affecting carbon fluxes in TDF. A previous study by Becknell et al. (2012) showed precipitation to account for 55% of the variation in biomass among mature TDF sites. Other analyses into the interrelations of environmental conditions showed water balance depended on soil moisture availability, atmospheric evaporative demand, and the transpiration capacity of the tree (Reich and Borchert, 1982). The interplay of environmental parameters makes controls difficult to identify individually. The 2013 and 2016 seasons showed parallel drivers (LE and VPD) accounting for the majority of GPP variability. This indicates atmospheric evaporation demand as the principal controlling factor of productivity and water balance status during these seasons. Conversely, focus on the drought events of 2014 and 2015 show a shift in importance towards soil water moisture. Latent heat flux, representing the evaporative demand, still had noticeable contributions during drought periods. Assuming active regulation by vegetation to minimize water loss through evaporation during water scarcity (Borchert, 1994; Reich and Borchert, 1988; Reich, 1995; Sobrado, 1997), the presence of LE as a governing factor during drought may represent the minimum evaporative regulation demand. The high relative importance of VWC across both drought periods could point towards a common regulation mechanism and strategy in response to drought.

Whole season analysis of 2014 and 2015 drought years showed similar results to non-drought years, where the interplay of a suite of environmental variables informed GPP patterns. The main difference in parameter importance was an increasing importance of soil moisture during drought. The shifting in variable importance about ecosystem productivity (from soil water moisture during droughts to evaporative demands during non-drought periods) demonstrates the ability of this TDF to adjust to limited water resources. These observations align with functional convergence theory

(Bloom et al., 1985; Field, 1991; Mooney and Glumon, 1979, 1982) which states that investment on CO2 fixation will vary with resource availability, resulting in productivity being curtailed when faced with limiting resource availability that prevents utilization of additional capacity.

2.5 Conclusions

This study assessed the effect of drought on phenology and carbon dynamics. Our results show significant changes in phenology closely linked to seasonal water availability patterns. Water limitations had important effects on start of season, drought recovery, and senescence. Water status should not be interpreted as a cause to phenology, but rather an alteration to the timing of the progression between phenologic cycles. Forest carbon dynamics were also affected by water scarcity and drought severity. Reductions in seasonal productivity were observed during both drought years. The 2014 season showed post-drought recovery levels comparable to non-drought states that point to a notable drought resilience capacity. However, the severity of the 2015 drought did not allow in-season recovery. Instead, the recovery was observed during the 2016 season, where we observed higher productivity and an extended phenologic cycle. Alterations to phenology and forest productivity appear to be important drought coping strategies for tropical dry forests. The magnitude of the fluxes and the duration of phases can be readily applied toward refinement of larger scale flux estimates as well as vegetation model parametrization and validation.

Acknowledgements: This research and ideas was supported by the Inter-American Institute for Global Chance Research (IAI) CRN3-025, which is supported by the National Science Foundation of the United States (Grant GEO-1128040). Additional support was provided by the National Science and Engineering Research Council of Canada (NSERC-Discovery Grant Program), and IBM Alberta Center for Advance. Thanks to Peter Carlson, Ana Cristina Castro, and Jose Antonio Guzman for their technical and logistical support. We thank Roger Blanco and Maria Marta Chaverria Daiz, and the rest of the Area de Conservacion Guanacaste (ACG) personnel for extensive field support and knowledge.

2.6 References

Allen, K., Dupuy, J.M., Gei, M.G., Hulshof, C., Medvigy, D., Pizano, C., Salgado-Negret, B., Smith, C.M., Trierweiler, A., Van Bloem, S.J. and Waring, B.G., 2017. Will seasonally dry tropical forests be sensitive or resistant to future changes in rainfall regimes?. Environmental Research Letters, 12(2), p.023001.

Aubinet, M., Grelle, A., Ibrom, A., Rannik, Ü., Moncrieff, J., Foken, T., Kowalski, A.S., Martin, P.H., Berbigier, P., Bernhofer, C. and Clement, R., 1999. Estimates of the annual net carbon and water exchange of forests: the EUROFLUX methodology. Advances in ecological research, 30, pp.113-175.

Baldocchi, D.D., Hincks, B.B. and Meyers, T.P., 1988. Measuring biosphere-atmosphere exchanges of biologically related gases with micrometeorological methods. Ecology, 69(5), pp.1331-1340.

Baldocchi, D., 1997. Measuring and modelling carbon dioxide and water vapour exchange over a temperate broad-leaved forest during the 1995 summer drought. Plant, Cell & Environment, 20(9), pp.1108-1122.

Balvanera, P., Castillo, A. and MartÍnez-Harms, M.J., 2011. Ecosystem services in seasonally dry tropical forests. In Seasonally Dry Tropical Forests (pp. 259-277). Island Press/Center for Resource Economics.

Becknell, J.M., Kucek, L.K. and Powers, J.S., 2012. Aboveground biomass in mature and secondary seasonally dry tropical forests: A literature review and global synthesis. Forest Ecology and Management, 276, pp.88-95.

Birch, H.F., 1958. The effect of soil drying on humus decomposition and nitrogen availability. Plant and soil, 10(1), pp.9-31.

Bloom, A.J., Chapin III, F.S. and Mooney, H.A., 1985. Resource limitation in plants-an economic analogy. Annual review of Ecology and Systematics, 16(1), pp.363-392.

Bonal, D., Burban, B., Stahl, C., Wagner, F., & Hérault, B. 2016. The response of tropical rainforests to drought—lessons from recent research and future prospects. Annals of forest science, 73(1), pp.27-44.

Borchert, R., 1994. Soil and stem water storage determine phenology and distribution of tropical dry forest trees. Ecology, 75(5), pp.1437-1449.

Cao, S. and Sanchez-Azofeifa, A., 2017. Modeling seasonal surface temperature variations in secondary tropical dry forests. International Journal of Applied Earth Observation and Geoinformation, 62, pp.122-134.

Castillo, A., Magaña, A., Pujadas, A., Martínez, L. and Godínez, C., 2005. Understanding the interaction of rural people with ecosystems: a case study in a tropical dry forest of Mexico. Ecosystems, 8(6), pp.630-643.

Chadwick, R., Good, P., Martin, G. and Rowell, D.P., 2016. Large rainfall changes consistently projected over substantial areas of tropical land. Nature Climate Change, 6(2), p.177.

Chevan, A. and Sutherland, M., 1991. Hierarchical partitioning. The American Statistician, 45(2), pp.90-96.

Daubenmire, R., 1972. Phenology and other characteristics of tropical semi-deciduous forest in north-western Costa Rica. The Journal of Ecology, pp.147-170.

Eamus, D. and Prior, L., 2001. Ecophysiology of trees of seasonally dry tropics: comparisons among phenologies. Advances in Ecological Research, 32, pp.113-197.

Fajardo, L., Gonzalez, V., Nassar, J.M., Lacabana, P., Portillo, Q., Carlos, A., Carrasquel, F. and Rodriguez, J.P., 2005. Tropical dry forests of Venezuela: characterization and current

conservation status. Biotropica, 37(4), pp.531-546.

Field, C.B., 1991. Ecological scaling of carbon gain to stress and resource. In Response of plants to multiple stresses (pp. 35-65). Academic Press San Diego.

Genizi, A., 1993. Decomposition of R 2 in multiple regression with correlated regressors. Statistica Sinica, pp.407-420.

Gillespie, T.W., Grijalva, A. and Farris, C.N., 2000. Diversity, composition, and structure of tropical dry forests in Central America. Plant ecology, 147(1), pp.37-47.

Goulden, M. L., Miller, S. D., Da Rocha, H. R., Menton, M. C., de Freitas, H. C., & de Sousa, C. A. D. 2004. Diel and seasonal patterns of tropical forest CO2 exchange. Ecological Applications, 14(sp4), pp42-54.

Gromping U., 2006. relaimpo: Relative Importance of Regressors in Linear Models. R package version 1.1-1.

Hanan, N.P., Burba, G., Verma, S.B., Berry, J.A., Suyker, A. and Walter-Shea, E.A., 2002. Inversion of net ecosystem CO_2 flux measurements for estimation of canopy PAR absorption. Global Change Biology, 8(6), pp.563-574.

Hanson, P.J., Amthor, J.S., Wullschleger, S.D., Wilson, K.B., Grant, R.F., Hartley, A., Hui, D., Hunt Jr, E.R., Johnson, D.W., Kimball, J.S. and King, A.W., 2004. Carbon and water cycle simulations for an upland oak forest using 13 stand-level models: intermodel comparisons and evaluations against independent measurements. Ecol. Monogr, 74, pp.443-489.

Huemmrich, K.F., Black, T.A., Jarvis, P.G., McCaughey, J.H. and Hall, F.G., 1999. High temporal resolution NDVI phenology from micrometeorological radiation sensors. Journal of Geophysical Research: Atmospheres, 104(D22), pp.27935-27944.

Huete, A. R., Didan, K., Shimabukuro, Y. E., Ratana, P., Saleska, S. R., Hutyra, L. R., ... & Myneni,

R. 2006. Amazon rainforests green-up with sunlight in dry season. Geophysical research letters, 33(6).

Hutyra, L.R., Munger, J.W., Saleska, S.R., Gottlieb, E., Daube, B.C., Dunn, A.L., Amaral, D.F., De Camargo, P.B. and Wofsy, S.C., 2007. Seasonal controls on the exchange of carbon and water in an Amazonian rain forest. Journal of Geophysical Research: Biogeosciences, 112(G3).

Hutyra, L.R., Munger, J.W., Hammond-Pyle, E., Saleska, S.R., Restrepo-Coupe, N., Daube, B.C., de Camargo, P.B. and Wofsy, S.C., 2008. Resolving systematic errors in estimates of net ecosystem exchange of CO 2 and ecosystem respiration in a tropical forest biome. agricultural and forest meteorology, 148(8), pp.1266-1279.

Janzen, D.H., 1988. Tropical dry forests. Biodiversity, p.538.

Janzen, D.H., 2000. Costa Rica's Area de Conservación Guanacaste: a long march to survival through non-damaging biodevelopment. Biodiversity, 1(2), pp.7-20.

Jarvis, P., Rey, A., Petsikos, C., Wingate, L., Rayment, M., Pereira, J., Banza, J., David, J., Miglietta, F., Borghetti, M. and Manca, G., 2007. Drying and wetting of Mediterranean soils stimulates decomposition and carbon dioxide emission: the “Birch effect”. Tree physiology, 27(7), pp.929-940.

Johnson, J.W., Lebreton J.M. 2004. History and Use of Relative Importance Indices in Organizational Research. Organizational Research Methods, 7, pp.238–257.

Jung, M., Reichstein, M. and Bondeau, A., 2009. Towards global empirical upscaling of FLUXNET eddy covariance observations: validation of a model tree ensemble approach using a biosphere model. Biogeosciences, 6(10), pp.2001-2013.

Kumar, J., Hoffman, F.M., Hargrove, W.W. and Collier, N., 2016. Understanding the representativeness of FLUXNET for upscaling carbon flux from eddy covariance

measurements. Earth Syst. Sci. Data Discuss, pp.1-25.

Kutsch, W. L., Hanan, N., Scholes, R. J., McHugh, I., Kubheka, W., Eckhardt, H., & Williams, C. 2008. Response of carbon fluxes to water relations in a savanna ecosystem in South Africa. Biogeosciences Discussions, 5(3), pp.2197-2235.

Li, W., Cao, S., Campos-Vargas, C. and Sanchez-Azofeifa, A., 2017. Identifying tropical dry forests extent and succession via the use of machine learning techniques. International Journal of Applied Earth Observation and Geoinformation, 63, pp.196-205.

Lieberman, D., 1982. Seasonality and phenology in a dry tropical forest in Ghana. The Journal of Ecology, pp.791-806.

Lindeman, R.H. and Lindeman, R.H., 1980. Introduction to bivariate and multivariate analysis (No. 04; QA278, L553.).

Maass, J.M., Balvanera, P., Castillo, A., Daily, G.C., Mooney, H.A., Ehrlich, P., Quesada, M., Miranda, A., Jaramillo, V.J., García-Oliva, F. and Martínez-Yrizar, A., 2005. Ecosystem services of tropical dry forests: insights from longterm ecological and social research on the Pacific Coast of Mexico. Ecology and society: a journal of integrative science for resilience and sustainability, 10(1), pp.1-23.

Malhi, Y., Roberts, J.T., Betts, R.A., Killeen, T.J., Li, W. and Nobre, C.A., 2008. Climate change, deforestation, and the fate of the Amazon. science, 319(5860), pp.169-172.

Malhi, Y., 2012. The productivity, metabolism and carbon cycle of tropical forest vegetation. Journal of Ecology, 100(1), pp.65-75.

Moncrieff, J.B., Massheder, J.M., De Bruin, H., Elbers, J., Friborg, T., Heusinkveld, B., Kabat, P., Scott, S., Soegaard, H. and Verhoef, A., 1997. A system to measure surface fluxes of momentum, sensible heat, water vapour and carbon dioxide. Journal of Hydrology, 188, pp.589-611.

Mooney, H.A. and Gulmon, S.L., 1979. Environmental and evolutionary constraints on the photosynthetic characteristics of higher plants. In Topics in plant population biology (pp. 316-337). Macmillan Education UK.

Mooney, H.A. and Gulmon, S.L., 1982. Constraints on leaf structure and function in reference to herbivory. BioScience, 32(3), pp.198-206.

Murphy, P.G. and Lugo, A.E., 1986. Ecology of tropical dry forest. Annual review of ecology and systematics, 17(1), pp.67-88.

Papale, D. and Valentini, R., 2003. A new assessment of European forests carbon exchanges by eddy fluxes and artificial neural network spatialization. Global Change Biology, 9(4), pp.525-535.

Quesada, M., Sanchez-Azofeifa, G.A., Alvarez-Anorve, M., Stoner, K.E., Avila-Cabadilla, L., Calvo-Alvarado, J., Castillo, A., Espírito-Santo, M.M., Fagundes, M., Fernandes, G.W. and Gamon, J., 2009. Succession and management of tropical dry forests in the Americas: Review and new perspectives. Forest Ecology and Management, 258(6), pp.1014-1024.

Reichstein, M., Tenhunen, J.D., Roupsard, O., Ourcival, J.M., Rambal, S., Dore, S. and Valentini, R., 2002. Ecosystem respiration in two Mediterranean evergreen Holm Oak forests: drought effects and decomposition dynamics. Functional Ecology, 16(1), pp.27-39.

Reichstein, M., Tenhunen, J., Roupsard, O., Ourcival, J.M., Rambal, S., Miglietta, F., Peressotti, A., Pecchiari, M., Tirone, G. and Valentini, R., 2003. Inverse modeling of seasonal drought effects on canopy CO_2/H_2O exchange in three Mediterranean ecosystems. Journal of Geophysical Research: Atmospheres, 108(D23).

Reichstein, M., Falge, E., Baldocchi, D., Papale, D., Aubinet, M., Berbigier, P., Bernhofer, C., Buchmann, N., Gilmanov, T., Granier, A. and Grünwald, T., 2005. On the separation of net ecosystem exchange into assimilation and ecosystem respiration: review and improved algorithm. Global Change Biology, 11(9), pp.1424-1439.

Reich, P.B. and Borchert, R., 1982. Phenology and ecophysiology of the tropical tree, Tabebuia neochrysantha (Bignoniaceae). Ecology, 63(2), pp.294-299.

Reich, P.B. and Borchert, R., 1984. Water stress and tree phenology in a tropical dry forest in the lowlands of Costa Rica. The Journal of Ecology, pp.61-74.

Reich, P.B. and Borchert, R., 1988. Changes with leaf age in stomatal function and water status of several tropical tree species. Biotropica, pp.60-69.

Reich, P.B., 1995. Phenology of tropical forests: patterns, causes, and consequences. Canadian Journal of Botany, 73(2), pp.164-174.

Reichstein, M., Falge, E., Baldocchi, D., Papale, D., Aubinet, M., Berbigier, P., Bernhofer, C., Buchmann, N., Gilmanov, T., Granier, A. and Grünwald, T., 2005. On the separation of net ecosystem exchange into assimilation and ecosystem respiration: review and improved algorithm. Global Change Biology, 11(9), pp.1424-1439.

Sánchez-Azofeifa, G.A., Quesada, M., Rodriguez, J.P., Nassar, J.M., Stoner, K.E., Castillo, A., Garvin, T., Zent, E.L., Calvo-Alvarado, J.C., Kalacska, M.E. and Fajardo, L., 2005. Research priorities for neotropical dry forests. Biotropica, 37(4), pp.477-485.

Sobrado, M.A., 1997. Embolism vulnerability in drought-deciduous and evergreen species of a tropical dry forest. Acta Oecologica, 18(4), pp.383-391.

Verduzco, V. S., Garatuza-Payán, J., Yépez, E. A., Watts, C. J., Rodríguez, J. C., Robles-Morua, A., & Vivoni, E. R. 2015. Variations of net ecosystem production due to seasonal precipitation differences in a tropical dry forest of northwest Mexico. Journal of Geophysical Research: Biogeosciences, 120(10), pp2081-2094.

Waring, B.G. and Powers, J.S., 2016. Unraveling the mechanisms underlying pulse dynamics of soil respiration in tropical dry forests. Environmental Research Letters, 11(10), p.105005.

Whigham, D.F., Zugasty, T., Cabrera, C., O'neill, J. and Ley, E., 1990. The effect of annual variation in precipitation on growth and litter production in a tropical dry forest in the Yucatan of Mexico. Tropical Ecology, 31(2), pp.23-34.

Zelazowski, P., Malhi, Y., Huntingford, C., Sitch, S. and Fisher, J.B., 2011. Changes in the potential distribution of humid tropical forests on a warmer planet. Philosophical Transactions of the Royal Society of London A: Mathematical, Physical and Engineering Sciences, 369(1934), pp.137-160.

Zuber, V. and Strimmer, K., 2010. High-dimensional regression and variable selection using CAR scores. arXiv preprint arXiv:1007.5516.

2.7 Figures:

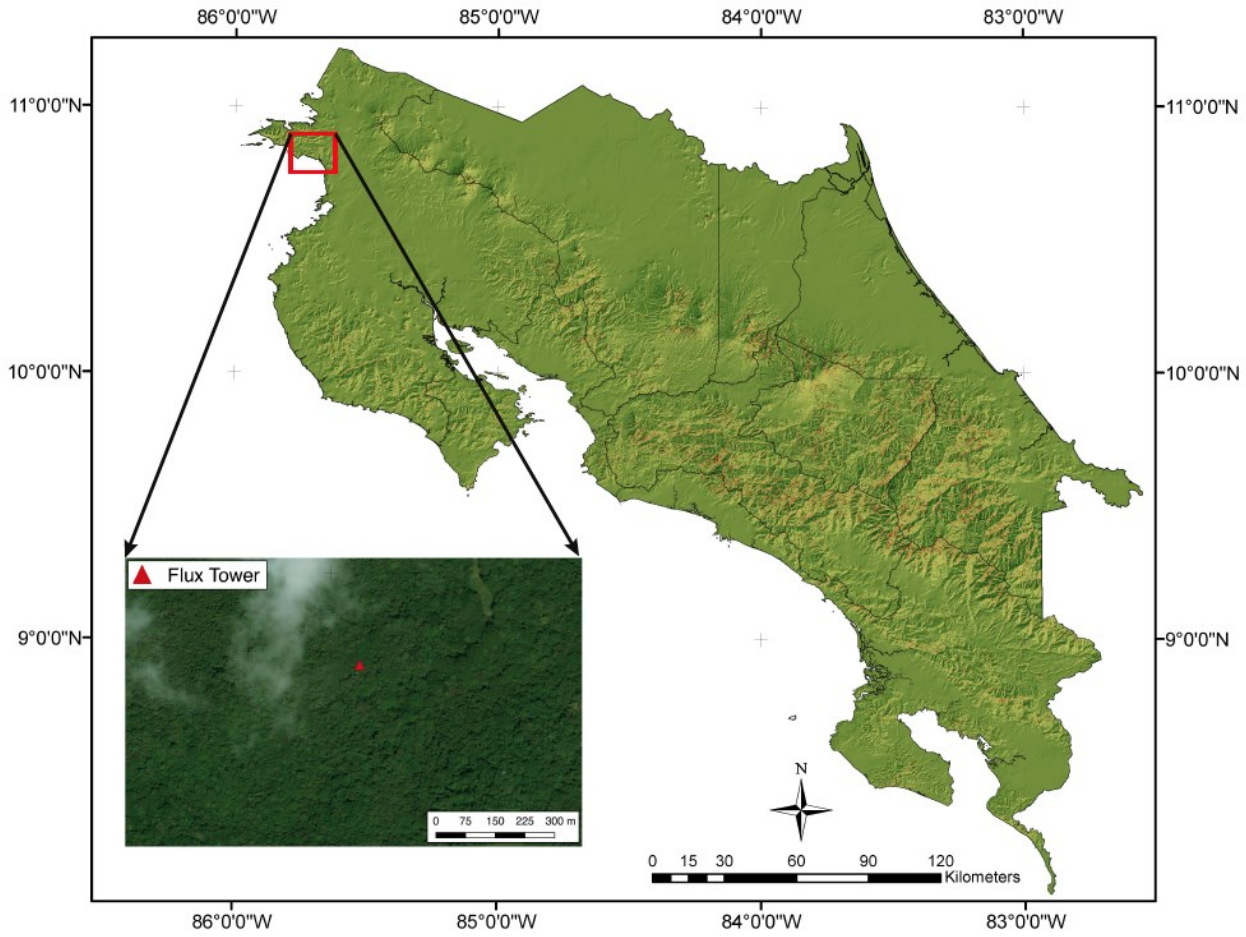

Figure 2.1: Location of Santa Rosa National Park and Environmental Monitoring Super Site. Red triangle shows the location of the flux tower within a secondary tropical dry forest (TDF). Tower contains eddy covariance system, meteorological sensors, and proximal remote sensing sensors.

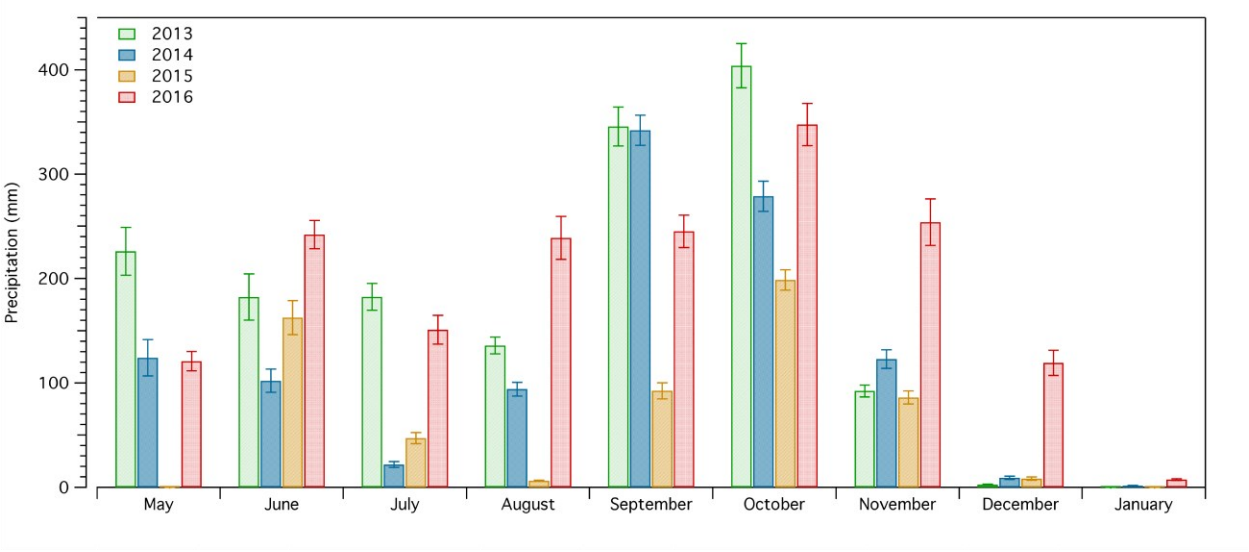

Figure 2.2: Monthly precipitation for 2013, 2014, 2015, and 2016 growing seasons.

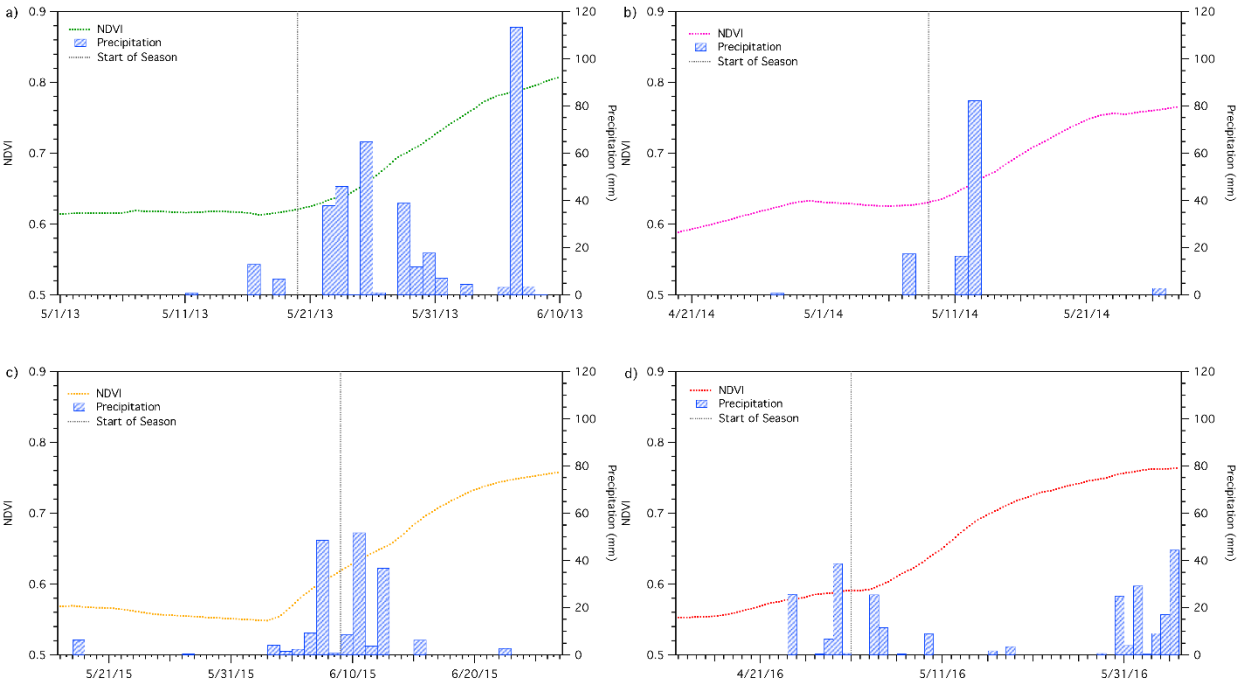

Figure 2.3: Pre-season precipitation patterns and NDVI changes for the (a) 2013 season, (b) 2014 season, (c) 2015 season, and (d) 2016 season. NDVI and precipitation patterns are shown for periods leading up to the start of season (gray line) and into green-up.

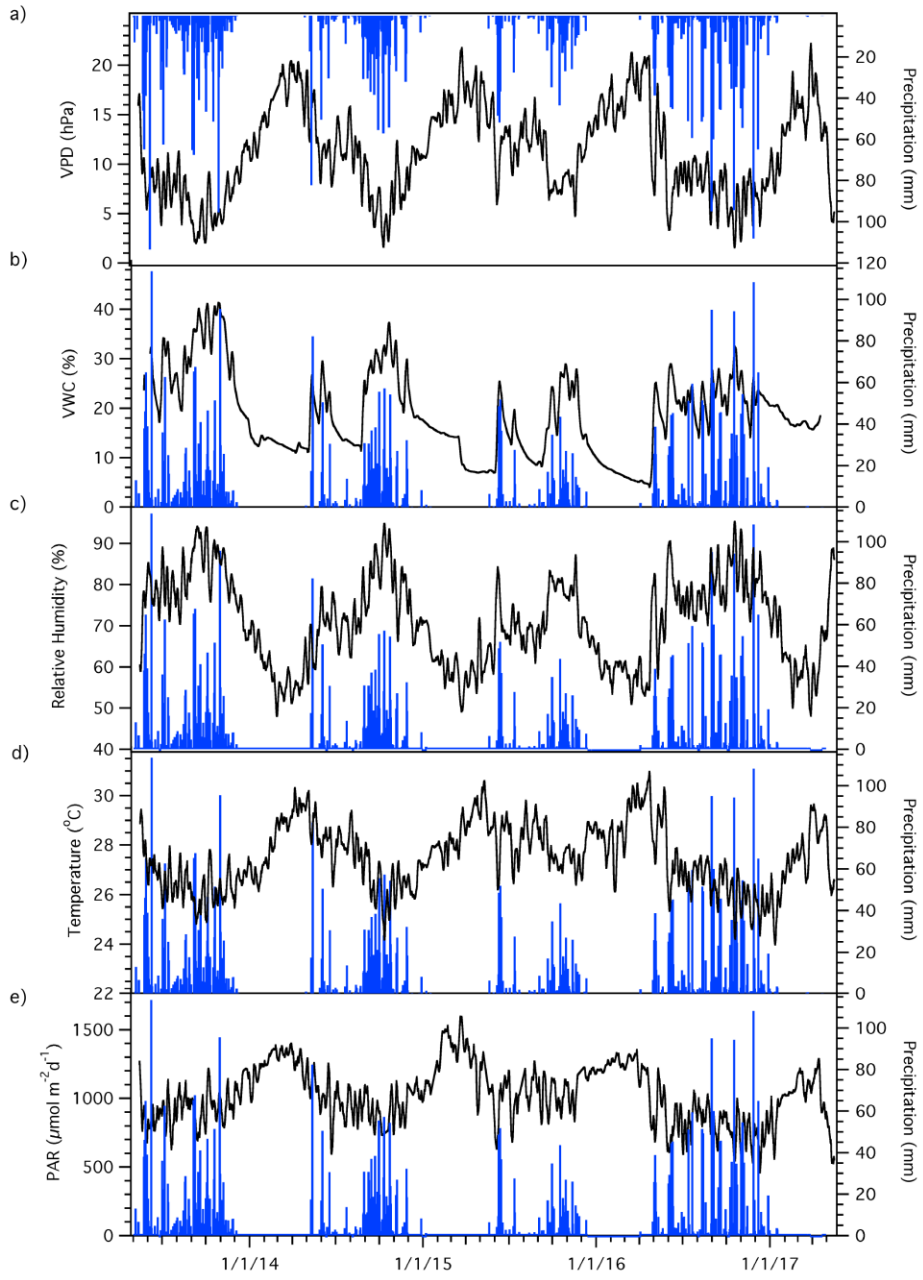

Figure 2.4: Time series of mean daytime a) VPD, b) VWC, c) RH, d) T, and e) PAR, with daily cumulative precipitation.

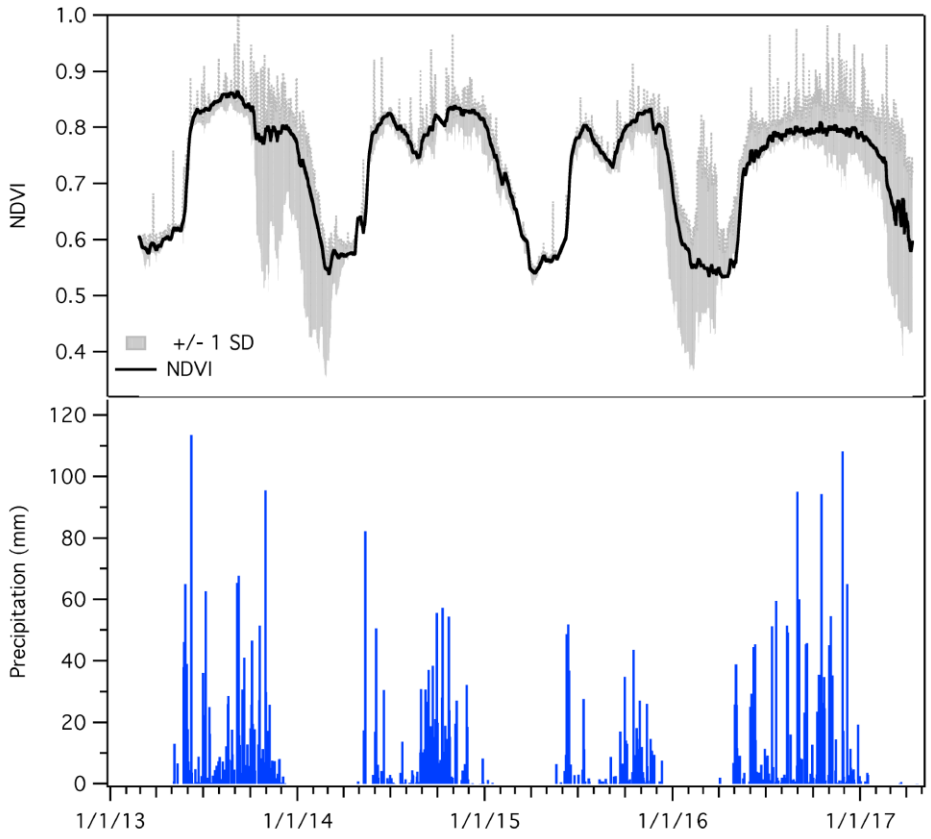

Figure 2.5: Time series the a) phenology cycle derived from mean daily NDVI values and b) seasonal precipitation (mm) throughout the four-year period. Precipitation data were collected manually and corroborated with electronic tipping bucket precipitation measurements.

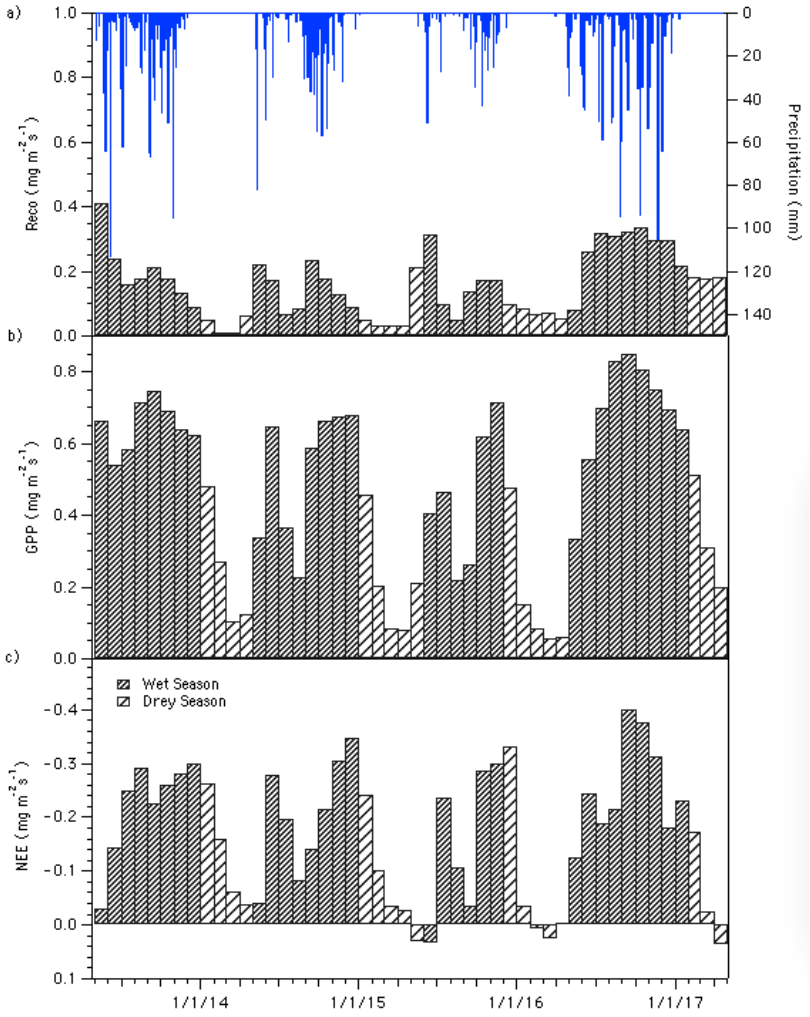

Figure 2.6: Monthly time series of average (a) R_{eco} (mg m^{-2} s^{-1}), (b) GPP (mg m^{-2} s^{-1}), and (c) NEE (mg m^{-2} s^{-1}). Shaded patterns indicate wet or dry season. Precipitation histogram (mm) is shown in blue.

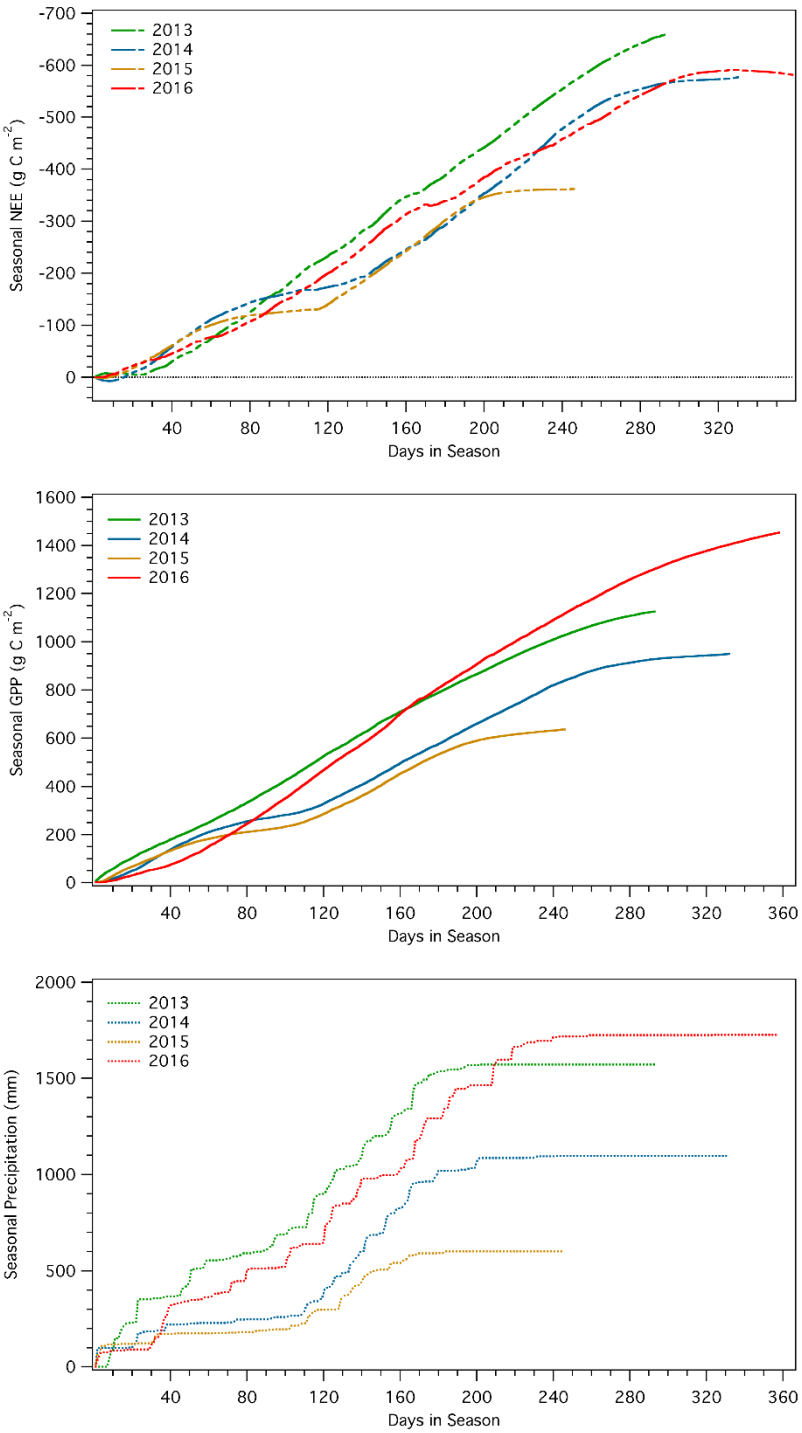

Figure 2.7: Time series of (a) seasonal cumulative net ecosystem CO_2 exchange (NEE g C m^{-2}), (b) seasonal cumulative gross primary productivity (GPP g C m^{-2}), and (c) cumulative precipitation (mm), for 2013, 2014, 2015, and 2016 seasons.

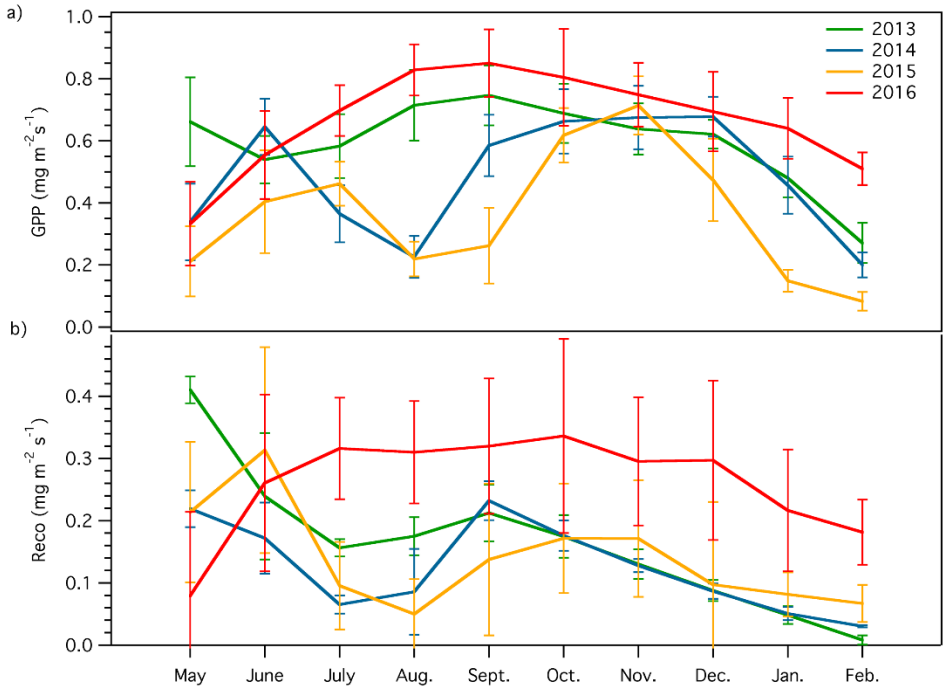

Figure 2.8: Monthly mean seasonal (2013-2016) comparison of (a) gross primary productivity (GPP mg m^{-2} s^{-1}), and (b) ecosystem respiration (R_{eco} mg m^{-2} s^{-1}).

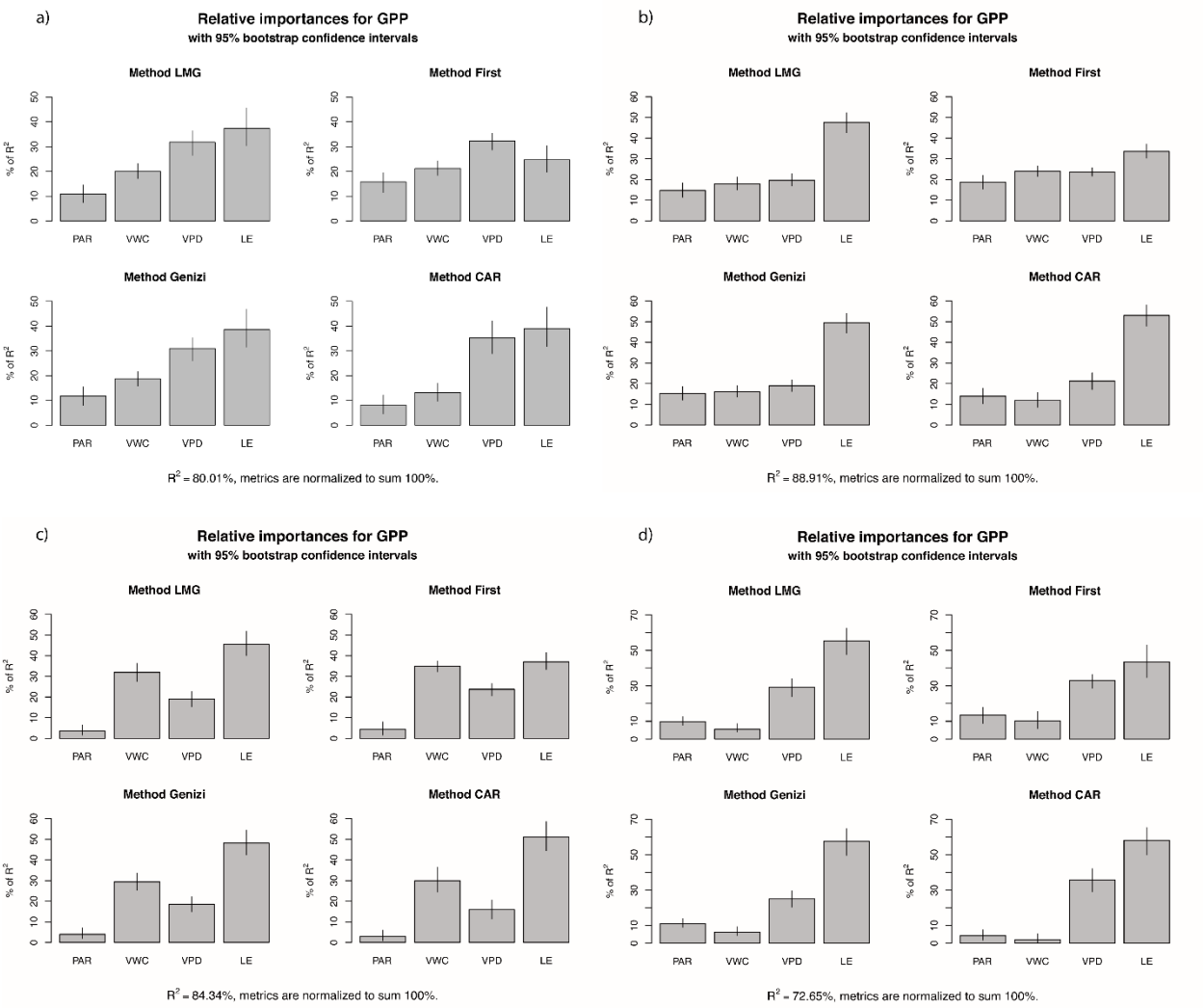

Figure 2.9: Relative importance analysis of environmental parameters PAR, VWC, VPD, and LE about GPP for (a) 2013, (b) 2014, (c) 2015, and (d) 2016 growing seasons. Four relative importance models were used including LMG, First, Genizi, and CAR. GLM accounted for 80.01%, 89.91%, 84.34%, and 72.65% of 2013, 2014, 2015, and 2016 GPP variability, respectively.

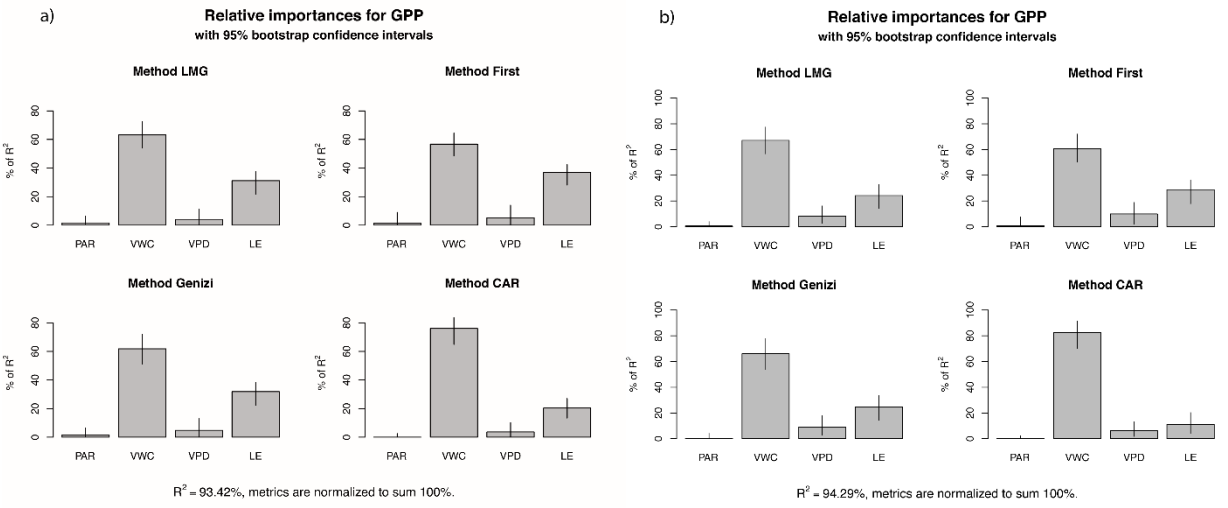

Figure 2.10: Relative importance analysis of GLM GPP = PAR + VWC + VPD + LE for drought event in (a) 2014 and (b) 2015. Four relative importance models were used including LMG, First, Genizi, and CAR. GLM accounted for 93.42% and 94.29% of 2014 and 2015 GPP variability, respectively.

Table 2.1: Precipitation totals (mm) grouped by phenologic stage.

	2013	**2014**	**2015**	**2016**
Green-up	531.1	101.7	159.5	221.4
Maturity	1219.8	993.0	433.0	1504.3
Senescence	0.0	1.6	8.3	1.0
Seasonal Total	1570.9	1096.0	600.8	1726.6
Pre-Season Total	20.5	18.2	74.0	72.6

Table 2.2: Summary of seasonal maximums, minimums, mean, and standard deviation values of meteorological parameters PAR, VWC, VPD, RH, and T.

	2013				2014			
	Max.	**Min.**	**Mean.**	**SD**	**Max.**	**Min.**	**Mean.**	**SD**
PAR (µmol m^{-2} s^{-1})	1387.43	283.67	996.83	239.94	1613.01	367.42	1060.75	266.22
VWC (%)	42.87	10.33	25.76	9.23	40.42	7.4	19.65	7.1
VPD (hPa)	28.22	0.65	8.58	4.44	22.17	0.42	11.22	4.55
RH (%)	97.84	38.08	76.84	11.14	98.57	48.69	70.82	10.73
Temp (ºC)	30.59	22.99	26.65	1.17	29.86	23.3	27.42	1.31

	2015				2016			
	Max.	**Min.**	**Mean.**	**SD**	**Max.**	**Min.**	**Mean.**	**SD**
PAR (µmol m^{-2} s^{-1})	1390.75	445.69	1082.64	192.94	1276.25	158.75	877.88	235.24
VWC (%)	31.65	7.1	15.12	5.48	35.45	13.54	20.76	4.17
VPD (hPa)	21.57	3.23	11.79	3.55	23.64	0.58	9.87	4.79
RH (%)	90.7	49.18	70.14	8.19	98.05	40.48	73.58	11.58
Temp (°C)	30.42	25.35	28.05	1.04	30.93	24.02	26.91	1.36

Table 2.3: Dates and changes (Δ) in green-up, maturity, senescence, and total season length in days using 2013 for length comparisons.

	2013	**2014**	**2015**	**2016**	**Δ (2013-2014)**	**Δ (2013-2015)**	**Δ (2013-2016)**
Start of Green-up	20-May	09-May	09-Jun	01-May	11	-20	19
Start of Maturity	10-Jun	28-May	27-Jun	06-Jun	13	-17	4
Start of Senescence	27-Dec	02-Jan	24-Nov	20-Jan	-6	33	-24
End of Season	03-Mar	06-Apr	09-Feb	23-Apr	-34	22	-51

Table 2.4: Length of each phenology stage (days) for each growth season within the four-year study period (2013-2016).

	2013	**2014**	**2015**	**2016**
Green-up	21	19	18	36
Maturity	200	219	150	228
Senescence	66	94	77	94
Total Season	287	332	245	358

CHAPTER 3 – Testing of Automated Photochemical Reflectance Index Sensors as Proxy Measurements of Light Use Efficiency in an Aspen Forest

Abstract

Commercially available autonomous photochemical reflectance index (PRI) sensors are a new development in the remote sensing field that offer novel opportunities for a deeper exploration of vegetation physiology dynamics. In this study, we evaluated the reliability of autonomous PRI sensors (SRS-PRI) developed by METER Group Inc. as proxies of light use efficiency (LUE) in an aspen (*Populus tremuloides*) forest stand. Before comparisons between PRI and LUE measurements were made, the optical SRS-PRI sensor pairs required calibrations to resolve diurnal and seasonal patterns properly. An offline diurnal calibration procedure was shown to account for variable sky conditions and diurnal illumination changes affecting sensor response. Eddy covariance measurements provided seasonal gross primary productivity (GPP) measures as well as apparent canopy quantum yield dynamics (α). LUE was derived from the ratio of GPP to absorbed photosynthetically active radiation (APAR). Corrected PRI values were derived after diurnal and midday cross-calibration of the sensor's 532 nm and 570 nm fore-optics, and closely related to both LUE ($R^2 = 0.62$, $p < 0.05$) and α ($R^2 = 0.72$, $p < 0.05$). A LUE model derived from corrected PRI values showed good correlation to measured GPP ($R^2 = 0.77$, $p < 0.05$), with an accuracy comparable to results obtained from an α driven LUE model ($R^2 = 0.79$, $p < 0.05$). The automated PRI sensors proved to be suitable proxies of light use efficiency. The onset of continuous PRI sensors signifies new opportunities for explicitly examining the cause of changing PRI, LUE, and productivity over time and space. As such, this technology represents great value for the flux, remote sensing and modeling community.

Keywords: remote sensing; PRI; LUE model; eddy covariance

3.1. Introduction

The light use efficiency (LUE) model [1,2] has provided an avenue for quantifying the terrestrial carbon cycle using remote sensing data [3,4]. The LUE model can be conceptualized as being driven by structural and pigment pool changes in vegetation and, secondly, by the physiological status described by the vegetation's photosynthetic process [5]. The structural component is quantified by the amount of photosynthetically active radiation absorbed by the canopy (APAR); while the

physiological component is described as the efficiency by which the absorbed light, or light use efficiency (LUE), is used to fix carbon during a specific period. Much work has been done in displaying a relationship between optical remote sensing and the APAR term, although it is not without error and complexity [6–11]. However, as LUE variability can be driven by multiple individual and combined factors, the connection between efficiency and remote sensing signals have been harder to characterize, leading to considerable uncertainty in many ecosystems [12–14]. Some of the physiological effects on light use efficiency include changing climatic conditions, temperature, water availability, phenology, vegetation functional type, and vegetation species [15–22]. These complex interactions confound the parametrization of in LUE in global productivity models, and, as such, efforts continue towards the better accounting of efficiency changes that would, in turn, lead to more accurate CO_2 flux estimations.

Developments in proximal and spaceborne remote sensing have led to advances in estimating vegetation LUE at the leaf level, stand level, and whole ecosystem resolutions [14,23–25]. One of the main proposed tools to do so is through the use of the photochemical reflectance index (PRI). First developed in leaf level studies, this vegetation index has been shown to be a proxy of xanthophyll pigment activity and closely linked to photosystem II (PSII) photochemical efficiency [23,26,27]. During periods of light saturation and excess energy PSII centers remain in a reduced state, leaving them susceptible to photoinhibitory damage [28]. Non-photochemical quenching (NPQ) performed through the chemical transformation of carotenoid pigments that compose the xanthophyll cycle prevent damage to photosynthetic centers. More specifically, NPQ of excess light is done through the de-epoxidation of violaxanthin to the photoprotective pigment zeaxanthin, with antheraxanthin acting as a transitional pigment [28–30]. De-epoxidation provides a sink for excess energy and a method of light regulation that can be measured optically via the PRI [27,31,32]. PRI tracks short-term decreases in reflectance at 531nm that occur in response to increased zeaxanthin concentrations and shrinking chloroplast (associated with increased thylakoid pH) resulting from xanthophyll de-epoxidation [23,27]. The index uses reflectance at 570 nm (insensitive to NPQ) as a reference band.

Testing of PRI over seasonal timescales for foliar, canopy and ecosystem level scales has shown PRI to be a good indicator of physiological efficiency across different vegetation types and scales, however, with numerous temporal and spatial challenges [24]. Radiative transfer modeling studies have identified a number of confounding factors including leaf area distribution, soil type, and view and illumination angles affect the interpretation of PRI [33,34]. Additionally, in situ studies have shown a strong effect of chlorophyll/carotenoid ratios on seasonal PRI [24]. These changes in

pigment pool sizes can account for a significant proportion of seasonal PRI (constitutive) changes, compared to those driven by xanthophyll cycle activity (facultative changes), and lead to misrepresentations of the PRI-photosynthetic relationship [19,35–38]. As such, seasonal studies are needed to characterize the effects of vegetation structure changes and identify the facultative and constitutive components in PRI [39]. However, few long-term studies with the necessary dense time-series measurements over varying ecosystems exist, and some of these rely on satellite-based data with low temporal resolutions that do not allow the separation of facultative and constitutive effects. Perhaps for this reason, some comparisons of satellite-based PRI and LUE across ecosystems have resulted in contrasting PRI-LUE relationships for different ecosystems [40,41].

The lack of accessible and cost-effective data, available at meaningful temporal or spatial scales, has limited the testing of PRI functionality at ecosystem levels. For example, a 16-day MODIS composite lacks the temporal resolution to resolve short-term xanthophyll cycle changes. This has contributed to slow integration and comparison to micrometeorological data and ecosystem monitoring networks [42]. However, the recent availability of inexpensive PRI specific narrowband radiometers [43–45] has opened the possibility of attaining continuous PRI measurements at low cost. The high temporal resolution of automated optical sensor systems would allow improved accounting of physical and physiological variables affecting diurnal and seasonal PRI measurements and help interpret LUE changes over a phenological cycle. Additionally, continuous PRI measurements allow for their integration with eddy covariance flux measurements, which in turn provides additional ecophysiological validation for PRI as an LUE proxy at ecosystem scales.

For this study, we utilized newly commercially developed automated PRI spectral reflectance (SRS-PRI) radiometers and eddy covariance data to explore the LUE dynamics in a deciduous boreal forest. As such, the objectives of this paper are to (1) determine if automated SRS-PRI values can be used as a proxy of canopy light use efficiency and apparent canopy quantum yield over an aspen forest and (2) to explore how continuous PRI measurements can be leveraged to better inform ecosystem scale LUE models.

3.2. Materials and Methods

3.2.1. Study Area

The study was conducted at the Peace River Environmental Monitoring Super Site (PR-EMSS) within the Ecosystem Management Emulating Natural Disturbance (EMEND) site, located

approximately 90 km northwest of Peace River, AB, Canada (Figure 3.1). This region is part of the Lower Foothills Natural Subregion [46]. The study plot, located at 56°44′38.10″ N, 118°20′38.08″ W, with an altitude of 867 m ASL, is characterized as an old growth stand of trembling aspen (*Populus tremuloides*). There are two vertical vegetation layers; the understory reaching a height of 3 m, while the overstory canopy growing to 12–15 m. Its topography is slightly sloping (<2%) in the west direction. The predominant wind direction is from the west. Mean annual air temperature is 0.6 °C and mean annual precipitation is 436.2 mm, with approximately 29% falling as snow [47]. Soils are primarily Orthic and Dark Gray Luvisols and have a depth of 1 m on average [48]. The study site has been monitored since 2013 with an eddy covariance system and meteorological station installed on a 30 m tower located at the eastern edge of the forest stand. Proximal remote sensing sensors, comprising of PRI and broadband spot radiometers mounted on the tower allowed the tracking of forest stand phenology, as well as monitoring the incoming and canopy reflected light. A wireless sensor network (WSN) continually measured the transmitted photosynthetic photon flux density (PPFD) within the canopy, providing continuous measurements of fraction of absorbed photosynthetically active radiation (fAPAR).

3.2.2. Reflectance Measurements and Vegetation Indices

3.2.2.1. Spectral Reflectance Sensors (SRS)

Spectral data was collected through the use of commercial automated SRS-PRI sensors with an Em50 datalogger (METER Group. Inc., Pullman, WA, USA). PRI sensors contain photodiodes with interference filters at selected peak wavelengths 532 ± 2 and 570 ± 2 nm with 10 nm full width half maximum (FWHM) bandwidths. Photodiode and filter construction was based on prototypes reviewed by Garity et al. [43]. Downward looking PRI pairs contain field stops, restricting the field of view (FOV) at 36°. Upward looking pairs contain Teflon cosine diffusers allowing near 180° FOV. They provide continuous irradiance measurements used to normalize radiance spectral responses measured through the downward looking sensor pair. Upwelling and downwelling PRI sensors were placed on a 25 m tower and positioned 10° off-nadir at an approximate distance of 10–12 m from the top of the canopy, representing a footprint of approximately 50 m^2 towards the eddy covariance area of influence.

Each sensor produced a radiance and irradiance output, for each waveband (532 nm and 570 nm) at 1-minute intervals throughout the 2015 season. Data points were filtered to remove precipitation events which caused significant signal noise attributed to water droplets accumulating on the flat Teflon cosine diffusers of the hemispherical sensor pair. Uncorrected reflectance at each waveband was expressed as the ratio of measured radiance (r) to irradiance (i) (Equation (1) and (2)) and used to calculate uncorrected PRI (Equation (3)):

$$\rho_{532} = \frac{r_{532}}{i_{532}} \quad (1)$$

$$\rho_{570} = \frac{r_{570}}{i_{570}} \quad (2)$$

$$\text{PRI} = \frac{\rho_{532} - \rho_{570}}{\rho_{532} + \rho_{570}} \quad (3)$$

where ρ represents reflectance at a specific wavelength. Calculated PRI values were averaged over 30 min to match eddy covariance binned measurements. PRI values were expressed as scaled PRI (sPRI) using the formula [49,50]:

$$\text{sPRI} = \frac{(1 + \text{PRI})}{2} \quad (4)$$

which transformed PRI values into a 0–1 range commonly used in remote sensing vegetation indices. Before and after field deployment, the sensors underwent a series of cross-calibration and sensor response validation experiments. Details of these experiments are outlined in Sections 2.2.2 and 2.2.3 below.

3.2.2.2. SRS-PRI Sensor Cross-Calibration

A cross-calibration procedure is required to account for differences in sensor response and fore-optics [51]. The cross-calibration process allows for the normalization of irradiance and radiance outputs under varying light conditions. Gamon et al. [44] outlined a procedure for both midday and diurnal cross-calibration, noting that diurnal calibrations best represent xanthophyll cycle epoxidation states. Due to the remoteness of our study site and the manual nature of cross-calibration, both the midday and diurnal cross-calibration procedures were done prior and subsequently to field deployment, following the general principles outlined by Gamon et al. [44].

SRS-PRI sensors were placed at the height of 30 cm over a 99% reflective white standard panel (Spectralon, Labsphere Inc., North Sutton, NH, USA), ensuring that the downward-looking sensor's

FOV covered the standard. The upward-looking sensor simultaneously monitored the sky's irradiance conditions. The sensor pair measured continuously over a 23-day period. A pyranometer (SP-110, Apogee Instruments Inc., Logan, UT, USA) logged on a wireless sensor node (ENV-LINK-MINI, LORD Microstrain® Sensing Systems, Williston, VT, USA) was used to monitor incident radiation, sampled at 1-minute intervals. This radiation data was used to characterize the various illumination conditions over the experimental period, which varied from overcast to clear and sunny conditions. A solar radiation calculator (SolRad), developed by the Washington State Department of Ecology, provided modeled global radiation on a horizontal surface using the Ryan-Stolzenbach model [52]. Percent illumination was derived by comparing modeled to measured radiation data throughout the experiment. The 23-day experimental period allowed us to capture a nearly complete spectrum of illumination conditions (15–100%) over a full set of diurnal solar elevations (0°–56°). Solar elevations, defined as the angle between the horizon and the sun, were determined using NOAA's solar position calculator (https://www.esrl.noaa.gov/gmd/grad/solcalc/).

Cross-calibration responses as a function of illumination were calculated for every 3° solar elevations bin throughout the diurnal range. Three-degree bins were chosen as they represented approximately 30 min time intervals during the morning and evening periods where solar elevation changed most rapidly. A set of cross-calibration functions were derived for each sensor waveband. Percent illumination and solar elevations were calculated for onsite data collected during the 2015 season. Cross-calibration ratios derived from the set of empirical calibration functions were used to calculate corrected reflectance ($\rho_{corrected}$) as follows:

$$\rho_{corrected} = \frac{\rho_{uncorrected}}{'Cross-calibration\ ratio'} = \frac{r_{target}/i_{sky}}{r_{standard}/i_{sky}} \quad (5)$$

where r_{target} represents radiance from the canopy, $r_{standard}$ represents radiance from the white standard, and i_{sky} represents irradiance from sky conditions. Midday cross-correlation functions were also derived for each sensor waveband and used to calculate midday corrected reflectance following Equation (5). Diurnal and midday corrected reflectance were used to calculated (diurnal and midday)

corrected PRI following Equation (3). Corrected PRI values were averaged over 30 min to match eddy covariance data.

3.2.2.3. Sensor Response Validation

A dual-channel field spectrometer (Unispec-DC, PP-Systems, Amesbury, MA, USA) was used to validate the spectral response of the SRS-PRI sensors independently. Additionally, diurnal spectrometer measurements were collected in concert with cross-calibration data to confirm the effect and accuracy of mid-day vs. diurnal cross-calibration efforts. The Unispec-DC is a high precision spectrometer able to provide simultaneous measurements of radiance and irradiance, has a spectral range of 310–1100 nm, and a 3.3 nm FWHM. The upwelling/radiance was collected using a 2 m fiber optic cable (600 µm HCS LOH, SMA-Custom Ferrule-100 mm, Uni-684, PP Systems) with a 9 mm FOV restrictor providing a modified FOV of 18°. For the downwelling/irradiance, a similar 2 m fiber optic cable was used (600 µm HCS LOH, SMA-Custom Ferrule-25 mm, Uni-686, PP Systems) with the addition of a cosine head (UNI435, PP Systems) allowing near 180° FOV.

Validation experiments consisted of the sampling the diurnal response of a ~1 m tall *Populus tremuloides* seedling stand, simultaneously, with the field spectrometer and SRS sensors, throughout a 5-day period. The spectrometer's radiance fore-optic and SRS-PRI field-of-view pair were placed at matching height (0.37 m) above the canopy, producing a target footprint of about 1.0 m^2. The SRS-PRI sensors log every minute continuously throughout the diurnal cycle; while the spectrometer measurements were collected every minute for 10 min on the hour throughout the diurnal cycle.

Spectrometer reflectance data was corrected using a 99% reflective white standard panel (Spectralon, Labsphere Inc.). Corrected reflectance was expressed as:

$$\rho_{corrected} = \frac{\mathrm{r_{target}}}{\mathrm{i_{sky}}} \times \frac{\mathrm{i_{sky}}}{\mathrm{r_{standard}}} \quad (6)$$

where $\rho_{corrected}$ represents corrected reflectance. The first term (r_{target}/i_{sky}) represents the raw reflectance, expressed as a ratio of the upwelling radiance to the downwelling irradiance over the target. The second term ($i_{sky}/r_{standard}$) represents the cross-calibration value, calculated as a ratio of the downwelling irradiance to the radiance of the standard panel [44]. Corrected reflectance at 531 nm and 570 nm was used to derive a scaled photochemical reflectance index (sPRI). Corrected sPRI measurements from SRS-PRI sensors were compared to the spectrometer derived sPRI to validate the accuracy of these automated sensors.

3.2.3. Broad Band Optical Sensors and Wireless Sensor Network (WSN)

A wireless sensor network (WSN), composing of 36 nodes, was used to measure the fraction of absorbed photosynthetically active radiation (*f*APAR). The WSN sensor nodes were arranged in a hexagonal pattern, spaced every 20 m over a one-hectare plot located within the flux footprint. The spatial extent of the WSN footprint accounted for approximately 55% of measured flux measurements. Additional details on the WSN deployment and technical capabilities can be found in Rankine et al. [53]. Individual nodes were outfitted with an upward and downward facing quantum sensors (SQ-110, Apogee Instruments Inc.), providing transmitted PPFD and soil reflected PPFD measurements, respectively. Additional nodes were placed on the flux tower, positioned above the canopy. Upward and downward looking quantum sensor pairs provided measurements of incident and reflected PPFD, respectively. The sampling interval of WSN nodes was 15 min. *f*APAR was calculated using the equation:

$$f\text{APAR} = 1 - t - r + (t \times r_s) \quad (7)$$

where t is the fraction of transmitted radiation, r is the reflected radiation from the canopy, and r_s is the soil reflectance component.

A broadband normalized difference vegetation index (NDVI) was derived from upward and downward looking quantum and pyranometer pairs installed on the flux tower, positioned above the canopy. Spot radiometers had a sampling interval of 10 min. Broadband NDVI was calculated using the equation:

$$\text{NDVI} = (\rho\text{PYR} - \rho\text{PPFD})/(\rho\text{PYR} + \rho\text{PPFD}) \quad (8)$$

where ρPYR is the solar radiation reflectance calculated from the upwelling:downwelling radiation from pyranometer pairs; and ρPPFD is the total reflectance of PPFD derived from upwelling: downwelling PPFD sensor pairs. Broadband NDVI values have been shown as adequate proxies of narrowband NDVI measurements [54]. Seasonal NDVI values were used to identify phenologic stages. A second derivative function was used to identify the transitions from maturity to leaf senescence (21 August 2015).

3.2.4. Light Use Efficiency Calculations

LUE was derived following traditional remote sensing methodology through the rearrangement of the LUE model as follows:

$$\mathrm{LUE} = \frac{\mathrm{GPP}}{(f\mathrm{APAR} \times \mathrm{PPFD})} = \frac{\mathrm{GPP}}{\mathrm{APAR}} \quad (9)$$

where GPP is the gross primary productivity, derived from eddy covariance measurements, and the absorbed photosynthetically active radiation (APAR) is the product of *f*APAR and PPFD. LUE values were derived at both diurnal and seasonal time scales. LUE values were expressed as 30 min. binned averages.

3.2.5. Micrometeorology Measurements

3.2.5.1. Micrometeorology Instrumentation and Processing

The eddy covariance (EC) method [55–57] was used to measure net ecosystem CO_2 exchange (NEE) (μmol m^{-2} s^{-1}), (latent heat (LE) (W m^{-2}), and sensible heat (H) (W m^{-2}) fluxes during the 2016 growth cycle. This consisted of a fast response (20 Hz) closed-path infrared gas analyzer (IRGA) (model EC155, Campbell Scientific Inc., Logan, UT, USA) and a three-dimensional sonic anemometer (model CSAT-3A, Campbell Scientific Inc.). The system was installed on a scaffold tower at 25 m above the forest floor. The sonic anemometer and IRGA share integrated electronics and communications to reduce logging lag, as part of the CPEC200 EC system (Campbell Scientific). Both sensors have a sampling frequency of 20 Hz, logged with a CR3000 datalogger (Campbell Scientific, Logan). A complete weather station (model HOBO U-30-NRC Weather Station, Onset Computer Corp., Bourne, MA, USA) provide ancillary meteorological variables including temperature (T_{air}), relative humidity (RH), vapor pressure deficit (VPD), precipitation, soil temperature, soil volumetric water content (VWC), soil heat fluxes, and net radiation. Remote communication to all micrometeorological instrumentation was provided through an Iridium satellite connection (Upward Innovations Inc., East Falmouth, MA, USA).

High-frequency eddy covariance data was processed using EddyPro® software (LI-COR Inc., Lincoln, NE, USA) and IBM streams® (IBM, Armonk, NY, USA). Vertical CO_2 flux (NEE) (μmol m^{-2} s^{-1}) was expressed as the product of mean air density and the covariance between instantaneous vertical wind velocity and concentration fluctuations.

$$\mathrm{NEE} = -\rho_a \overline{w's'} \quad (10)$$

where ρ_a is the dry air density (mol m^{-3}), w is the instantaneous vertical wind speed (m s^{-1}), and s is the molar mixing ratio (mol mol^{-1} dry air). The negative sign follows meteorological notation, where negative NEE values represented net CO_2 uptake into an ecosystem, and positive values represent net CO_2 release into the atmosphere.

Eddy covariance data corrections included time lag correction [58], despiking data outliers [59], double coordinate rotation [60], high-pass and low-pass filtering [56,61], and Webb-Pearman-Leuning (WPL) correction [62]. Fluxes were calculated at 30-minute block averages. Flux-footprint analysis' were performed following the Kljun et al. [63] parametrization. Precipitation events were not explicitly removed from the dataset. However, diagnostic/error flags associate with IRGA and SAT instrument failure, including during heavy rainfall, were used as a filter. A requirement of 80% data coverage was applied for each 30-minute averaging interval.

3.3.5.2. Flux Partitioning

Eddy covariance NEE measurements were partitioned into gross ecosystem productivity (GPP) (µmol m^{-2} s^{-1}) and respiration (R_{eco}) (µmol m^{-2} s^{-1}). R_{eco} was calculated using the Reichstein et al. [64] partitioning algorithm. Periods of poor mixing, identified by low frictional velocity ($u^* < 0.21$ m s^{-1}) and representing possible unreliable NEE measurements, were removed. A light-response curve model [65–68] was used as an independent method for GPP derivation and calculations of apparent quantum yield. This method uses rectangular hyperbolic functions to express the response of photosynthesis to radiation, using the general expression:

$$\mathrm{NEE} = -\left(\frac{A_{max} \cdot \alpha \cdot \mathrm{PPFD}}{A_{max} + \alpha \cdot \mathrm{PPFD}}\right) + R_{10} Q_{10}^{(\mathrm{T_{air}} - 10)/10} \quad (11)$$

where A_{max} is the maximum carbon assimilation, or GPP, (µmol m^{-2} s^{-1}) at maximum photosynthetic photon flux density (PPFD*)* (µmol m^{-2} s^{-1}); α is the apparent quantum yield calculated from the initial slope of the light-response curve (mol CO_2 mol^{-1} PPFD); R_{10} is the ecosystem respiration rate at 10 °C (µmol m^{-2} s^{-1}); Q_{10} is the respiration temperature response coefficient during temperature changes of 10 °C; and T_{air} is the air temperature (°C). A_{max}, α, R_{10} and Q_{10} variables are resulting outputs of the non-linear least square, Gauss-Newton, regressions applied (using the statistical package Systat10, Systat Software, Inc., San Jose, CA, USA, 2000), of the input diurnal

meteorological (PPFD and T_{air}) and NEE flux data. Before light-response curves were derived, NEE data was binned over two days to derive representative diurnal patterns.

3.3. Results

3.3.1. Sensor Calibrations and Validation

For each of the SRS-PRI sensor pairs (532 nm and 570 nm), cross-calibration ratios showed a strong linear relationship to illumination but varied in response to solar elevation. At low elevations, functions had steeper slopes and, therefore, showed higher sensitivity to illumination changes (Figure 3.2a). Illumination sensitivity decreased as solar elevation increased and functions were near horizontal at solar elevations of >52°, which represented peak solar noon elevations at our site. For both the 532 nm and 570 nm pairs, the difference in signal (radiance – irradiance) between the hemispherical and field stop fore-optics over the white balance (Figure 3.2b) decreased with diffused light observed cloudy conditions. This effect leads to calibration functions with negative slopes where cross-calibration ratios were higher during low illumination than high illumination. Boxplot distributions of cross-calibration functions (Figure 3.3) show an overall decrease in variability as sun elevation increased towards higher solar elevations. This was expected as low sun angles cause higher specular reflectance. However, generally, cross-calibration ratios were within range of theoretical radiance/irradiance ratio value of 0.318 [69].

The diurnal corrections were applied by first matching the empirical cross-calibrations functions with the solar elevations of each SRS-PRI data points. Then, the derived percent illumination of each point was used to automatically determine the cross-calibration multipliers and derive new corrected reflectance SRS-PRI values. Scaled photochemical reflectance index (sPRI) values were derived from corrected SRS-PRI. A similar process was applied for the midday correction procedure; however, instead of accounting for continuous changes in solar elevation, only daily solar noon elevations were used to select the appropriate empirical cross-calibration response. Solar noon elevations at our site varied from 24.28° to 56.36° (fall and summer, respectively). Both diurnal and midday cross-calibration procedures (Figure 3.4a) had a significant effect on the sPRI diurnal pattern. Each of the corrections caused a downward shift in midday sPRI values as well as a sharper recovery during the start and end of the day. These patterns more closely represented the spectrometer derived sPRI diurnal pattern than that formed by the uncorrected SRS-sPRI values. In particular, the dynamic

pattern of the diurnal cross-calibration best represented the reference spectrometer shape. Regression analysis (Figure 3.4b) of diurnal corrected SRS-sPRI values and spectrometer sPRI showed a strong linear correlation ($R^2 = 0.78$, $p < 0.05$). Midday corrected and uncorrected values were also significantly correlated to spectrometer sPRI ($R^2 = 0.72$, $p < 0.05$ and $R^2 = 0.62$, respectively).

3.3.2. Meteorological and Carbon Flux Data

Seasonal time series of net ecosystem exchange (NEE), gross primary productivity (GPP), and respiration (R_{eco}) were compared to meteorological variables and allowed the identification of climatic drivers directing intra-seasonal variability in carbon fluxes. Key connections between carbon fluxes and meteorological variables provided indications of the underlying mechanisms affecting vegetation efficiency over the season and during individual phenologic stages (maturity and leaf senescence). A more detailed analysis of carbon fluxes and meteorological data can be found in appendix A. PPFD appeared to be a strong driver of productivity during maturity. Comparison of diurnal patterns of GPP and PPFD (Figure 3.5) showed significant correlations during the months of June ($R^2 = 0.91$, $p < 0.05$), July ($R^2 = 0.90$, $p < 0.05$), August ($R^2 = 0.85$, $p < 0.05$), and September ($R^2 = 0.80$, $p < 0.05$). Productivity during the leaf senescence months, April and October, showed no association to PPFD conditions.

A combination of meteorological factors affecting apparent quantum yield (α) made it hard to determine the proportion of effect of each variable and how these may change over the growing season. However, some key components were identified and further discussed in the appendix A. Seasonal comparison of GPP and α (Figure 3.6a) were poorly correlated ($R^2 = 0.33$) over the whole season. However, during leaf senescence, (Figure 3.6b) as GPP starts to decline, GPP and α showed similar temporal changes and were significantly correlated ($R^2 = 0.73$, $p < 0.05$).

3.3.3. Comparison of Light Use Efficiency Parameters and Canopy Structure Parameters

SRS-sPRI values were compared to LUE and α to determine its suitability as a proxy of light use efficiency. Comparison of SRS-sPRI and LUE time series (Figure 3.7a) showed similar seasonal patterns and were significantly correlated ($R^2 = 0.62$, $p < 0.05$). PRI was also able to resolve periods of high LUE changes.

However, smaller fluctuations observed throughout the LUE time series were not as clearly resolved by the SRS sensors. Further separation of the LUE–SRS-sPRI relationship by phenologic stages (Figure 3.8a) showed higher correlation during maturity ($R^2 = 0.54$) than during leaf senescence ($R^2 = 0.43$). Also, higher variability in SRS-sPRI values was observed during maturity ($\sigma = 0.15$) than during leaf senescence ($\sigma = 0.069$). Correlation analysis of SRS-sPRI and α (Figure 3.7b) showed a strong significant correlation ($R^2 = 0.72$, $p < 0.05$). Temporal dynamics of α were also able to be better tracked by SRS-sPRI, especially during maturity (Figure 8b) ($R^2 = 0.67$). During leaf senescence (Figure 3.8b), SRS-sPRI started to increasingly depart from α values leading to a weaker relationship ($R^2 = 0.51$). Comparison of LUE and α (Figure 3.7c) resulted in highly correlated arrays ($R^2 = 0.88$, $p < 0.05$). The α time series followed the dynamic changes in LUE but with less short term variations, likely due to the 2-day temporal binning methodology used to calculate the α term.

Parametrization of light use efficiency must be done on the basis of green vegetation [5]. As collected fAPAR values represented the total light conditions of the forest stand, an NDVI-*f*APAR relationship (Figure 3.9) was established to ensure that fAPAR was, in fact, a good proxy of vegetation greenness changes. Daily NDVI and *f*APAR values strongly correlated ($R^2 = 0.96$, $p < 0.05$), but the relationship was non-linear. NDVI was seen to saturate as values reached above approximately 0.65 (*f*APAR ≈ 0.75). The effect of canopy structure and pigment pool changes on the PRI signal was evaluated by comparing SRS-sPRI values with measured *f*APAR. Analysis of the seasonal relationship (Figure 3.10a) showed *f*APAR and SRS-sPRI as being poorly correlated ($R^2 = 0.14$, $p > 0.05$). The seasonal time series was further divided into maturity and leaf senescence, and correlations were derived (Figure 3.10a). During maturity, we observed a poor relationship between *f*APAR and SRS-sPRI values, suggesting a minimal effect of canopy structure on PRI signals. However, during leaf senescence, a linear relationship ($R^2 = 0.52$, $p < 0.05$) formed between *f*APAR and SRS-sPRI values. To confirm the effect of canopy structure on efficiency during maturity and leaf senescence, the same comparisons were performed using LUE values, and lead to comparable results (Figure 3.10b).

3.3.4. Light Use Efficiency Models

SRS-sPRI and α values were used to derive light use efficiency models and compared to GPP to assess each model's accuracy. APAR values were also compared to GPP (Figure 3.11a) to determine its contributing proportion to the overall model. APAR closely tracked temporal changes in GPP

throughout maturity, however, during leaf fall GPP and APAR show differing paths. The LUE model constructed from α values (Figure 3.11b) was significantly correlated to GPP ($R^2 = 0.79$, $p < 0.05$). The model's closest association to GPP occurred during leaf senescence, as GPP started to decline. The light use efficiency model driven by the SRS-sPRI dataset (Figure 3.11c) had very similar results to that of the α based model and showed significant correlations to GPP ($R^2 = 0.77$, $p < 0.05$). Again, the GPP and models' paths were most closely associated during senescence, as leaf fall initiated.

3.4. Discussion

As suggested in other studies [70–73], our results show that a cross-calibration must be performed to properly calibrate automatic optical sensors. Uncalibrated SRS-PRI values did not have good agreement with spectrometer PRI values. Unlike results from Gamon et al. [44], both diurnal and midday calibrations noticeably improved the ability to resolve diurnal PRI patterns. Although we do not know the reason for this difference in calibration outcomes, one possibility may be that our aspen stand could represent more a heterogeneous structure and illumination conditions. Wind conditions that are common at our calibration site could help randomize the leaf orientation so that both the spectrometer and SRS sensors measure similar sunlit and shaded leaf proportions. Our contrasting results advocate for the importance of characterizing site-specific light fields that can vary in complexity between different canopy structures and may affect the ability to resolve diurnal dynamics accurately. A lack of ability to accurately resolve diurnal PRI patterns becomes problematic when diurnal patterns of the xanthophyll cycle and light use efficiency is wanted [39,44,78].

Although cross-calibrations provided more accurate PRI values, errors remain. In general, the main discrepancy between the SRS-PRI sensors and spectrometer measurements occurred as we moved away from midday. This suggests that the factory SRS sensors sensitivity cannot resolve the full range of reflectance changes. Uncalibrated SRS sensors result in an overestimation of PRI and LUE and modeled GPP values if used within a LUE model. To prevent erroneous PRI values that can lead to the mischaracterization of light use efficiency, we recommend regular calibrations and corrections of SRS sensors [71,73]. Diurnal cross-calibration procedures confirmed that an offline calibration is possible and can be used to correct the effects of illumination and solar elevation on radiance and irradiance measurements. However, it is important to note that our procedure did not account for changes in solar azimuth that lead to changes in directional reflectance [74,75]. Solar

azimuth changes will have a meaningful impact in high latitude ecosystems as angles will vary significantly from start to peak growing season. Real-time calibrations would account from changes in solar azimuth. However, given the constant manual intervention needed during real-time cross-calibrations, we believe our procedure to be a good compromise. The offline diurnal calibration was able to resolve diurnal PRI pattern (and xanthophyll cycle changes) more accurately than midday calibrations. The diurnal cross-calibrations results corroborate previous findings showing the effect of sun-canopy-sensor geometry on PRI values [33,43,76,77].

The strong correlation between SRS-sPRI and LUE (R^2 = 0.62) show that automated SRS-PRI sensors can be used as a proxy for light use efficiency. It is important to note the observed relationship between SRS-sPRI and LUE was stronger than the mean of 27 broadleaf forests reported correlations (R^2 = 0.59) reviewed by Zhang et al. [24]. Comparison between SRS-sPRI and apparent canopy quantum yield showed an even stronger correlation with an R^2 = 0.72 that represents the upper third quartile boundary of the broadleaf forest PRI-LUE correlation meta-analysis. Although quantum yield is not equivalent to light use efficiency, the strong correlation between α and LUE (R^2 = 0.88) show that α can be used as an adequate proxy of LUE when PPFD is the primary driving variable of productivity. As such, the strong correlation of between SRS-sPRI and α provide even more evidence that PRI values from the SRS sensors can serve as a proxy for efficiency.

Although sPRI was well correlated to light use efficiency parameters, their association appeared to vary within different developmental stages. The close correlation between sPRI, LUE (R^2 = 0.54) and α (R^2 = 0.67) during maturity show ability to track the facultative changes of xanthophyll cycle pigment pools. This was further supported by the weak correlation between *f*APAR and sPRI (R^2 = 0.14), indicating the low effect of vegetation structure that drives constitutive pigment pool changes [38]. During leaf senescence sPRI was less strongly correlated to efficiency parameters (light use efficiency R^2 = 0.43, quantum yield R^2 = 0.51) and correlated with *f*APAR (R^2 = 0.52), suggesting that the PRI signal is influenced by canopy changes. In deciduous vegetation, senescence marks a period of substantial changes in canopy structure composition as leaves start to senesce and fall. During this marked period of structural variation, senescence PRI would most likely represent a mixture of facultative and constitutive changes, with constitutive changes confounding the physiological signal from leaves. This aligns with studies [79,80] suggesting that dominant effects of canopy structure can confound physiological leaf traits detection. Future parametrization of LUE models will need to take into account PRI's contrasting effect on photosynthetic activity during different time periods [21]. The high temporal resolution of the automatic SRS-PRI sensors and their

ability to serve as a proxy of LUE at different temporal scales could be useful towards the better parametrization of LUE models.

A close analysis of PRI and light use efficiency parameters provided some underlying mechanism affecting efficiency at our site. The close relationship of α and GPP during senescence indicate that efficiency changes are influenced by canopy structure, this being the primary driving mechanism of GPP changes. Coinciding efficiency peaks present in sPRI, LUE and α time series were associated with high water availability (soil and atmospheric), lower temperatures and low PPFD. In the context of PRI, we can infer that periods of low PPFD would account for the little need for non-photochemical quenching as canopy would not be exposed to saturating light conditions. Diffused light conditions have been shown to result in higher canopy light use efficiency [81–83] and could explain the increases in LUE rates. This effect of diffused light on light use efficiency rates has been difficult to account for in remote sensing modeling as most of the driving data come from non-continuous satellite-based imagery. Continuous PRI measurements have the potential to solve this, as illumination can be used to classify continuous datasets into illumination groups and used to empirically describe the effects of different light conditions on LUE through time.

Many described canopy scale variables have been described that can confound PRI signals including canopy structure, view and illumination angles, soil types, shadow fractions, phenology and pigment pools [19,21,38,84,85]. One approach to mitigate some of these effects is through the normalization of PRI (calculating daily ΔPRI) [86]. This has been shown to reduce the effects of canopy structure, vegetation cover, and soil background. Although not applied in this study, PRI normalization is a topic of future work as it may improve PRI-LUE relationships from continuous sensors. Some of the variables previously mentioned also impact our sPRI dataset. We can also assume that our continuous measurements will have a wide range of impacts as the higher temporal resolution will naturally capture more of these interactions. Although quantifying the individual effect of each impacting variable is difficult, we believe that continuous datasets provide the ability to explicitly examine the cause of changing PRI over time and space. This has been a criticism of studies using non-continuous PRI measurements such as those from satellite platforms, where their low temporal resolution cannot resolve short-term reflectance changes and instead changes primarily represent changing pigment pools [38,39].

Both the sPRI and α LUE models were able to track the overall progression of GPP. Still, some of the short-term dynamic changes observed in GPP during maturity were better captured by APAR the sPRI and α derived LUE models. We can attribute this to the strong association between incident

light and productivity during peak GPP months. During peak GPP months, canopy structure remains mostly unchanged; thus APAR variability is driven by PPFD dynamics. During leaf senescence, PPFD was no longer associated with GPP and lead to the differences seen between APAR and GPP trends. Overall, the α driven LUE model showed to be the most accurate. The sPRI LUE model followed closely and was able to track seasonal changes in productivity. Evaluation of APAR, sPRI and LUE model results indicate that construction of LUE models needs to consider the changing contribution of the individual model variables through time and within different ecosystems. This follows Garbulsky et al. [14] concept suggesting that canopy efficiency can change between vegetation and environmental conditions. Exploration of this concept has been hard to test due to lack of continuous datasets that would allow mechanistic and comparative analysis within and across biomes. Continuous SRS-sPRI offer new opportunities to explore diurnal and seasonal changes in vegetation physiology.

3.5. Conclusions

An offline diurnal calibration was able to characterize the optical sensor's response and allowed us to resolve diurnal and seasonal PRI patterns. Corrected PRI values from SRS sensor proved to be appropriate proxies of light use efficiency. Our results contribute to the growing research indicating that continuous PRI sensors can be used to track diurnal and seasonal changes in efficiency. Still, it is important to define facultative and constitutive proportions within the PRI observations and how this may change over different ecosystems and growth stages. Studies on the explicit effect of environmental conditions on PRI signals will also prove to be important since the higher resolution of continuous measurements will need to be accurately characterized. In general, we see continuous PRI sensors as having numerous benefits for explicitly examining the cause of changing PRI, LUE, and productivity over time and space. For this reason, we see this technology of great value for the flux, remote sensing and modeling community.

Author Contributions: Conceptualization, S.Castro. and A.Sanchez-Azofeifa.; Methodology, S.Castro.; Formal Analysis, S.Castro.; Investigation, S.Castro.; Resources, A.Sanchez-Azofeifa.; Data Curation, A.Sanchez-Azofeifa.; Writing-Original Draft Preparation, S.Castro.; Writing-Review & Editing, S.Castro. and A.Sanchez-Azofeifa; Supervision, A.Sanchez-Azofeifa.; Project Administration, A.Sanchez-Azofeifa.; Funding Acquisition, A.Sanchez-Azofeifa.

Funding: This research was funded by a grant from the Canada Foundation for Innovation (CFI), Discovery Grant from the National Science and Engineering Research Council of Canada (NSERC) and IBM Alberta Center for Advance.

Acknowledgments: We would also like to acknowledge the support of EMEND, and DMI Peace River Pulp Division, Peter Carlson, Iain Sharp, and Jose Antonio Guzman, for their technical and logistical support. Thank you to Amy Castro for her patience and support.

Conflicts of Interest: The authors declare no conflict of interest.

3.6 References

1. Monteith, J.L. Solar radiation and productivity in tropical ecosystems. *J. Appl. Ecol.* **1972**, *9*, 747–766.

2. Monteith, J.L. Climate and the efficiency of crop production in Britain. *Philos. Trans. R. Soc. Lond. B* **1977**, *281*, 277–294.

3. Huete, A.; Ponce-Campos, G.; Zhang, Y.; Restrepo-Coupe, N.; Ma, X.; Moran, M. Monitoring photosynthesis from space. In *Land Resources Monitoring, Modeling, and Mapping with Remote Sensing*; Remote Sensing Handbook; CRC Press: Boca Raton, FL, USA, 2015; pp. 3–22.

4. Schimel, D.; Pavlick, R.; Fisher, J.B.; Asner, G.P.; Saatchi, S.; Townsend, P.; Miller, C.; Frankenberg, C.; Hibbard, K.; Cox, P. Observing terrestrial ecosystems and the carbon cycle from space. *Glob. Chang. Biol.* **2015**, *21*, 1762–1776.

5. Gitelson, A.A.; Gamon, J.A. The need for a common basis for defining light-use efficiency: Implications for productivity estimation. *Remote Sens. Environ.* **2015**, *156*, 196–201.

6. Sellers, P.J. Canopy reflectance, photosynthesis and transpiration. *Int. J. Remote Sens.* **1985**, *6*, 1335–1372.

7. Sellers, P.J. Canopy reflectance, photosynthesis, and transpiration, II. The role of biophysics in the linearity of their interdependence. *Remote Sens. Environ.* **1987**, *21*, 143–183.

8. Myneni, R.B.; Williams, D.L. On the relationship between FAPAR and NDVI. *Remote Sens. Environ.* **1994**, *49*, 200–211.

9. Asrar, G.M.; Myneni, R.B.; Choudhury, B.J. Choudhury. Spatial heterogeneity in vegetation canopies and remote sensing of absorbed photosynthetically active radiation: A modeling study. *Remote Sens. Environ.* **1992**, *41*, 85–103.

10. Gobron, N.; Pinty, B.; Aussedat, O.; Chen, J.M.; Cohen, W.B.; Fensholt, R.; Gond, V.; Huemmrich, K.F.; Lavergne, T.; Mélin, F.; et al. Evaluation of fraction of absorbed photosynthetically active radiation products for different canopy radiation transfer regimes: Methodology and results using Joint Research Center products derived from SeaWiFS against ground-based estimations. *J. Geophys. Res. Atmos.* **2006**, *111*, doi:10.1029/2005JD006511.

11. Widlowski, J.-L. On the bias of instantaneous FAPAR estimates in open-canopy forests. *Agric. For. Meteorol.* **2010**, *150*, 1501–1522.

12. Field, C.B.; Gamon, J.A.; Peñuelas, J. Remote sensing of photosynthesis. In *Ecophysiology of Photosynthesis*; Schulze, E.-D., Caldwell, M.M., Eds.; Ecological Studies; Springer: Berlin/Heidelberg, Germany; New York, NY, USA, 1994; Volume 100, pp. 511−527.

13. Garbulsky, M.F.; Peñuelas, J.; Papale, D.; Ardö, J.; Goulden, M.L.; Kiely, G.; Richardson, A.D.; Rotenberg, E.; Veenendaal, E.M.; Filella, I. Patterns and controls of the variability of radiation use efficiency and primary productivity across terrestrial ecosystems. *Glob. Ecol. Biogeogr.* **2010**, *19*, 253–267.

14. Garbulsky, M.F.; Peñuelas, J.; Gamon, J.; Inoue, Y.; Filella, I. The photochemical reflectance index (PRI) and the remote sensing of leaf, canopy and ecosystem radiation use efficiencies: A review and meta-analysis. *Remote Sens. Environ.* **2011**, *115*, 281–297.

15. Jarvis PG, Leverenz JW. Productivity of temperate, deciduous and evergreen forests. InPhysiological plant ecology IV 1983 (pp. 233-280). Springer, Berlin, Heidelberg.

16. Ruimy, A.L.; Jarvis, P.G.; Baldocchi, D.D.; Saugier, B. CO_2 fluxes over plant canopies and solar radiation: A review. *Adv. Ecol. Res.* **1995**, *26*, 1–68.

17. Gamon, J.A.; Serrano, L.; Surfus, J. The photochemical reflectance index: An optical indicator of photosynthetic radiation use efficiency across species, functional types, and nutrient levels. *Oecologia* **1997**, *112*, 492–501.

18. Ahl, D.E.; Gower, S.T.; Mackay, D.S.; Burrows, S.N.; Norman, J.M.; Diak, G.R. Heterogeneity of light use efficiency in a northern Wisconsin forest: Implications for modeling net primary production with remote sensing. *Remote Sens. Environ.* **2004**, *93*, 168–178.

19. Sims, D.A.; Gamon, J.A. Relationships between leaf pigment content and spectral reflectance across a wide range of species, leaf structures and developmental stages. *Remote Sens. Environ.* **2002**, *81*, 337–354.

20. Jenkins, J.P.; Richardson, A.D.; Braswell, B.H.; Ollinger, S.V.; Hollinger, D.Y.; Smith, M.L. Refining light-use efficiency calculations for a deciduous forest canopy using simultaneous tower-based carbon flux and radiometric measurements. *Agric. For. Meteorol*. **2007**, *143*, 64–79.

21. Gamon, J.A.; Huemmrich, K.F.; Wong, C.Y.; Ensminger, I.; Garrity, S.; Hollinger, D.Y.; Noormets, A.; Peñuelas, J. A remotely sensed pigment index reveals photosynthetic phenology in evergreen conifers. *Proc. Natl. Acad. Sci. USA* **2016**, *113*, 13087–13092.

22. Zhang, C.; Filella, I.; Liu, D.; Ogaya, R.; Llusià, J.; Asensio, D.; Peñuelas, J. Photochemical reflectance index (PRI) for detecting responses of diurnal and seasonal photosynthetic activity to experimental drought and warming in a mediterranean shrubland. *Remote Sens*. **2017**, *9*, 1189.

23. Peñuelas, J.; Filella, I.; Gamon, J.A. Assessment of photosynthetic radiation-use efficiency with spectral reflectance. *New Phytol.* **1995**, *131*, 291–296.

24. Zhang, C.; Filella, I.; Garbulsky, M.; Peñuelas, J. Affecting factors and recent improvements of the photochemical reflectance index (PRI) for remotely sensing foliar, canopy and ecosystemic radiation-use efficiencies. *Remote Sens.* **2016**, *8*, 677.

25. Garbulsky, M.F.; Filella, I.; Verger, A.; Peñuelas, J. Photosynthetic light use efficiency from satellite sensors: From global to Mediterranean vegetation. *Environ. Exp. Bot.* **2014**, *103*, 3–11.

26. Gamon, J.A.; Field, C.B.; Bilger, W.; Björkman, O.; Fredeen, A.L.; Peñuelas, J. Remote sensing of the xanthophyll cycle and chlorophyll fluorescence in sunflower leaves and canopies. *Oecologia* **1990**, *85*, 1–7.

27. Gamon, J.A.; Penuelas, J.; Field, C.B. A narrow-waveband spectral index that tracks diurnal changes in photosynthetic efficiency. *Remote Sens. Environ.* **1992**, *41*, 35–44.

28. Björkman, O.; Demmig-Adams, B. Regulation of photosynthetic light energy capture, conversion, and dissipation in leaves of higher plants. In *Ecophysiology of Photosynthesis*; Springer: Berlin/Heidelberg, Germany, 1995; pp. 17–47.

29. Demmig-Adams, B.; Adams, W.W., III; Logan, B.A.; Verhoeven, A.S. Xanthophyll cycle-dependent energy dissipation and flexible photosystem II efficiency in plants acclimated to light stress. *Funct. Plant Biol.* **1995**, *22*, 249–260.

30. Demmig-Adams, B.; Adams, W.W., III. The role of xanthophyll cycle carotenoids in the protection of photosynthesis. *Trends Plant Sci.* **1996**, *1*, 21–26.

31. Gamon, J.A. *The Dynamic 531-Nanometer A Reflectance Signal: A Survey of Twenty Angiosperm Species*; Gilmore Hall 202-3050 Maile Way Honolulu, Hawaii 96822 Office of the Director; American Society of Plant Physiologists: Rockville, MA, USA, 1993; p. 172.

32. Gamon, J.A.; Surfus, J.S. Assessing leaf pigment content and activity with a reflectometer. *New Phytol*. **1999**, *143*, 105–117.

33. Barton, C.V.; North, P.R. Remote sensing of canopy light use efficiency using the photochemical reflectance index: Model and sensitivity analysis. *Remote Sens. Environ.* **2001**, *78*, 264–273.

34. Cheng, Y.B.; Middleton, E.M.; Zhang, Q.; Corp, L.A.; Dandois, J.; Kustas, W.P. The photochemical reflectance index from directional cornfield reflectances: Observations and simulations. *Remote Sens. Environ.* **2012**, *124*, 444–453.

35. Stylinski, C.; Gamon, J.; Oechel, W. Seasonal patterns of reflectance indices, carotenoid pigments and photosynthesis of evergreen chaparral species. *Oecologia* **2002**, *131*, 366–374.

36. Filella, I.; Porcar-Castell, A.; Munné-Bosch, S.; Bäck, J.; Garbulsky, M.F.; Peñuelas, J. PRI assessment of long-term changes in carotenoids/chlorophyll ratio and short-term changes in de-epoxidation state of the xanthophyll cycle. *Int. J. Remote Sens.* **2009**, *30*, 4443–4455.

37. Garrity, S.R.; Eitel, J.U.; Vierling, L.A. Disentangling the relationships between plant pigments and the photochemical reflectance index reveals a new approach for remote estimation of carotenoid content. *Remote Sens. Environ.* **2011**, *115*, 628–635.

38. Gamon, J.A.; Berry, J.A. Facultative and constitutive pigment effects on the Photochemical Reflectance Index (PRI) in sun and shade conifer needles. *Isr. J. Plant Sci.* **2012**, *60*, 85–95.

39. Gitelson, A.A.; Gamon, J.A.; Solovchenko, A. Multiple drivers of seasonal change in PRI: Implications for photosynthesis 2. Stand level. *Remote Sens. Environ.* **2017**, *190*, 198–206.

40. Nichol, C.J.; Lloyd, J.O.; Shibistova, O.; Arneth, A.; Röser, C.; Knohl, A.; Matsubara, S.; Grace, J. Remote sensing of photosynthetic-light-use efficiency of a Siberian boreal forest. *Tellus B Chem. Phys. Meteorol.* **2002**, *54*, 677–687.

41. Goerner, A.; Reichstein, M.; Tomelleri, E.; Hanan, N.; Rambal, S.; Papale, D.; Dragoni, D.; Schmullius, C. Remote sensing of ecosystem light use efficiency with MODIS-based PRI. *Biogeosciences* **2011**, *8*, 189–202.

42. Gamon, J.A. Reviews and syntheses: Optical sampling of the flux tower footprint. *Biogeosciences* **2015**, *12*, 4509–4523.

43. Garrity, S.R.; Vierling, L.A.; Bickford, K. A simple filtered photodiode instrument for continuous measurement of narrowband NDVI and PRI over vegetated canopies. *Agric. For. Meteorol.* **2010**, *150*, 489–496.

44. Gamon, J.A.; Kovalchuck, O.; Wong, C.Y.; Harris, A.; Garrity, S.R. Monitoring seasonal and diurnal changes in photosynthetic pigments with automated PRI and NDVI sensors. *Biogeosciences* **2015**, *12*, 4149–4159.

45. Van Leeuwen, M.; Kremens, R.L.; van Aardt, J. Tracking diurnal variation in photosynthetic down-regulation using low cost spectroscopic instrumentation. *Sensors* **2015**, *15*, 10616–10630.

46. Alberta Environmental Protection. *Natural Regions and Subregions of Alberta: A Summary*; Publ. I/531 and Map, 1 Sheet; Alberta Environmental Protection: Edmonton, AB, Canada, 1994.

47. Atmospheric Environment Service. *Canadian Climate Normals (19511980)*; Precipitation Environment Canada: Downsview, ON, Canada, 1982; Volume 3, p. 602

48. Soil Classification Working Group. *The Canadian System of Soil Classification*; Publication 1646 (Revised); Agriculture and Agri-Food Canada: Ottawa, ON, Canada, 1998; p. 187.

49. Rahman, A.F.; Cordova, V.D.; Gamon, J.A.; Schmid, H.P.; Sims, D.A. Potential of MODIS ocean bands for estimating CO_2 flux from terrestrial vegetation: A novel approach. *Geophys. Res. Lett.* **2004**, *31*, doi:10.1029/2004GL019778.

50. Goerner, A.; Reichstein, M.; Rambal, S. Tracking seasonal drought effects on ecosystem light use efficiency with satellite-based PRI in a Mediterranean forest. *Remote Sens. Environ.* **2009**, *113*, 1101–1111.

51. Gamon, J.A.; Rahman, A.F.; Dungan, J.L.; Schildhauer, M.; Huemmrich, K.F. Spectral Network (SpecNet)—What is it and why do we need it? *Remote Sens. Environ.* **2006**, *103*, 227–235.

52. Ryan, P.J.; Stolzenbach, K.D. *Engineering Aspects of Heat Disposal from Power Generation*; Harleman, D.R.F., Ed.; RM Parson Laboratory for Water Resources and Hydrodynamics, Department of Civil Engineering, Massachusetts Institute of Technology: Cambridge, MA, USA, 1972.

53. Rankine, C.J.; Sanchez-Azofeifa, G.A.; MacGregor, M.H. Seasonal wireless sensor network link performance in boreal forest phenology monitoring. In Proceedings of the 2014 Eleventh Annual IEEE International Conference on Sensing, Communication, and Networking (SECON), Singapore, 30 June–3 July 2014; pp. 302–310.

54. Huemmrich, K.F.; Black, T.A.; Jarvis, P.G.; McCaughey, J.H.; Hall, F.G. High temporal resolution NDVI phenology from micrometeorological radiation sensors. *J. Geophys. Res. Atmos.* **1999**, *104*, 27935–27944.

55. Baldocchi, D.D.; Hincks, B.B.; Meyers, T.P. Measuring biosphere-atmosphere exchanges of biologically related gases with micrometeorological methods. *Ecology* **1988**, *69*, 1331–1340.

56. Moncrieff, J.B.; Massheder, J.M.; De Bruin, H.; Elbers, J.; Friborg, T.; Heusinkveld, B.; Kabat, P.; Scott, S.; Søgaard, H.; Verhoef, A. A system to measure surface fluxes of momentum, sensible heat, water vapour and carbon dioxide. *J. Hydrol.* **1997**, *188*, 589–611.

57. Aubinet, M.; Grelle, A.; Ibrom, A.; Rannik, Ü.; Moncrieff, J.; Foken, T.; Kowalski, A.S.; Martin, P.H.; Berbigier, P.; Bernhofer, C.; et al. Estimates of the annual net carbon and water exchange of forests: The EUROFLUX methodology. In *Advances in Ecological Research*; Academic Press: Cambridge, MA, USA, 1999; Volume 30, pp. 113–175.

58. Moore, C.J. Frequency response corrections for eddy correlation systems. *Bound.-Layer Meteorol.* **1986**, *37*, 17–35.

59. Vickers, D.; Mahrt, L. Quality control and flux sampling problems for tower and aircraft data. *J. Atmos. Ocean. Technol.* **1997**, *14*, 512–526.

60. Finnigan, J.J. A re-evaluation of long-term flux measurement techniques part II: Coordinate systems. *Bound.-Layer Meteorol.* **2004**, *113*, 1–41.

61. Moncrieff, J.; Clement, R.; Finnigan, J.; Meyers, T. Averaging, detrending, and filtering of eddy covariance time series. In *Handbook of Micrometeorology*; Springer: Dordrecht, The Netherlands, 2004; pp. 7–31.

62. Webb, E.K.; Pearman, G.I.; Leuning, R. Correction of flux measurements for density effects due to heat and water vapour transfer. *Q. J. R. Meteorol. Soc.* **1980**, *106*, 85–100.

63. Kljun, N.; Calanca, P.; Rotach, M.W.; Schmid, H.P. A simple parameterisation for flux footprint predictions. *Bound.-Layer Meteorol.* **2004**, *112*, 503–523.

64. Reichstein, M.; Falge, E.; Baldocchi, D.; Papale, D.; Aubinet, M.; Berbigier, P.; Bernhofer, C.; Buchmann, N.; Gilmanov, T.; Granier, A.; et al. On the separation of net ecosystem exchange into assimilation and ecosystem respiration: Review and improved algorithm. *Glob. Chang. Biol.* **2005**, *11*, 1424–1439.

65. Flanagan, L.B.; Johnson, B.G. Interacting effects of temperature, soil moisture and plant biomass production on ecosystem respiration in a northern temperate grassland. *Agric. For. Meteorol.* **2005**, *130*, 237–253.

66. Glenn, A.J.; Flanagan, L.B.; Syed, K.H.; Carlson, P.J. Comparison of net ecosystem CO_2 exchange in two peatlands in western Canada with contrasting dominant vegetation, Sphagnum and Carex. *Agric. For. Meteorol.* **2006**, *140*, 115–135.

67. Syed, K.H.; Flanagan, L.B.; Carlson, P.J.; Glenn, A.J.; Van Gaalen, K.E. Environmental control of net ecosystem CO_2 exchange in a treed, moderately rich fen in northern Alberta. *Agric. For. Meteorol.* **2006**, *140*, 97–114.

68. Adkinson, A.C.; Syed, K.H.; Flanagan, L.B. Contrasting responses of growing season ecosystem CO_2 exchange to variation in temperature and water table depth in two peatlands in northern Alberta, Canada. *J. Geophys. Res. Biogeosci.* **2011**, *116*, doi:1029/2010JG001512.

69. Monteith, J.L. *Principles of Environmental Physics*; Elsevier: New York, NY, USA, 1973.

70. Balzarolo, M.; Anderson, K.; Nichol, C.; Rossini, M.; Vescovo, L.; Arriga, N.; Wohlfahrt, G.; Calvet, J.C.; Carrara, A.; Cerasoli, S.; et al. Ground-based optical measurements at European flux sites: A review of methods, instruments and current controversies. *Sensors* **2011**, *11*, 7954–7981.

71. Harris, A.; Gamon, J.A.; Pastorello, G.Z.; Wong, C.Y.S. Retrieval of the photochemical reflectance index for assessing xanthophyll cycle activity: A comparison of near-surface optical sensors. *Biogeosciences* **2014**, *11*, 6277–6292.

72. Drolet, G.; Wade, T.; Nichol, C.J.; MacLellan, C.; Levula, J.; Porcar-Castell, A.; Nikinmaa, E.; Vesala, T. A temperature-controlled spectrometer system for continuous and unattended measurements of canopy spectral radiance and reflectance. *Int. J. Remote Sens.* **2014**, *35*, 1769–1785.

73. Pacheco-Labrador, J.; Martín, M.P. Nonlinear response in a field portable spectroradiometer: Characterization and effects on output reflectance. *IEEE Trans. Geosci. Remote Sens.* **2014**, *52*, 920–928.

74. Deering, D.W.; Leone, P. A sphere-scanning radiometer for rapid directional measurements of sky and ground radiance. *Remote Sens. Environ.* **1986**, *19*, 1–24.

75. Kimes, D.S. Dynamics of directional reflectance factor distributions for vegetation canopies. *Appl. Opt.* **1983**, *22*, 1364–1372.

76. Hilker, T.; Coops, N.C.; Hall, F.G.; Black, T.A.; Wulder, M.A.; Nesic, Z.; Krishnan, P. Separating physiologically and directionally induced changes in PRI using BRDF models. *Remote Sens. Environ.* **2008**, *112*, 2777–2788.

77. Galvão, L.S.; Breunig, F.M.; dos Santos, J.R.; de Moura, Y.M. View-illumination effects on hyperspectral vegetation indices in the Amazonian tropical forest. *Int. J. Appl. Earth Obs. Geoinf.* **2013**, *21*, 291–300.

78. Gitelson, A.A.; Gamon, J.A.; Solovchenko, A. Multiple drivers of seasonal change in PRI: Implications for photosynthesis 1. Leaf level. *Remote Sens. Environ.* **2017**, *190*, 110–116.

79. Knyazikhin, Y.; Schull, M.A.; Stenberg, P.; Mottus, M.; Rautiainen, M.; Yang, Y.; Marshak, A.; Latorre Carmona, P.; Kaufmann, R.K.; Lewis, P.; et al. Hyperspectral remote sensing of foliar nitrogen content. *Proc. Natl. Acad. Sci. USA* **2013**, *110*, E185–E192,

80. Townsend, P.A.; Serbin, S.P.; Kruger, E.L.; Gamon, J.A. Disentangling the contribution of biological and physical properties of leaves and canopies in imaging spectroscopy data. *Proc. Natl. Acad. Sci. USA* **2013**, *110*, E1074, doi:10.1073/pnas.1300952110.

81. Norman, J.M.; Arkebauer, T.J. Predicting canopy light-use efficiency from leaf characteristics. *Model. Plant Soil Syst.* **1991**, 31, 125–143.

82. Choudhury, B.J. Estimating gross photosynthesis using satellite and ancillary data: Approach and preliminary results. *Remote Sens. Environ.* **2001**, *75*, 1–21.

83. Gu, L.; Baldocchi, D.; Verma, S.B.; Black, T.A.; Vesala, T.; Falge, E.M.; Dowty, P.R. Advantages of diffuse radiation for terrestrial ecosystem productivity. *J. Geophys. Res. Atmos.* **2002**, *107*, ACL-2.

84. Drolet, G.G.; Huemmrich, K.F.; Hall, F.G.; Middleton, E.M.; Black, T.A.; Barr, A.G.; Margolis, H.A. A MODIS-derived photochemical reflectance index to detect inter-annual variations in the photosynthetic light-use efficiency of a boreal deciduous forest. *Remote Sens. Environ.* **2005**, *98*, 212–224.

85. Hilker, T.; Coops, N.C.; Nesic, Z.; Wulder, M.A.; Black, A.T. Instrumentation and approach for unattended year round tower based measurements of spectral reflectance. *Comput. Electron. Agric.* **2007**, *56*, 72–84.

86. Liu, L.; Zhang, Y.; Jiao, Q.; Peng, D. Assessing photosynthetic light-use efficiency using a solar-induced chlorophyll fluorescence and photochemical reflectance index. *Int. J. Remote Sens.* **2013**, *34*, 4264–4280.

3.7. Figures

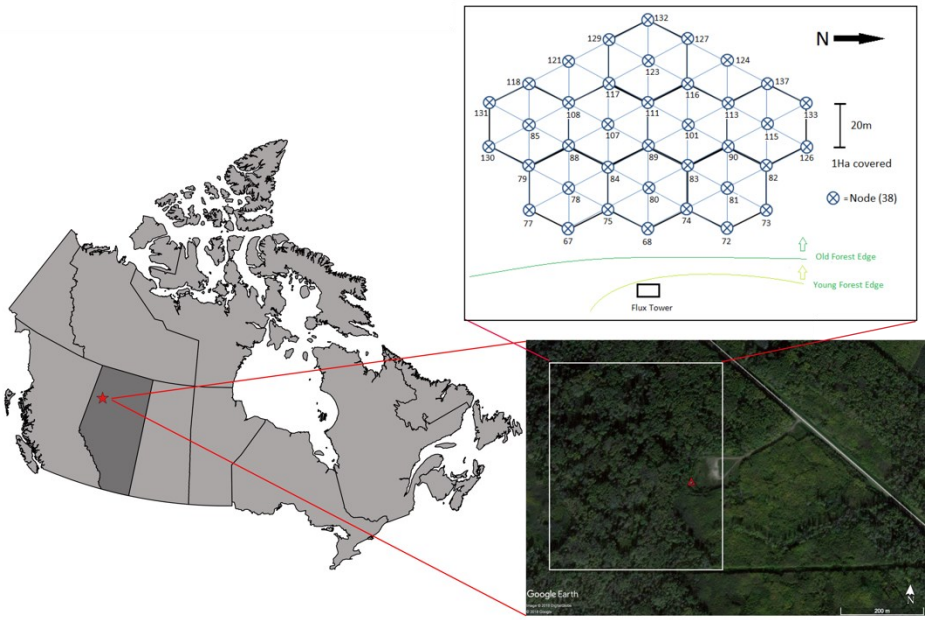

Figure 3.1. Location of the Peace River Environmental Monitoring Super Site (red star). Red triangle shows the location of the flux tower at the edge of an old growth deciduous boreal forest. The tower contains eddy covariance system, meteorological sensors, and proximal remote sensing sensors. A Wireless Sensor Network (WSN) composing of 36 nodes is located east of the eddy covariance tower, within the flux footprint.

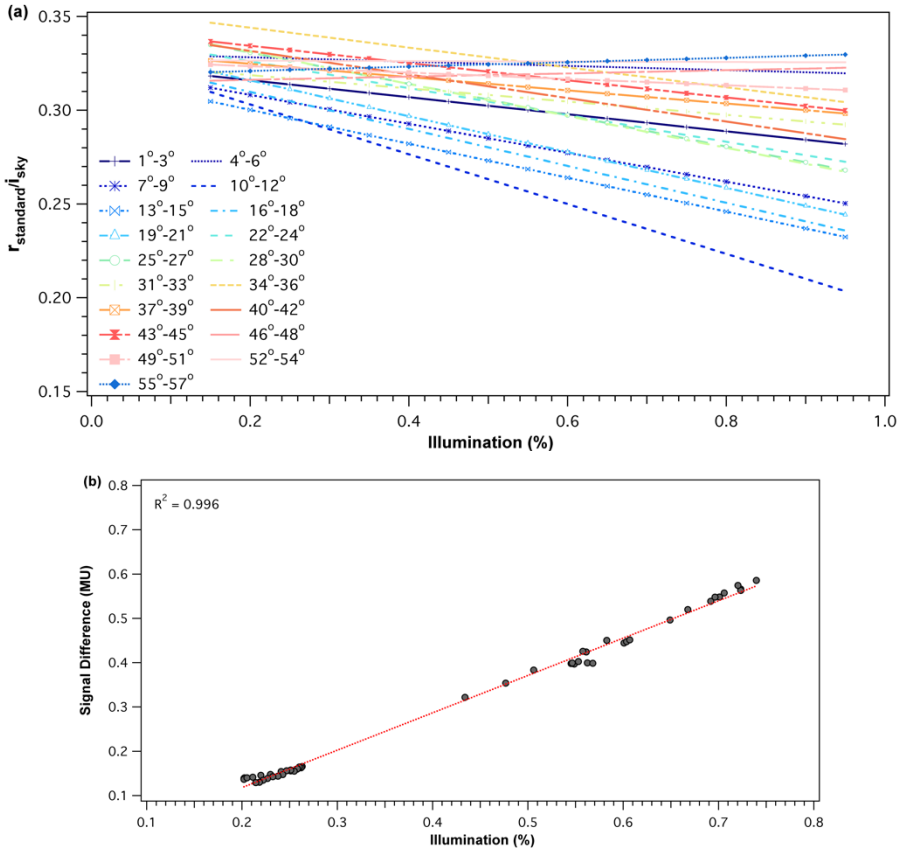

Figure 3.2. (**a**) Example of midday and diurnal cross-calibration functions for the 532 nm SRS-PRI fore-optic. Cross-calibration ratios are shown as a function of sun elevation (binned every 3°). Illumination of 100% represents clear and sunny sky conditions. (**b**) Example of the observed signal difference (radiance – irradiance), in machine units, as a function of illumination percentage for the 41°–43° solar elevation bin. Radiance and irradiance measurements were collected from the 532 nm SRS-PRI sensor pair.

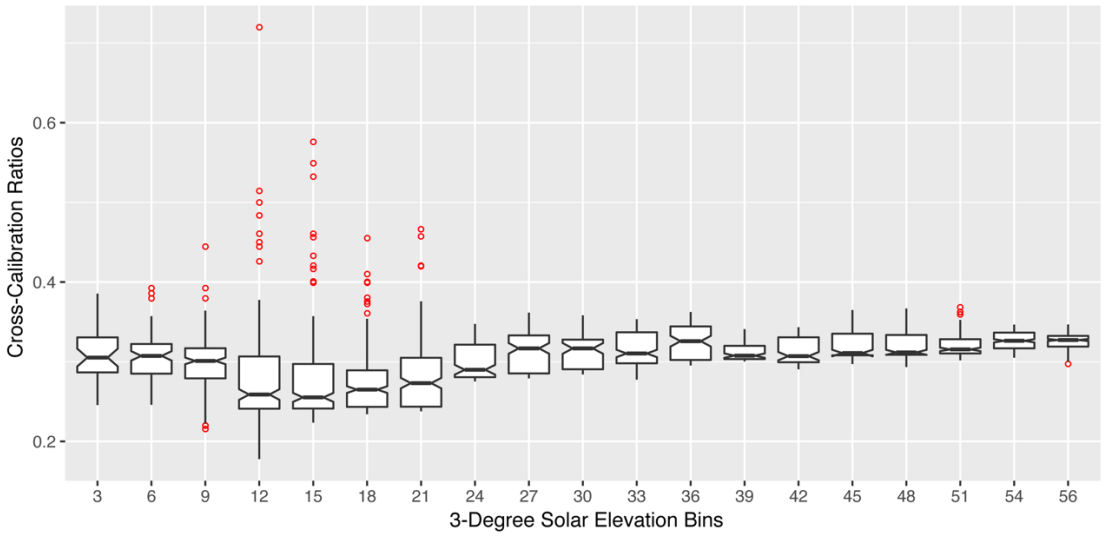

Figure 3.3. Boxplot distribution of diurnal cross-calibration ratios for the 532 nm SRS-PRI fore-optic. Each boxplot represents a 3° solar elevation bin. Red points represent outliers and were observed more often in low solar elevation bins.

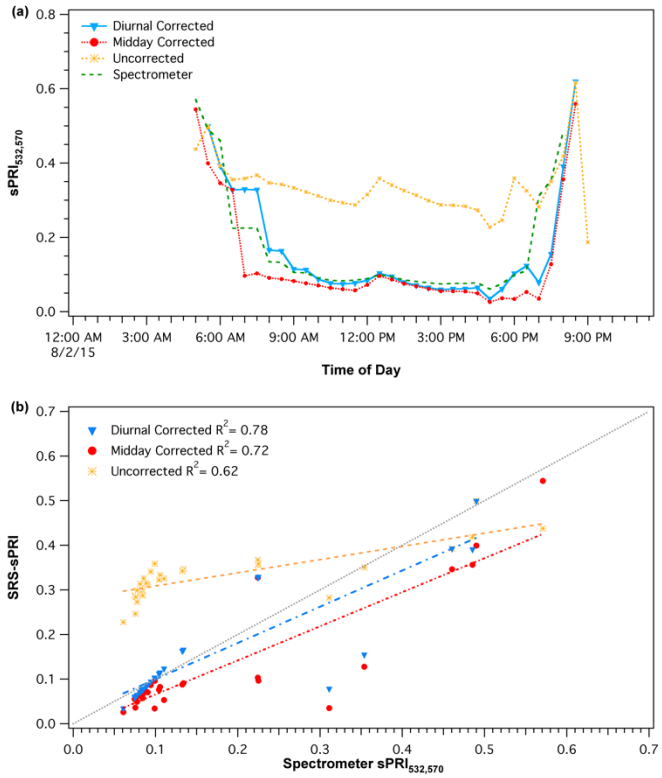

Figure 3.4. (**a**) Comparison of uncorrected and corrected (diurnal and midday) PRI diurnal patterns. (**b**) Comparison of spectrometer PRI measurements with uncorrected and corrected

SRS-PRI measurements. The diurnal cross-calibration procedure shows the strongest and closest correlation to spectrometer readings and 1:1 (gray) line.

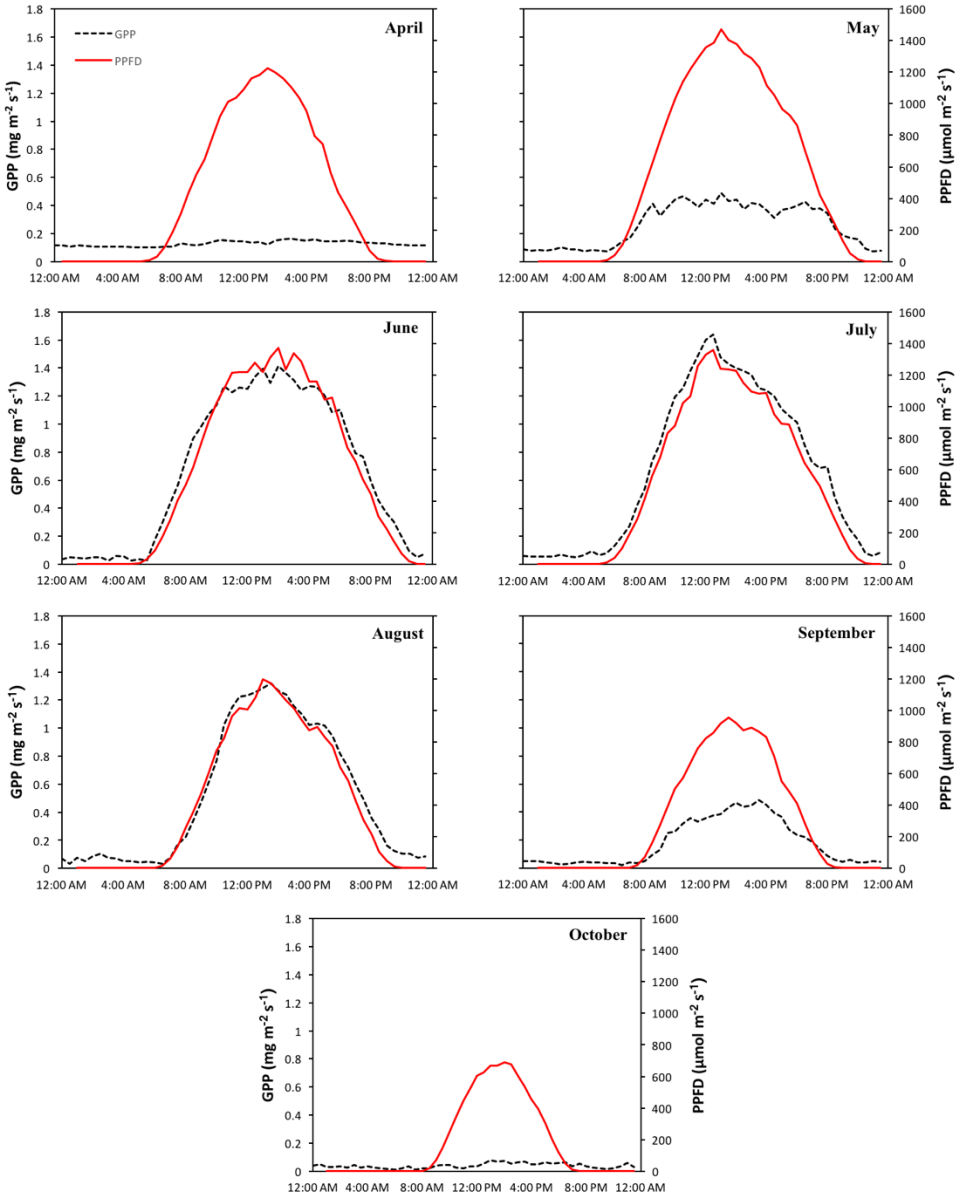

Figure 3.5. Mean diurnal monthly pattern of gross primary productivity (GPP) (black dotted line) and photosynthetic photon flux density (red line) for the growing season (April–October).

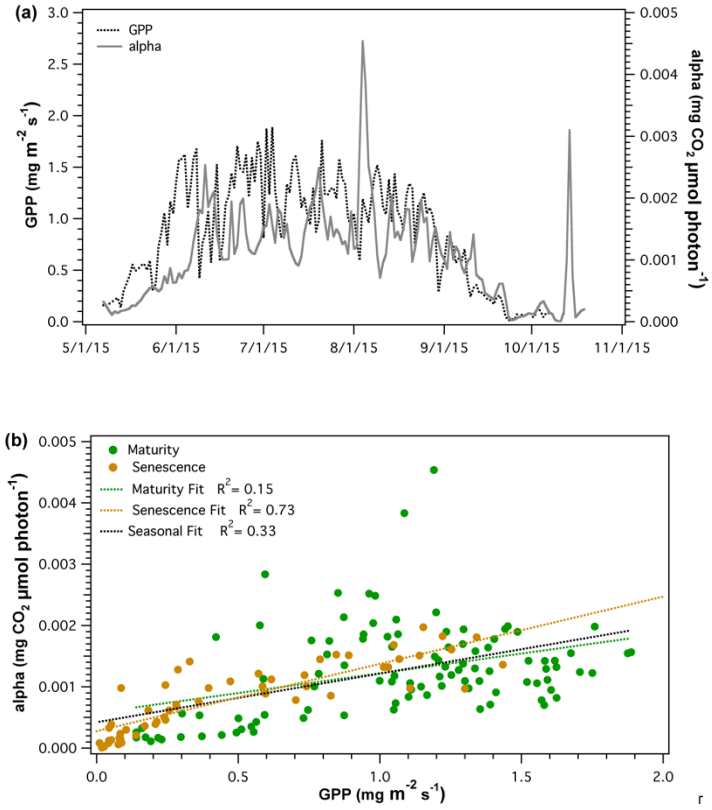

Figure 3.6. (**a**) Time series and (**b**) regression analysis of gross primary productivity (GPP) and apparent canopy quantum yield (alpha). Correlation between GPP and alpha was analyzed for the whole season (black), maturity (green), and leaf senescence (brown).

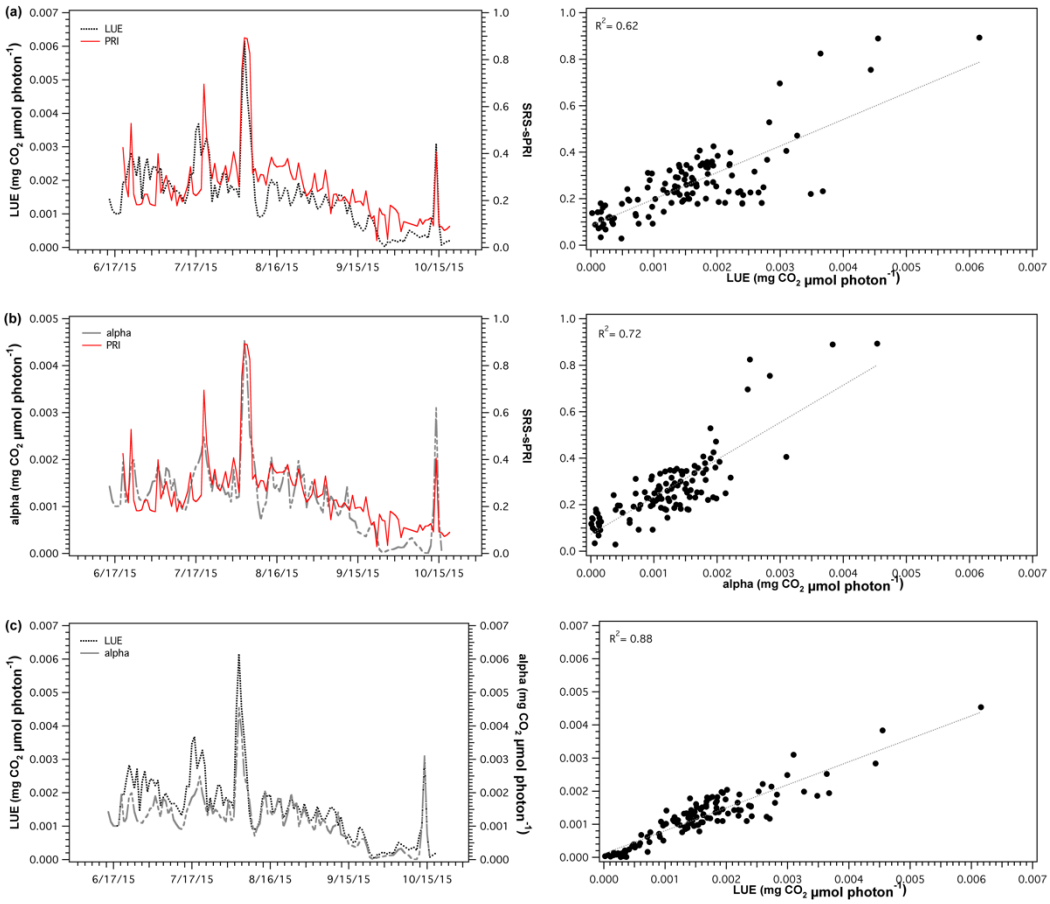

Figure 3.7. Time series (left panels) and regression plots (right panels) of (**a**) light use efficiency (LUE) and scaled photochemical reflectance index from SRS sensors (SRS-sPRI), (**b**) apparent quantum yield (alpha) and SRS-sPRI, and (**c**) LUE and α. Dotted lines in regressions plots (right panels) show linear regressions fitted to the data.

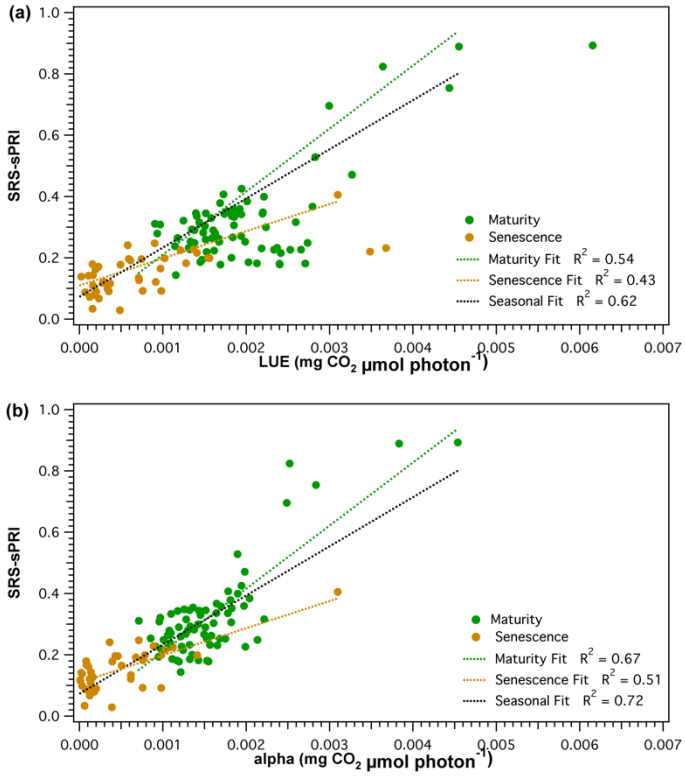

Figure 3.8. Seasonal (black), maturity (green), and leaf senescence (brown) correlations of scaled photochemical reflectance index from SRS sensors (SRS-sPRI) and (**a**) light use efficiency (LUE), and (**b**) apparent quantum yield (alpha). Dotted lines show linear fits.

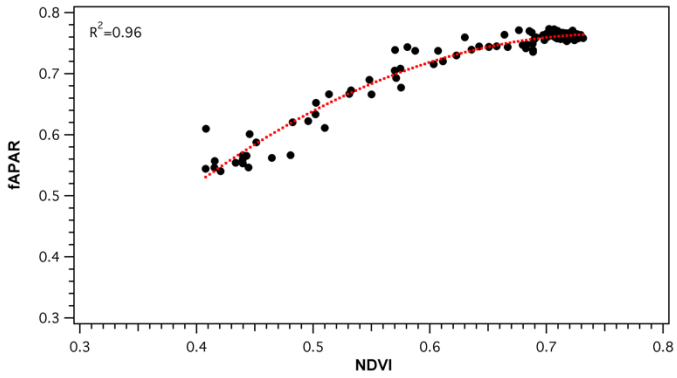

Figure 3.9. NDVI-*f*APAR relationships derived from daily values. NDVI was calculated from broadband spot radiometer sensors. *f*APAR was derived from the wireless sensor network (WSN) composing of 36 nodes measuring canopy transmitted light. Dotted line represents polynomial regression fitted to the data: y = -1.9596 χ^2 + 2.954x – 0.3484, R^2 = 0.96.

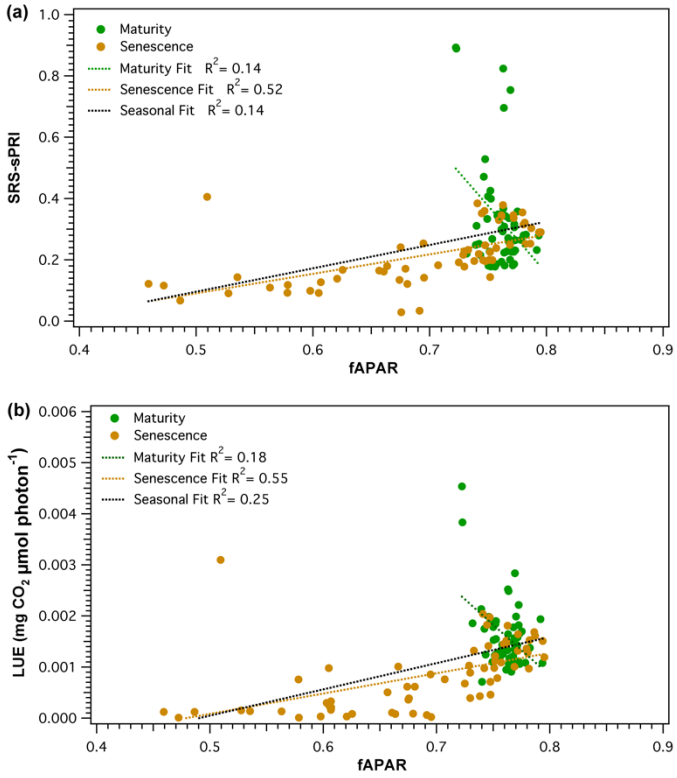

Figure 3.10. Relationship between fraction of absorbed photosynthetically active radiation (*f*APAR) and (**a**) scaled photochemical reflectance index from SRS sensors (SRS-sPRI), and (**b**) light use efficiency (LUE). Comparisons are shown for the combined season (black) as well separated into maturity (green) and leaf senescence (brown) phenologic stages.

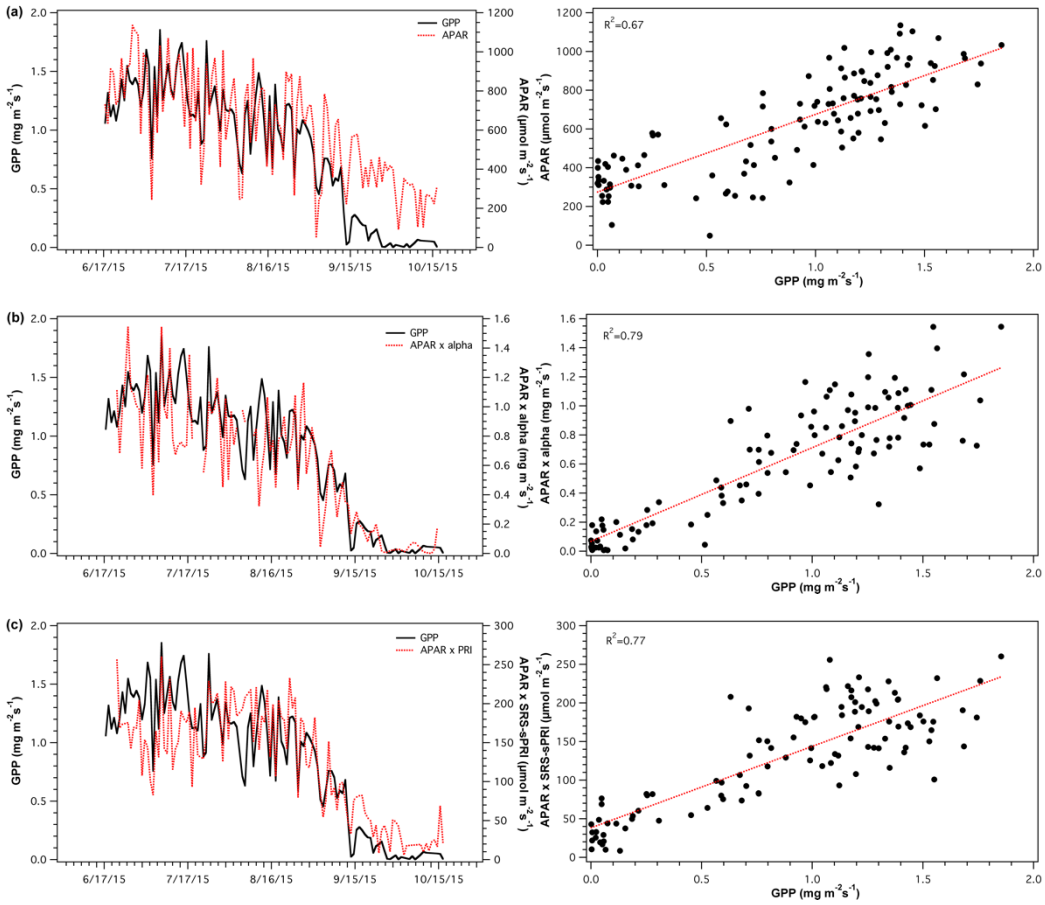

Figure 3.11. Time series (top panels) and regressions (bottom panels) of (**a**) absorbed photosynthetically active radiation (APAR) and gross primary productivity (GPP), (**b**) light use efficiency (LUE) model driven by apparent quantum yield (α) and GPP, and (**c**) light use efficiency (LUE) model driven by scaled photochemical reflectance index from SRS sensors (sPRI) and GPP

CHAPTER 4 – Effect of temporal aggregation and phenology on *LUE* model variables and productivity in two deciduous forests.

Abstract

The integration of optical and flux data requires temporal aggregation. In this study, we explore the effect of temporal aggregation of these two different data types by assessing the impact of various aggregation periods in the context of ecosystem productivity and its ecological relevance. Optical remote sensing and eddy covariance flux data collected over four years from a Tropical Dry Forest (TDF) and a Deciduous Boreal Forest (DBF) were used in the analysis. Light use efficiency model variables (PAR, $fAPAR_{green}$, $APAR_{green}$, and LUE) were derived, temporally aggregated over the diurnal period at 1hr increasing intervals and compared to gross primary productivity, derived from flux measurements. Temporal aggregation analysis was performed at the seasonal scale as well as divided by phenological stage (green-up, maturity, and senescence). Seasonal aggregation analysis showed little effect on $fAPAR_{green}$ derived from TDF and DBF. Aggregation of PAR, $APAR_{green}$ and LUE_{green} variables from TDF and DBF showed significant changes in correlation to GPP. Aggregation analysis as a function of optical phenology produced contrasting results to seasonal aggregations. This was especially the case for TDF fAPAR during green-up, where aggregation produced significant changes in correlation to GPP ($\Delta r^2 \approx 0.34\text{-}0.39$, $p < 0.05$). A relative importance analysis provided a quantitative measure of contribution by each LUE model variable towards ecosystem productivity. Relative importance analysis was done at both the seasonal level as well as with data divided by individual phenophases (green-up, maturity, and senescence). Previous knowledge of seasonal and phenological ecosystem functions was combined with relative importance metrics to put ecological context in our results. Findings validate the hypothesis that physiological and structural contributions to the LUE model change between vegetation and provides new evidence of an effect of environmental condition and phenology on LUE model parametrization.

4.1 Introduction

The systematic integration of optical remote sensing with eddy covariance datasets has provided the opportunity to explore in detail the mechanistic drivers of productivity operating at finer temporal and spatial scales (Gamon, 2015). The evaluation of the individual and combined processes allows for a deeper understanding of the variables driving seasonal carbon cycle dynamics and productivity modelling (Falge et al., 2002; Law et al., 2002). The integration of remote sensing and

micrometeorological data can be done using the light-use efficiency (LUE) model as the unifying concept. First proposed by Monteith (1972, 1977), the *LUE* model states that total yield, or productivity, can be quantified by the amount of Photosynthetically Active Radiation (PAR) absorbed by a given canopy, and the efficiency by which that radiation is transformed to fixed carbon over time. The model can be mathematically expressed as:

$$\text{Total Yield} = \varepsilon \int_0^t APAR\,dt \qquad (1)$$

where *APAR* (μmol m^{-2} s^{-1}) is the Absorbed Photosynthetically Active Radiation (μmol m^{-2} s^{-1}) by a given vegetation structure, and ε represents the physiological parameter of LUE. Conceptually, the LUE model can be separated into two components: one structural and another physiological (Gamon, 2015). APAR describes the structural component by quantifying the amount of vegetation present. LUE quantifies the physiological response of plants to changing environmental conditions (Monteith 1972, 1977). As such, the LUE model can be directly parameterized by remote sensing data and is conventionally expressed in terms of Gross Primary Productivity (GPP). Although it can be expressed using different formulations and parametrizations, the model is generally expressed as:

$$\begin{aligned} GPP &= (fAPAR \times PAR) \times LUE \\ &= (APAR) \times LUE \end{aligned} \qquad (2)$$

where fAPAR is the fraction of Absorbed Photosynthetically Active Radiation (fAPAR), and the PAR and ε terms are as stated previously. The primary connection between remote sensing and the LUE model is based on combining PAR and fAPAR measurements to determine the APAR term, providing a measure of potential photosynthetic activity by green vegetation (Sellers, 1985; Sellers et al., 1987; Hall et al. 1992; Gamon et al. 1995; Myneni and Williams, 1994; Gitelson and Gamon, 2015). LUE models using remote sensing have been used to estimate global productivity at various temporal and spatial dimensions including ecosystem and global scales (Potter et al., 1993; Prince and Goward, 1995; Landsberg and Waring, 1997; Cramer et al., 1999; Law et al., 2000; Coops et al., 2005). Traditionally, models have been parameterized at global scales and by vegetation type. However, current trends are moving away from vegetation specific parametrization and more towards biophysical conditions of a given ecosystem (Potter et al., 1993a; Yuan et al., 2007, 2010, 2014).

As research priorities continue to move towards exploring individual ecosystems and

functions, the integration of remote sensing and flux measurements represents an important development in multidisciplinary science; an approach that can provide significant insight into ecosystem functioning (Gamon, 2015). Remote sensing driven *LUE* models offer the ability to sample sites with high heterogeneity, complex topography, and other non-ideal sites for the eddy covariance technique (Running et al., 2004; Hilker et al., 2008). In turn, eddy covariance can provide direct physiological validation to remote sensing empirical observations. Integrated National Aeronautics and Space Administration (NASA) field campaigns, First International Satellite Land Surface Climatology Project Field Experiment (FIFE) (Sellers et al., 1992) and Boreal Ecosystem-Atmosphere Study (BOREAS) (Sellers et al., 1997), were the first large scale studies of remote sensing and flux integration towards a fuller understanding of ecosystem physiology and ecology. The integration of remotes sensing and flux data has been shown to provide greater insight into the underlying controls on ecosystem-atmospheric interactions than would be possible with either method applied independently (Gamon, 2015).

One of the challenges of integrating optical and flux data arises from the difference in their temporal scales. To realize a successful integration of remote sensing data and flux data, an in-depth assessment exploring temporal aggregation effects and its ecological relevance is necessary. To date, analysis of the effect of temporal aggregation on the LUE model is limited within the scientific body. Published studies have largely focused on the effect of aggregation on individual LUE variables. For the fAPAR variable, conventional wisdom has traditional assumed a that daily integrated measurements correlate to satellite-derived instantaneous measurements (Baret et al., 2011; Camacho et al.,2013; Martinez et al., 2013). However recent studies comparing ground fAPAR measurements to satellite derived products in boreal forest (Majasalmi et al., 2017; Putzenlechner et al., 2019) and Tropical Dry Forest (TDF) (Putzenlechner et al., 2019) suggest significant differences between instantaneous and diurnal aggregated fAPAR measurements. Likewise, studies comparing diurnal and midday LUE values, calculated over in a variety of ecosystems, showed them to be poorly correlated (Sims et al., 2005; Chen et al., 2009). The discrepancy between instantaneous and daily values for both the fAPAR and LUE variables put into question the reliability of point measurements (e.g. satellite collections) and highlights the need for a systematic analysis of the effect of temporal aggregation on the LUE model.

Functional responses of different vegetation in response to environmental limitations (Ustin and Gamon, 2010) has also been suggested as an additional complexity in the parametrization of the LUE model (Garbulsky et al., 2011; Gamon, 2015). In this context, Garbulsky et al. (2011) proposed

that the contributions of the structural and physiological components of the LUE model towards carbon fluxes should vary across ecosystems. Dominant component contribution would also relate to the hypothesis of vegetation *optical types* (Ustin and Gamon, 2010), where vegetation traits, canopy structure, and phenology affect the mechanisms of ecosystem productivity. Testing of Gabrulsky's et al. (2011) hypothesis has proven difficult due to the need for replicated (flux and optical) instrumentation and experimental design that is not common (Gamon, 2015).

To address the knowledge gaps mentioned above the objectives of this study are to (1) determine the effect of temporal aggregation on LUE model variables over the season and through the phenological stages (green-up, maturity, and senescence), and (2) identify the *LUE* model components that drive ecosystem productivity and how they change seasonally and through phenology. The analysis was done on datasets collected over 2 years from two different forest types, deciduous boreal forest (DBF) and tropical dry forest (TDF), instrumented with matching optical and flux sensors.

4.2 Materials and Methods

4.2.1 Study Sites

Data collected from two deciduous forest sites were used for this study (Table 4.1); the first site is a Canadian mixed boreal forest, and the second site is a Tropical Dry Forest (TDF) in Costa Rica. The Deciduous Boreal Forest (DBF) dataset spans the 2015 and 2016 growing seasons of an old-growth trembling aspen (*Populus tremuloides*) stand, collected at the Peace River Environmental Monitoring SuperSite (PR-EMSS) (Castro and Sanchez-Azofeifa, 2018). The PR-EMSS is located approximately 90km northwest of Peace River, Alberta, Canada (Figure 1a) (56° 44.635' N, 118° 20.635' W) and forms part of the Lower Foothills ecological unit, based on the provincial classification system (Alberta Environmental Protection, 1994; Natural Regions Committee, 2006). Key instrumentation components and deployment at the PR-EMSS include a 30m tower containing an eddy covariance and full meteorological station, providing detailed micrometeorological and biometric data of an old-growth *P. tremuloides* stand (Castro and Sanchez-Azofeifa, 2018). Proximal remote sensing sensors mounted above the canopy allow for the tracking of forest optical phenology and light (incoming and reflected) conditions used to derive greenness vegetation indices. An understory wireless sensor network (WSN) provided continuous transmitted Photosynthetically Active Radiation (PAR) quantities and was used to calculate the continuous fraction of Absorbed PAR (fAPAR) (Putzenlechner et al., 2019; 2020). The WSN was located within the flux footprint.

Further detail on site characteristics and instrumentation deployment at the PR-EMSS is discussed by Castro and Sanchez-Azofeifa (2018) and Putzenlechner et al. (2019; 2020).

TheTDF dataset was likewise composed of micrometeorological and proximal remote sensing data collected in an intermediate successional stage forest (10°44.206' N, 85°37.034 W) within the Santa Rosa National Park Environmental Monitoring SuperSite (SRNP-EMSS) during the 2013 to 2016 growing seasons (Castro et al. 2018). The SRNP-EMSS is located in the northwest province of Guanacaste, Costa Rica, and is part of the Area de Conservacion Guanacaste (ACG) conservation area. Similar to the PR-EMSS, the SRNP-EMSS site derived micrometeorological and biometric data from an eddy covariance system, and a fully instrumented meteorological station mounted on a 35m tower located within the forest stand. Phenological and canopy greenness changes were tracked through broadband spot radiometers mounted on a south-facing arm extending from another 35m tower located within the flux footprint. Also, within the flux footprint, a WSN measured canopy transmitted light dynamics that, combined with above canopy downwelling light conditions, allowed direct fAPAR calculations. Further detail on site characteristics and instrumentation deployment at the SRNP-EMSS can be found in Castro et al. (2018) and Putzenlechner et al. (2019; 2020).

4.2.2. Eddy Covariance Instrumentation Processing and partitioning

Identical eddy covariance (EC) systems were used to measure forest Net Ecosystem Exchange (NEE) (μmol $m^{-2}s^{-1}$) at both the DBF and TDF sites. Fluxes were measured through an integrated EC system as part of the CPEC200 system (Campbell Scientific, Logan, UT, USA). The system was composed of a close-path infrared gas analyzer (IRGA) (model EC155, Campbell Scientific Inc., Logan, UT, USA) and a three-dimensional sonic anemometer (model CSAT-3A, Campbell Scientific Inc., Logan, UT, USA), logged at a sampling frequency of 20 Hz through a CR3000 datalogger (Campbell Scientific, Logan, UT, USA).

EC data from both the DBF and TDF sites were processed using the post-acquisition software EdiRe (http://www.geos.ed.ac.uk/abs/research/micromet/EdiRe) and EddyPro Software (LI-COR Inc., Lincoln, NE, USA). Flux processing steps included time lag correction (Moore,1986), low and high-frequency losses due to attenuation in close path systems (Moncrieff et al., 1997), data de-spiking (Vickers and Marhart, 1997), double coordinate rotation (Finnigan et al., 2003), and Webb-Pearman-Leuning correction (Webb et al., 1980). Fluxes were calculated as 30-minute block averages. Diagnostic flags associated with the IRGA and sonic anemometer instruments were used to filter the flux datasets further and allowed the identification and removal of errors caused by

precipitation events. Filtered NEE datasets from the DBF and TDF sites were partitioned into gross primary productivity (GPP) and respiration (Reco) components through the use of light-response curves models outlined by Flanagan et al. (2005) and Hutyra et al. (2007), respectively. Hyperbolic functions derived from the light-response curves were used to calculate apparent quantum yield (α) values. Additional details on the DBF and TDF flux datasets can be found in Castro and Sanchez-Azofeifa (2018) and Castro et al. (2018), respectively.

4.2.3 Canopy Structure and Phenology

Upward and downward-looking quantum and pyranometer pairs installed above the canopy were used to calculate a broadband normalized difference vegetation index (NDVI). These spot radiometers provided continuous measurements at a logging interval of 10 minutes. Broadband NDVI was calculated as:

$$NDVI = \frac{(\rho PYR - \rho PAR)}{(\rho PYR + \rho PAR)} \quad (3)$$

where ρPYR is the solar radiation reflectance calculated as the ratio of upwelling:downwelling radiation from pyranometer pair; and ρPAR is the Photosynthetically Active Radiation (PAR) reflectance calculated as the ratio of upwelling:downwelling PAR sensor pair. Broadband NDVI indices have been shown to be accurate proxies of narrowband NDVI (Huemmrich et al., 1999). Seasonal NDVI changes were used to identify stages of green-up, maturity, senescence, and dormancy at the PR-EMSS and SR-EMSS study sites. Transitions between phenological stages were identified through the use of second derivative statistics.

4.2.4 Wireless Sensor Network (WSN) and fraction of absorbed PAR measurements

Both of the TDF and DBF WSNs consisted of self-powered nodes (model ENV-Link-Mini-LXRS, LORD MicroStrain, Cary, NC, USA) equipped with upward and downward quantum *PAR* sensors (model SQ-110, Apogee, Logan, UT, USA) with 180^{o} field of view. Nodes within the WSN were placed within the flux footprints of each site and were synchronized to log simultaneously every 10 minutes, providing instantaneous measurements of transmitted PAR and soil reflected PAR throughout the seasons. To ensure the representative sampling of light variability and overcome possible bias effect of sampling location, both WSNs consisted of more than 10 nodes (Widlowski,

2010; Putzenlechner et al. 2019). The PR-EMSS WSN was comprised by 36 nodes, while the SRNP-EMSS WSN consisted of 14 nodes. To maximize sensing area coverage and sensor connectivity, both networks were arranged in a hexagonal pattern (Mortazavi et al., 2014; Younis and Akkaya, 2008). Nodes were spaced every 20m to minimize the effect of spatial autocorrelation based on sensing footprint (Montgomery and Chazdon, 2001).

Radiation dynamics measured through the WSNs were used in combination with above canopy radiation measurements to calculate the fraction of absorbed photosynthetically active radiation (fAPAR) for each node at each collection site. A 4-flux fAPAR was calculated using the equation:

$$fAPAR = 1 - t - r + (t \times r_s) \quad (4)$$

where *t* is the fraction of transmitted radiation, *r* is the reflected radiation from the canopy, and *rs* is the soil reflectance component. To better match the spatial area of the sites' flux footprints, individual node fAPAR values were spatially averaged over the whole network. Noting that not all transmitted light is used for photosynthesis, the photosynthetic component of vegetation, $fAPAR_{green}$, was calculated as (Hall et al., 1992):

$$fAPAR_{green} = fAPAR_{total} \times \left({}^{NDVI_{green}}\!/_{NDVI_{total}} \right) \quad (5)$$

where green *NDVI* is the photosynthetically functional component of the total *NDVI*. Equation (5) was derived as a variant of the common method (Hall et al., 1992) for calculating the photosynthetic ($fAPAR_{green}$) fraction of transmitted light that uses the ratio of LAI_{green}:LAI_{total}. This *NDVI* based method was chosen to maintain the high temporal resolution of derived $fAPAR_{green}$ that would otherwise require high levels of interpolation by relying on monthly LAI collections.

4.2.5 Absorbed PAR, Light Use Efficiency (LUE) variables, and temporal aggregation

The Absorbed Photosynthetically Active Radiation (APAR) was calculated as the product of downwelling PAR and fAPAR. APAR was expressed as $APAR_{total}$ and $APAR_{green}$ at the PR-EMSS and the SRNP-EMSS, respectively.

The light use efficiency variable provides a quantitative measure of the efficiency by which absorbed radiation is used to fix carbon by vegetation, and is calculated as (Monteith, 1972; Monteith and

Moss, 1977):

$$LUE_{green} = \frac{GPP}{(fAPAR_{green} \times PAR)} = \frac{GPP}{APAR_{green}} \quad (6)$$

GPP was derived from the eddy covariance datasets. LUE values were expressed as LUE_{green}. The effect of temporal aggregation on LUE model variables was explored to determine how to best construct the model. The LUE model was expressed as:

$$GPP = \overbrace{(fAPAR \times PAR)}^{\text{III}} \times LUE \quad (7)$$
$$\text{[I]} \quad \text{[II]} \quad \text{[IV]}$$

Roman numerals noted in equation (7) denote the sequence by which the different LUE model terms were aggregated. Each of the continuous LUE model variables (fAPAR, PAR, APAR, and LUE) were temporally aggregated with increasing periods starting with instantaneous midday readings and increasing sequentially by one hour, centred at midday, over the diurnal cycle. For clarity, a conceptual figure (Figure 4. S1) has been provided in the supplementary material section that better illustrates the temporal aggregation process.

4.2.6 Analysis of LUE model variable contributions to productivity

To explore the relationship between LUE model variables on a seasonal basis, a Principal Component Analysis (PAC) was applied to centred and scaled 8hr aggregated GPP, $fAPAR_{green}$, PAR, and LUE_{green} datasets from the SRNP-EMSS and PR-EMSS. The $APAR_{green}$ variable was not included in the analysis to avoid the analogous contribution of canopy structure changes already represented by the $fAPAR_{green}$ term. A relative importance (RI) analysis based on the LUE model (equation 7) was preformed to explore the quantitative contribution of each LUE model variable to productivity (GPP). RI analysis was preformed at the seasonal scale as well as within individual phenological stages: green-up, maturity, and senescence. The Lindeman, Merenda and Gold (LMG) relative importance model (Chevan and Sutherland, 1991) was used as it accounts for the direct and combined effects of each regressor allowing a more effective r^2 decomposition (Gromping, 2006).

4.3 Results

4.3.1 Effect of Temporal Aggregation on Seasonal LUE Model Variables

Data aggregation had varying impacts on the different LUE model variables, and these were quantified for each variable through the comparison of coefficients of determination (r^2 values) for each aggregation period. Evaluation of the impact of $fAPAR_{green}$ aggregation for the 2013 growth season (Figure 4.1a) shows a relatively small increase in correlation ($\Delta r^2 = 0.03$) as aggregation was increased from 30 minutes to two hours. This increase was followed by a slight continuous decrease as aggregation was increased to 12hrs (full diurnal cycle). The change in r^2 between the maximum ($r^2 = 0.66$ at 2hr aggregation) and minimum ($r^2 = 0.57$ at 12hr aggregation) was statistically significant ($p < 0.05$). r^2 values for the 2014 $fAPAR_{green}$ aggregation were greater than those from the 2013 season (Figure 4.1b), likely associated with the added change in $fAPAR_{greeen}$ observed during the 2014 drought. Aggregation of the 2014 $fAPAR_{green}$ dataset showed an initial increase until 6hrs, followed by a gentle decline as periods increased. Variability in r^2 values (r^2 range of 0.73-0.75, $\Delta r^2 = 0.02$) throughout the aggregation analysis was smaller than in 2013, and r^2 changes were not statistically significant ($p > 0.05$). Similar patterns were observed for the 2015 and 2016 DBF datasets (Figure 4.1c, d), with no statistical difference associated with aggregation ($p > 0.05$). The lowe $fAPAR_{green}$-GPP correlation values at the PR-EMSS observed in 2016 are likely associated with the snow event observed during mid-senescence that accelerated leaf drop.

The testing of PAR aggregation showed a consistent generalized pattern across both biomes and seasons (Figure 4.2). Aggregation lead to continuous gradual increases in r^2, starting from minimum values that corresponded to instantaneous measurements (30 minutes), reaching maximum correlations at 8-10hrs, and followed by a slight decrease towards the total diurnal cycle. Due to the high variability of diurnal PAR values, this pattern was expected. Changes in r^2 due to aggregation totaled 0.092, 0.14, 0.12, and 1.1 for the 2013 (TDF), 2014 (TDF), 2015 (DBF), and 2016 (DBF) datasets, respectively, and these changes were statistically significant ($p < 0.05$).

The patterns for aggregation of $APAR_{green}$ (Figure 4.3) emerged as a combination of the patterns observed from the analysis of PAR and $fAPAR_{green}$ variables. As in the PAR analysis, aggregation lead to significant ($p < 0.05$) changes in r^2 values in all datasets and optimal aggregation periods were 8hrs (2013), 10hrs (2014), and 7hrs (2015 and 2016). Temporal aggregation was observed to have the greatest impact on the LUE_{green} variable (Figure 4.4). Both years at the SRNP-EMSS datasets showed significant initial increase in r^2 values during the first four hours of

aggregation (2013 $\Delta r^2 = 0.31$, 2014 $\Delta r^2 = 0.20$). This upsurge was followed by a slow but continuous increase, reaching maximum values at 8hrs ($r^2 = 0.70$ and $r^2 = 0.61$ for 2013 and 2014, respectively). Changes in LUE due to aggregation observed between instantaneous measurements and 8hr binned datasets were statistically significant ($p < 0.05$). LUE_{green} derived from the 2015 and 2016 DBF datasets was similarly affected by temporal aggregation. Major gains in r^2 metrics were observed during the first 5hrs (2015) and 4hrs (2016) of aggregation. Correlations for the 2015 and 2016 DBF seasons reached a maximum 9hrs ($r^2 = 0.61$) and 10hrs ($r^2 = 0.53$), respectively.

4.3.2 Effect of Temporal Aggregation and Phenology on LUE Model Variables

Aggregation analysis was also performed by dividing each season into phenological stages, specifically: green-up, maturity, and senescence. The purpose of incorporating phenology was to add incorporate the underlying factors that impact productivity within each growth stage (Castro et al., 2018; Castro and Sanchez-Azofeifa, 2018). Results from the aggregation analysis by phenology are summarized in Tables 4.2-4.5. Aggregation of TDF $fAPAR_{green}$ during green-up had a significant impact on correlations to GPP. Temporal aggregation resulted in changes in r^2 of 0.39 and 0.34 for the 2013 and 2014 seasons, respectively. These results stand in contrast to the insensitivity to aggregation observed in seasonal TDF $fAPAR_{green}$. Similar to seasonal analysis results, aggregation of 2013 maturity and senescence $fAPAR_{green}$ also exhibited limited changes in r^2 values. $fAPAR_{green}$ aggregation during the 2014 maturity showed significant changes ($p<0.05$), likely driven by changes in canopy structure observed during the 2014 drought (Castro et al., 2018). Results from the phenological assessment of $fAPAR_{green}$ aggregation for the 2015 and 2016 DBF seasons proved to be insensitive to temporal aggregation, and trajectories were similar to those resulting from the seasonal analysis. Phenological aggregation of PAR showed similar results to those observed during seasonal analysis as well. High variability in PAR in TDF 2014 maturity and DBF green-up (2015 and 2016) lead to very poor correlations with GPP and, as such, the effect of aggregation is hard to interpret.

The effect of aggregation on $APAR_{green}$ varied with phenology. At the TDF sites, aggregation during green-up and maturity resulted in significant changes ($p<0.05$) in r^2 values when comparing minimum and optimal aggregation periods. However, during senescence, $APAR_{green}$ for the 2013 and 2014 seasons was insensitive to aggregation. $APAR_{green}$ at the DBF sites also proved to be insensitive to aggregation during green-up, and during senescence of the 2014 season. $APAR_{green}$ still remained correlated to productivity throughout all the phenological stages. LUE_{green} remained sensitive to

aggregation ($p<0.05$) through all growth stages for all datasets. The largest impacts of aggregation on LUE were observed during senescence, where changes in r^2 values totalled 0.62, 0.27, 0.62, and 0.12 for 2013, 2014, 2015, and 2016 seasons, respectively.

4.3.3 LUE Model Variables contributions to productivity

Results from PCA analysis for the two primary contributing components are displayed in Figure 4. 5. PCA biplots show a similar correlation of variables within each study site. PC1 and PC2 represent 87.7%, 87.0%, 89.4%, and 93.1% of total variance for the 2013, 2014, 2015 and 2016 growing seasons, respectively. In TDF, the near orthogonal angle between GPP and PAR and opposing directions show a negative and poor correlation between these variables. In DBF, LUE_{green} and PAR variables appear to be poorly correlated; however, all variables seem to be correlated with GPP. Data pairs from TDF and DBF datasets show a sequential ordering according to the day of year (or day since start of season in TDF as seasons cover different calendar years), and indicate strong seasonality differentiating different stages of phenology.

Relative importance analysis of TDF growth seasons 2013 (Figure 4.6) and 2014 (Figure 4.7) showed a combination variable contributions accounting for 90% and 83% of GPP variance, respectively. In 2013, LUE_{green} appeared to be the most dominant variable, accounting for 45.6% of variance. RI analysis by phenology produced distinct results from those resulting from the seasonal analysis. During green-up ((Figure 4.6b and 7b), $fAPAR_{green}$ was the main driving variable of productivity (51.5%) followed by PAR (36.0%). $fAPAR_{green}$ and PAR relative contributions were significantly correlated. During maturity (Figure 4.6c), PAR accounted for over half (54.7%) of the variability in GPP, while LUE_{green} also had a considerable contribution to productivity with 39.3% of variability. 2013 senescence (Figure 4.6d) saw $fAPAR_{green}$ and LUE_{green} combining to account for approximately 87% of the total predictive ability of the combined variables (96.13%). RI analysis of the 2014 season resulted in different patterns to those observed in 2013. Over the season (Figure 4.7a), $fAPAR_{green}$ was the main driver of productivity with a 54.6% contribution. LUE_{green} remained an important driving variable throughout the season. During the 2014 maturity (Figure 4.7b), $fAPAR_{green}$ became a much more dominant variable and saw PAR influence diminish to negligible levels. Analysis of 2014 senescence relative importance variables and contributions (Figure 4.7d) were akin to those from 2013.

RI analysis of the DBF growth seasons 2015 and 2016 (Figure 4.8 & 4.9) showed similar patterns in variable importance and contributions at both the seasonal and phenological level. The

most notable difference was in the reduced importance of $fAPAR_{green}$ over the course of the 2016 season (variability contribution of 29.7% vs 43.8%) (Figure 4.8b). A slight increase of approx. 5% in 2016 LUE_{green} was also observed, but this change was within the 95% confidence interval of 2015 LUE_{green} importance metrics. During the 2015 and 2016 green-up, both LUE_{green} and $fAPAR_{green}$ combined to account for 90% and 81.2% of productivity variability, respectively (Figure 4.8b & 4.9b). In contrast, PAR was the dominant variable during maturity accounting for 74.7% of 2015 and 59.7% of 2016 productivity (Figure 4.8c & 4.9c). LUE_{green} also appeared to play a role (39% RI value) during 2016 maturity, pointing to possible periods of canopy stress during this time. RI analysis of DBF senescence followed very similar predictor results as during green-up (Figure 4.8d & 4.9d).

4.4 Discussion

4.4.1 Effect of temporal aggregation: seasonal scale.

Temporal aggregation analysis demonstrated the effect that temporal aggregation can have on the LUE model. This is significant when observed against estimations of productivity derived from remote sensing observations (Figures 4.1-4.4). This was most evident in the seasonal aggregation of LUE_{green} of both TDF and DBF study sites, where results indicated a significant change in correlation (r^2) values during the first 4 to 5 hours of aggregation. Instantaneous changes associated with non-photochemical quenching (NPQ) processes drive short term variability as fast (facultative) xanthophyll pigment changes respond to saturating light conditions (Deming-Adams and Adams, 1992; Gamon and Berry, 2012). Although these fast NPQ changes are essential in characterizing the physiological state of vegetation, high variability can occlude diurnal trends. Comparison of diurnal and midday LUE_{green} aggregation correlations show them to be significantly different ($p<0.05$), and results coincide with other studies showing a lack of correlation between midday and daily LUE values (Sims et al., 2005; Chen et al., 2009). These findings are relevant to the ongoing discussion on LUE calculations from satellite data (Drolet et al., 2005; Grace et al., 2007; Coops et al., 2010; Huemmrich et al., 2019) and how representative midday satellite LUE estimates are of daily LUE values.

The effect of aggregation on PAR resulted in a progressive rise of r^2 values. The observed increase in correlation to GPP with aggregation can be attributed to the averaging out of high diurnal variability in PAR measurements, especially at the TDF site where frequent rain and cloud cover lead

to dynamic illumination conditions (Yang and Slingo, 2001). The effect of aggregation on APAR is inherently influenced by downwelling radiation variability (Gu et al., 2002; Chen et al., 2009). This is important to consider in sites with variable sky illumination, such as in our TDF and DBF. Other studies have qualified radiation as diffused and direct light and used to derived APAR and fAPAR products and note that diffused light can increase bias in PAR products (Leuchner et al., 2011; Widlowski, 2010; Putzenlechner et al., 2019). However, studies on photosynthetic efficiency have shown LUE enhancement under diffused light (Gu et al., 2002; Choudhurry, 2001; Alton, 2008); and, as such, imply that filtering out diffused light conditions during LUE model parametrization would remove relevant photosynthetic events from productivity calculations. Therefore, special consideration should be taken to include measurements under all sky conditions that accounts for the complete impact of sky illumination on LUE model variables, as has been done in this study.

4.4.2 Effect of temporal aggregation: phenology scale.

Seasonal aggregation analysis resulted in consistent results regardless of forest type. However, aggregation by phenology produced some contrasting results to that of the seasonal analysis, as well as differences between the study sites. For example, aggregation of PAR during 2014 maturity showed no significant gains in r^2 with aggregation increases. Clear skies associated with drought conditions in 2014 reduced variability in illumination conditions that is typical through the rainy season in TDF (Yang and Slingo, 2001; Castro et al., 2018a). The lack of variability would reduce the averaging power of aggregation and likely accounts for the insensitivity of 2014 maturity PAR to temporal aggregation. Aggregation of $fAPAR_{green}$ by phenology also produced contrasting results to those observed in seasonal analysis, as observed during the 2013 and 2014 green-up. High variability in fAPAR during the start of the season is expected as the TDF goes from leafless to maximum leaf flush within 19-21 days, representing large changes in canopy structure (Castro et al., 2018). Contributing to the green-up variability in fAPAR is the underlying effect of variability in PAR as incoming radiation is a variable within the fAPAR formulation. As such, illumination variability due to common precipitation events during green-up would add to fAPAR variability and the effect of temporal aggregation. The changes in aggregation effects observed from the phenological analysis suggests the importance of considering possible functional response of vegetation during each phenological stage, and the need to consider changes in environmental limitations due to ecosystem disturbances such as droughts. The separate responses to aggregation observed throughout the phenological analysis compared to seasonal analysis patterns show the need to understand how

underlying mechanisms of productivity affect productivity and change through the phenological cycle. PCA analysis also points to the variability of influence associated with seasonality in LUE model parametrization. PCA vectors appeared to be weighted towards data points associated with maturity. For ecosystems where maturity represents a large portion of the growth cycle, as is the case in our TDF and DBF sites, seasonal correlations and responses to aggregation can be biased towards the underlying forces driving productivity during this phenological stage.

4.4.3 LUE model variable contributions to productivity

Resulting relative importance patterns from the different phenological stages can be explained in the context of the ecological processes at play during green-up, maturity, and senescence. TDF green-up is characterized by large canopy structure changes, as the canopy transitions from leafless to fully vegetative in a short period of time (approx. 20 days) (Castro et al., 2018). During this time, limiting variables to productivity, associated with water availability (Becknell et al., 2012; Reich and Borchet, 1982; Castro et al., 2018), do not constrain productivity due to regular precipitation events. As such, RI results from TDF green-up are as expected and identify $fAPAR_{green}$ as the main driver of productivity. Transition into maturity sees canopy structure reach maximum levels and remain plateaued until senescence (Castro et al., 2018). Under normal conditions, we would expect to see RI of maturity $fAPAR_{green}$ having little influence on productivity, as seen in 2013. However, a drought event during 2014 maturity lead to changes in canopy greenness and explains the uncharacteristic high relative importance of fAPARgreen during this period. TDF senescence is characterized by limited water resources that result in leaf drop (Borchert 1994, Reich and Borchert 1984). The combination of importance from $fAPAR_{green}$ and LUE_{green} observed in 2013 and 2014 senescence is explained by these canopy changes and vegetation stress caused by limiting water availability.

During the early growing season DBF phenology is largely controlled by temperature, where cool temperatures limit productivity (Chen et al., 2000). The combination of limited photosynthetic capacity, associated with low temperatures (Landsberg, 1986), and significant changes in canopy structure help explain results from the RI analysis that indicated LUE_{green} and $fAPAR_{green}$ as the main drivers of productivity during green-up. During phenology maturity, PAR was observed as the main driver of productivity for both 2015 and 2016 growing seasons. These results support by previous observations showing strong correlation of average diurnal patterns of PAR and GPP from the PR-EMSS site during summer months (Castro and Sanchez-Azofeifa, 2018). During late summer, DBF photosynthesis rates have been shown to decrease due to reduced illumination from contracting

diurnal periods and decreasing temperatures (Coursolle et al., 2006). As leaves reach a critical carbon balance and productivity becomes negative (respiration becomes a net cost), leaf-fall is triggered (Doi and Takahashi, 2008). The decreases in photosynthetic rates and onset leaf drop during senescence would be represented within the LUE model by changes in LUE and fAPAR, respectively. This would explain the high relative importance values of $fAPAR_{green}$ and LUE_{green} observed during the 2015 and 2016 senescence.

The replicated instrumentation at the PR-EMSS and SRNP-EMSS made these sites ideal for the testing of Garbulsky's et al. (2007) hypothesis. Our findings validated the hypothesis that the contributions of the physiological and structural component of the LUE model can change between vegetation and environmental conditions. Furthermore, our results extend this concept by suggesting that LUE model components can also change throughout vegetation phenology as environmental conditions (e.g. disturbances) impact an ecosystem's functional response. The difference in patterns between seasonal and phenological analysis suggests that the parametrization of the LUE model could better represent ecosystem functions if the model was parameterized by phenological stages.

4.5 Conclusion

As we consider the impact of data aggregation on the *LUE* model accuracy, it is also important to consider the impact of phenology and the ecosystem functional responses that characterize the dominant contributions affecting productivity. LUE model productivity calculated for phenology stages where canopy changes are prominent will be significantly affected by aggregation of variables associated with canopy structure (e.g. *NDVI, fAPAR, APAR*). Conversely, aggregation of *LUE* becomes of greater importance in biomes and phenological stages driven by ecophysiological changes, as seen in the TDF maturity and DBF senescence. Results from this study call for the incorporation of aggregation methodologies and consideration of phenological changes in productivity mechanisms in *LUE* modeling parametrization. Furthermore, this study illustrates how the integration of flux and remote sensing data can help to achieve a better understanding of underlying processes that can result in more accurate ecosystem productivity calculations.

4.6 References

Alberta Environmental Protection (1994). Natural Regions and Subregions of Alberta: A Summary; Publ. I/531 and Map, 1 Sheet; Alberta Environmental Protection: Edmonton, AB, Canada.

Alton, P. B. (2008). Reduced carbon sequestration in terrestrial ecosystems under overcast skies compared to clear skies. Agricultural and Forest Meteorology, 148(10), 1641-1653.

Becknell, J.M., Kucek, L.K. and Powers, J.S., (2012). Aboveground biomass in mature and secondary seasonally dry tropical forests: A literature review and global synthesis. Forest Ecology and Management, 276, pp.88-95.

Baret, F., Makhmara, H., Lacaze, R., Smets, B., (2011). BioPar Product User Manual LAI,FAPAR, FCover, NDVI Version 1 From SPOT/VEGETATION Data.

Borchert, R., (1994). Soil and stem water storage determine phenology and distribution of tropical dry forest trees. Ecology, 75(5), pp.1437-1449.

Camacho, F., Cernicharo, J., Lacaze, R., Baret, F., Weiss, M., (2013). Geov1: lai, Fapar essential climate variables and FCOVER global time series capitalizing over existing products. Part 2: validation and intercomparison with reference products. Remote Sens. Environ. 137, 310–329.

Castro, S., & Sanchez-Azofeifa, A. (2018). Testing of Automated Photochemical Reflectance Index Sensors as Proxy Measurements of Light Use Efficiency in an Aspen Forest. Sensors, 18(10), 3302.

Castro, S. M., G. A. Sanchez-Azofeifa, and H. Sato. (2018). “Effect of Drought on Productivity in a Costa Rican Tropical Dry Forest.” Environmental Research Letters 13(4).

Chen, J.M., Chen, W., Liu, J. & Cihlar, J. (2000) Annual carbon balance of Canada’s forests during

1895–1996. Global Biogeochemical Cycles, 14, 839–850.

Chen, J., Shen, M., & Kato, T. (2009). Diurnal and seasonal variations in light-use efficiency in an alpine meadow ecosystem: causes and implications for remote sensing. Journal of Plant Ecology, 2(4), 173-185.

Chevan A, Sutherland M (1991). "Hierarchical Partitioning." The American Statistician, 45, 90–96.

Choudhury, B.J. (2001). Estimating gross photosynthesis using satellite and ancillary data: approach and preliminary results. Remote Sensing Environ. 75:1–25.

Coursolle, C., Margolis, H.A., Barr, A.G., Black, T.A., Amiro, B.D., McCaughey, J.H., Flanagan, L.B., Lafleur, P.M., Roulet, N.T., Bourque, C.P.A., Arain, M.A., Wofsy, S.C., Dunn, A., Morgenstern, K., Orchansky, A.L., Bernier, P.Y., Chen, J.M., Kidston, J., Saigusa, N. & Hedstrom, N. (2006) Late-summer carbon fluxes from Canadian forests and peatlands along an east-west continental transect. Canadian Journal of Forest Research, 36, 783–800.

Coops, N. C., Waring, R. H., & Law, B. E. (2005). Assessing the past and future distribution and productivity of ponderosa pine in the Pacific Northwest using a process model, 3-PG. Ecological Modelling, 183(1), 107-124.

Coops, C., Hilker, T., Hall, F.G., Nichol, C.J., Drolet G.G. (2010). Estimation of light-use efficiency of terrestrial ecosystems from space: a status report. Bioscience, 60: 788-797

Cramer, W., Kicklighter, D. W., Bondeau, A., Iii, B. M., Churkina, G., Nemry, B., ... & Intercomparison, T. P. O. T. P. N. M. (1999). Comparing global models of terrestrial net primary productivity (NPP): overview and key results. Global change biology, 5(S1), 1-15.

Deming-Adams B, Adams WW III (1992) Photoprotection and other responses of plants to high light stress. Annu Rev Plant Physiol Plant Mol Biol 43:599–626

Doi, H. & Takahashi, M. (2008) Latitudinal patterns in the phenological responses of leaf colouring and leaf fall to climate change in Japan. Global Ecology and Biogeography, 17, 556– 561.

Drolet, G.G.; Huemmrich, K.F.; Hall, F.G.; Middleton, E.M.; Black, T.A.; Barr, A.G.; Margolis, H.A., (2005). A MODIS-derived photochemical reflectance index to detect inter-annual variations in the photosynthetic light-use efficiency of a boreal deciduous forest. Remote Sens. Environ. 98, 212–224

Gamon, J. A. (2015). Reviews and syntheses: Optical sampling of the flux tower footprint.

Gamon, J. A.,Field, C.B., Goulden, M., Griffin, K., Hartley, A., Joel, G., Peñuelas, J., Valentini, R. (1995). Relationship between NDVI, canopy structure, and photosynthesis in three Californian vegetation types. Ecological Applications, 5: 28-41.

Gamon, J.A., & Berry, J.A. (2012). Facultative and constitutive pigment effects on thePhotochemical Reflectance Index (PRI) in sun and shade conifer needles. Israel. Journal of Plant Sciences, 60: 85–95.

Garbulsky, M.F.; Peñuelas, J.; Gamon, J.; Inoue, Y.; Filella, I., (2011). The photochemical reflectance index (PRI) and the remote sensing of leaf, canopy and ecosystem radiation use efficiencies: A review and meta-analysis. Remote Sens. Environ, 115, 281–297

Gitelson, A.A.; Gamon, J.A., (2015). The need for a common basis for defining light-use efficiency: Implications for productivity estimation. Remote Sens. Environ., 156, 196–201.

Grace J., Nichol, C., Disney, M., Lewis, P., Quaife, T., Bowyer, P. (2007). Can we measure terrestrial photosynthesis from space directly, using spectral reflectance and fluorescence? Global Change Biology, 13:1487-1497.

Grömping, U. (2006). Relative importance for linear regression in R: the package relaimpo. Journal of statistical software, 17(1), 1-27.

Gu, L., Baldocchi, D., Verma, S. B., Black, T. A., Vesala, T., Falge, E. M., & Dowty, P. R. (2002). Advantages of diffuse radiation for terrestrial ecosystem productivity. Journal of

Geophysical Research: Atmospheres, 107(D6), ACL-2.

Hilker, T., Coops, N. C., Wulder, M. A., Black, T. A., & Guy, R. D. (2008). The use of remote sensing in light use efficiency based models of gross primary production: A review of current status and future requirements. *Science of the total environment*, *404*(2-3), 411-423.

Huemmrich, K. F., Campbell, P., Landis, D., & Middleton, E. (2019). Developing a common globally applicable method for optical remote sensing of ecosystem light use efficiency. Remote Sensing of Environment, 230, 111190.

Hutyra, L.R., Munger, J.W., Saleska, S.R., Gottlieb, E., Daube, B.C., Dunn, A.L., Amaral, D.F., De Camargo, P.B. and Wofsy, S.C., (2007). Seasonal controls on the exchange of carbon and water in an Amazonian rain forest. Journal of Geophysical Research: Biogeosciences, 112(G3).

Falge, E., Baldocchi. D., Tenhunen, J., Aubinet, M., Bakwin, P., Berbigier, P., Bernhofer, C., Burba, G., Clement, R., Davis, K.J. (2002). Seasonality of ecosystem respiration and gross primary production as derived from FLUXNET measurements. Agricultural and Forest Meteorology, 113: 53-74.

Finnigan, J.J., R. Clement, Y. Mahli, R. Leuning, H.A. Cleugh. (2003). A re-evaluation of long-term flux measurement techniques. Part I: averaging and coordinate rotation, Boundary-Layer Meteorology, 107, pp.1-48

Flanagan, L.B.; Johnson, B.G., (2005). Interacting effects of temperature, soil moisture and plant biomass production on ecosystem respiration in a northern temperate grassland. Agric. For. Meteorol., 130, 237–253.

Landsberg, J.J., (1986). Physiological Ecology of Forest Production. Academic Press, London, pp. 165–178.

Landsberg J. J., Waring R. H., (1997). A generalized model of forest productivity using simplified

concepts of radiation-use efficiency, carbon balance and partitioning. Forest Ecology and Management, 95:209-228.

Law, B. E., Waring, R., Anthoni, P. M., & Aber, J. D. (2000). Measurements of gross and net ecosystem productivity and water vapour exchange of a Pinus ponderosa ecosystem, and an evaluation of two generalized models. Global Change Biology, 6(2), 155-168.

Law, B.E., Falge, E., Gu, L., Baldocchi, D.D., Bakwin, P., Berbigier, P., Davis, K., Dolman, A.J., Falk, M., Fuentes, J.D. (2002). Environmental controls over carbon dioxide and water vapor exchange of terrestrial vegetation. Agricultural and Forest Meteorology, 113: 97-120.

Leuchner, M., Hertel, C., Menzel, A., (2011). Spatial variability of photosynthetically active radiation in European beech and Norway spruce. Agric. For. Meteorol. 151, 1226–1232.

Natural Regions Committee, (2006). Natural Regions and Subregions of Alberta. Compiled by D.J. Downing and W.W. Pettapiece. Government of Alberta. Pub. No. T/852.

Majasalmi, T., Stenberg, P., RAUTIAINEN, M., 2017. Comparison of ground and satellite based methods for estimating stand-level fPAR in a boreal forest. Agric. For. Meteorol. 232, 422–432.

Martínez, B., Camacho, F., Verger, A., García-Haro, F.J., Gilabert, M.A., (2013). Intercomparison and quality assessment of MERIS, MODIS and SEVIRI FAPAR.

Moore, C.J. (1986). Frequency response corrections for eddy correlation systems. Boundary-Layer Meteorol, 37: 17-35.

Moncrieff, J.B., Massheder, J.M., De Bruin, H., Elbers, J., Friborg, T., Heusinkveld, B., Kabat, P., Scott, S., Soegaard, H. and Verhoef, A., (1997). A system to measure surface fluxes of momentum, sensible heat, water vapour and carbon dioxide. Journal of Hydrology, 188, pp.589-611.

Montgomery, R.A., Chazdon, R.L., (2001). Forest structure, canopy architecture, and light forest

structure, canopy architecture, and light transmittance in tropical wet forests. Ecology 82, 2707–2718.

Monteith, J.L., (1972) Solar radiation and productivity in tropical ecosystems. J. Appl. Ecol., 9, 747–766.

Monteith, J.L., (1977). Climate and the efficiency of crop production in Britain. Philos. Trans. R. Soc. Lond. B, 281, 277–294.

Mortazavi, S.H., Salehe, M., MacGregor, M.H., (2014). Maximum WSN coverage in environments of heterogeneous path loss. International Journal of Sensor Networks 16, 185–198.

Myneni, R.B.; Williams, D.L. (1994). On the relationship between FAPAR and NDVI. Remote Sens. Environ., 49, 200–211.

Prince, S.D. and Goward, S.N. (1995). Global primary production: a remote sensing approach. Journal of Biogeography 22: 815–835.

Potter, C. S., Randerson, J. T., Field, C. B., Matson, P. A., Vitousek, P. M., Mooney, H. A., & Klooster, S. A. (1993). Terrestrial ecosystem production: a process model based on global satellite and surface data. Global Biogeochemical Cycles, 7(4), 811-841.

Putzenlechner, B., Castro, S., Kiese, R., Ludwig, R., Marzahn, P., Sharp, I., & Sanchez-Azofeifa, A. (2019). Validation of Sentinel-2 fAPAR products using ground observations across three forest ecosystems. Remote Sensing of Environment, 232, 111310.

Reich, P.B. and Borchert, R., (1982). Phenology and ecophysiology of the tropical tree, Tabebuia neochrysantha (Bignoniaceae). Ecology, 63(2), pp.294-299.

Reich, P.B. and Borchert, R., (1984). Water stress and tree phenology in a tropical dry forest in the lowlands of Costa Rica. The Journal of Ecology, pp.61-74

Running, S. W., Nemani, R. R., Heinsch, F. A., Zhao, M., Reeves, M., & Hashimoto, H. (2004). A continuous satellite-derived measure of global terrestrial primary production. *Bioscience*, *54* (6), 547-560.

Sellers, P.J., (1985). Canopy reflectance, photosynthesis and transpiration. Int. J. Remote Sens., 6, 1335–1372.

Sellers, P.J., (1987) Canopy reflectance, photosynthesis, and transpiration, II. The role of biophysics in the linearity of their interdependence. Remote Sens. Environ., 21, 143–183.

Sellers, P. J., Hall, F. G., Asrar, G., Strebel, D. E., & Murphy, R. E. (1992). An overview of the first international satellite land surface climatology project (ISLSCP) field experiment (FIFE). Journal of Geophysical Research: Atmospheres, 97(D17), 18345-18371.

Sellers, Piers J., et al. "BOREAS in 1997 (1997). Experiment overview, scientific results, and future directions." Journal of Geophysical Research: Atmospheres 102.D24: 28731-28769.

Sims, D.A., Rahman, A.F., Cordova, V.D., Baldocchi, D.D., et al. (2005). Midday values of gross CO2 flux and light use efficiency during satellite overpasses can used to directly estimate eight-day mean flux. Remote Sensing of Environment, 101: 1-12.

Ustin, S. L., & Gamon, J. A. (2010). Remote sensing of plant functional types. New Phytologist, 186 (4), 795-816.

Vickers, D. and Mahrt, L., (1997). Quality control and flux sampling problems for tower and aircraft data. Journal of Atmospheric and Oceanic Technology, 14(3), pp.512-526.

Webb, E.K., Pearman, G.I. and Leuning, R., (1980). Correction of flux measurements for density effects due to heat and water vapour transfer. Quarterly Journal of the Royal Meteorological Society, 106(447), pp.85-100.

Widlowski, J.-L., (2010). On the bias of instantaneous FAPAR estimates in open-canopy forests.

Agric. For. Meteorol. 150, 1501–1522.

Yang, G.-Y., Slingo, J., (2001). The diurnal cycle in the tropics. Mon. Weather Rev. 129, 784–801

Younis, M., Akkaya, K., (2008). Strategies and techniques for node placement in wireless sensor networks: a survey. Ad Hoc Netw. 6, 621–655

Yuan, W. P., Liu, S. G., Zhou, G. S., Zhou, G. Y., Tieszen, L. L., Baldocchi, D., Bernhofer, C., Gholz, H., Goldstein, A. H., Goulden, M. L., Hollinger, D. Y., Hu, Y., Law, B. E., Stoy, P. C., Vesal, T., Wofsy, S. C., and other AmeriFlux collaborators (2007) Deriving a light use efficiency 10 model from eddy covariance flux data for predicting daily gross primary production across biomes. Agr. Forest Meteorol., 143: 189–207.

Yuan, W. P., Liu, S. G., Yu, G. R., Bonnefond, J., Chen, J., Davis, K., Desai, A. R., Goldstein, A. H., Gianelle, D., Rossi, F., Suyker, A. E., and Verma, S. B. (2010) Global estimates of evapotranspiration and gross primary production based on MODIS and global meteorology 15 data. Remote Sens. Environ., 114: 1416–1431.

Yuan, W., Cai, W., Liu, S., Dong, W., Chen, J., Arain, M. A., ... & Genesio, L. (2014). Vegetation-specific model parameters are not required for estimating gross primary production. Ecological modelling, 292, 1-10.

4.7 Figures:

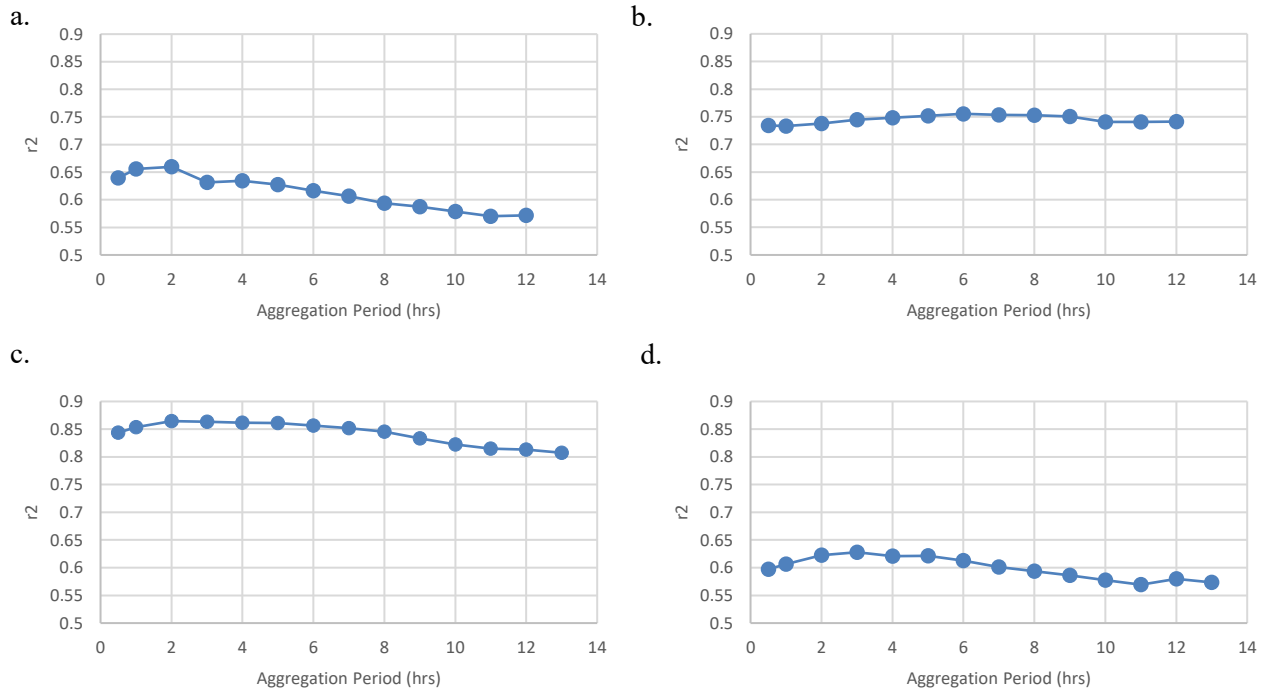

Figure 4.1- Coefficient of determination as a function of aggregation period (hours) for $fAPAR_{green}$ during the a) 2013 TDF, b) 2014 TDF, c) 2015 DBF, and d) 2016 DBF seasons.

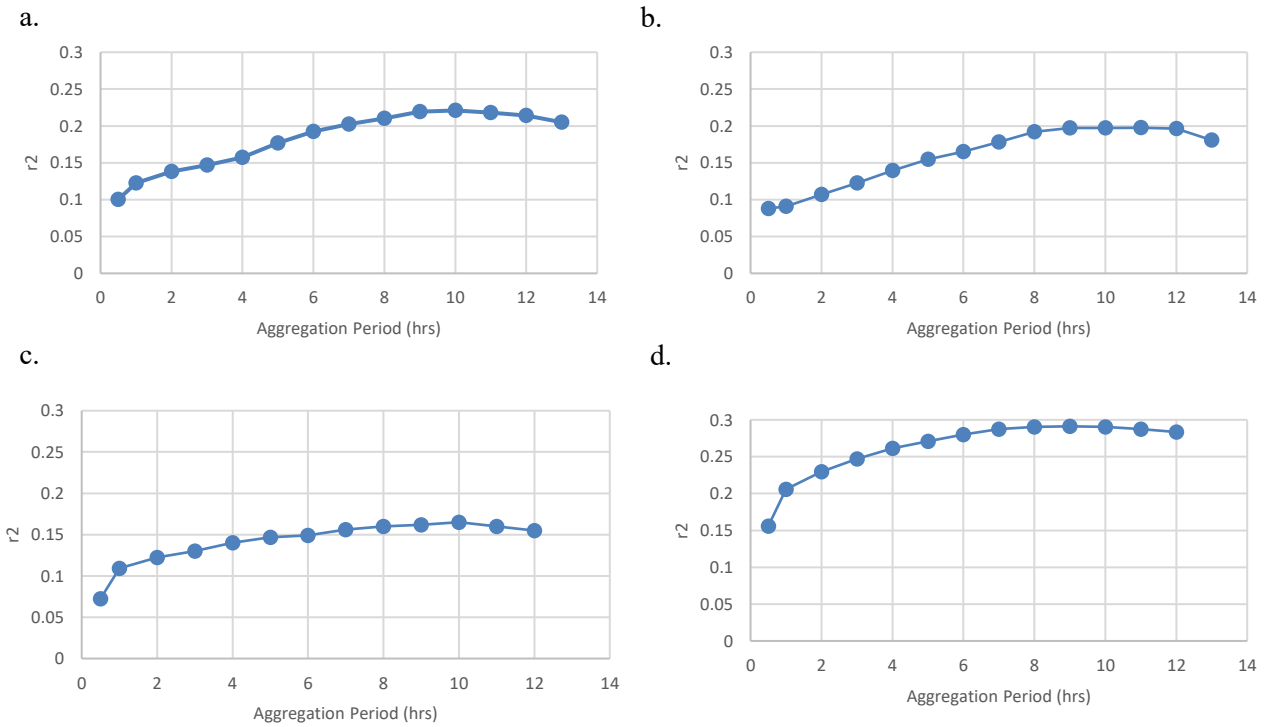

Figure 4.2- Coefficient of determination as a function of aggregation period (hours) for PAR during the a) 2013 TDF, b) 2014 TDF, c) 2015 DBF, and d) 2016 DBF seasons.

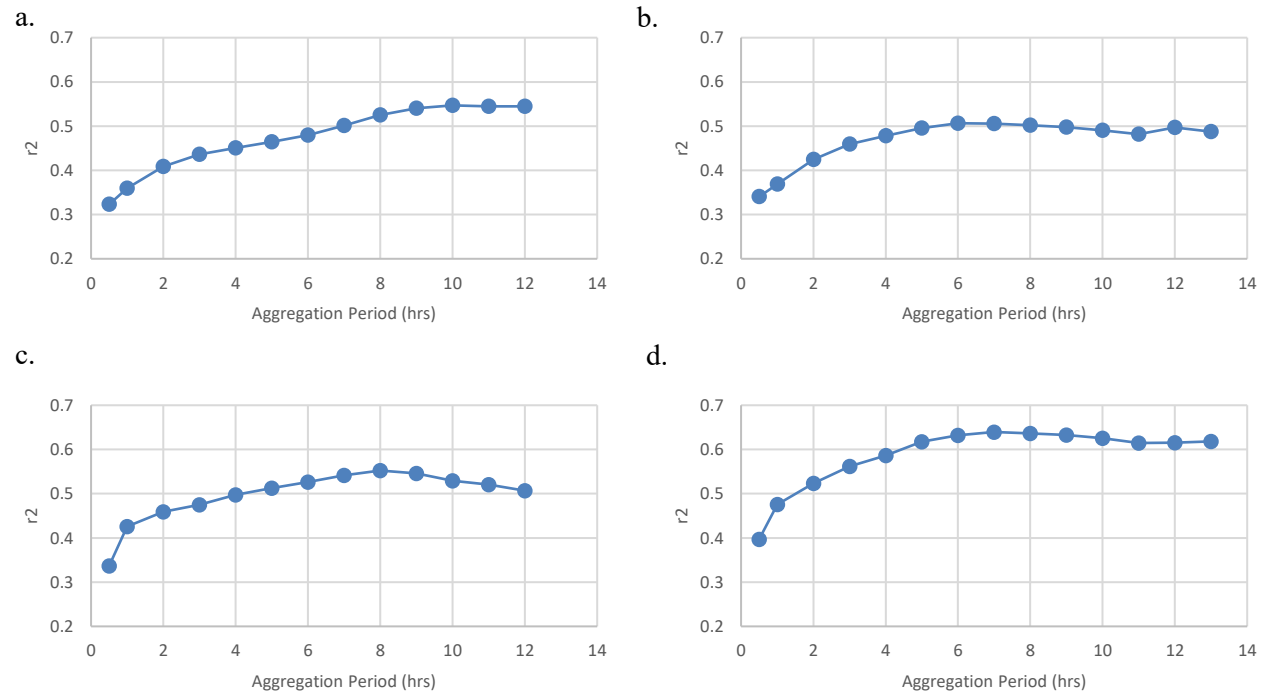

Figure 4.3 - Coefficient of determination as a function of aggregation period (hours) for $APAR_{green}$ during the a) 2013 TDF, b) 2014 TDF, c) 2015 DBF, and d) 2016 DBF seasons.

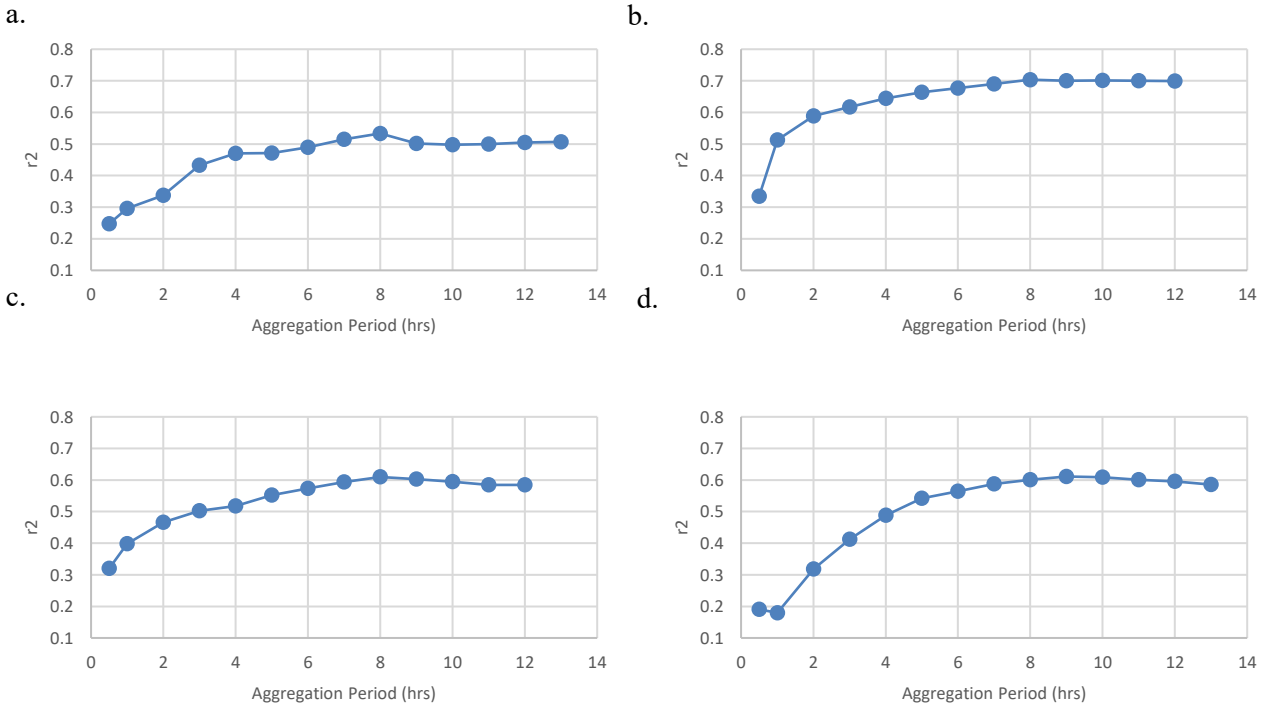

Figure 4.4 - Coefficient of determination as a function of aggregation period (hours) for LUE_{green} during the a) 2013 TDF, b) 2014 TDF, c) 2015 DBF, and d) 2016 DBF seasons.

a.

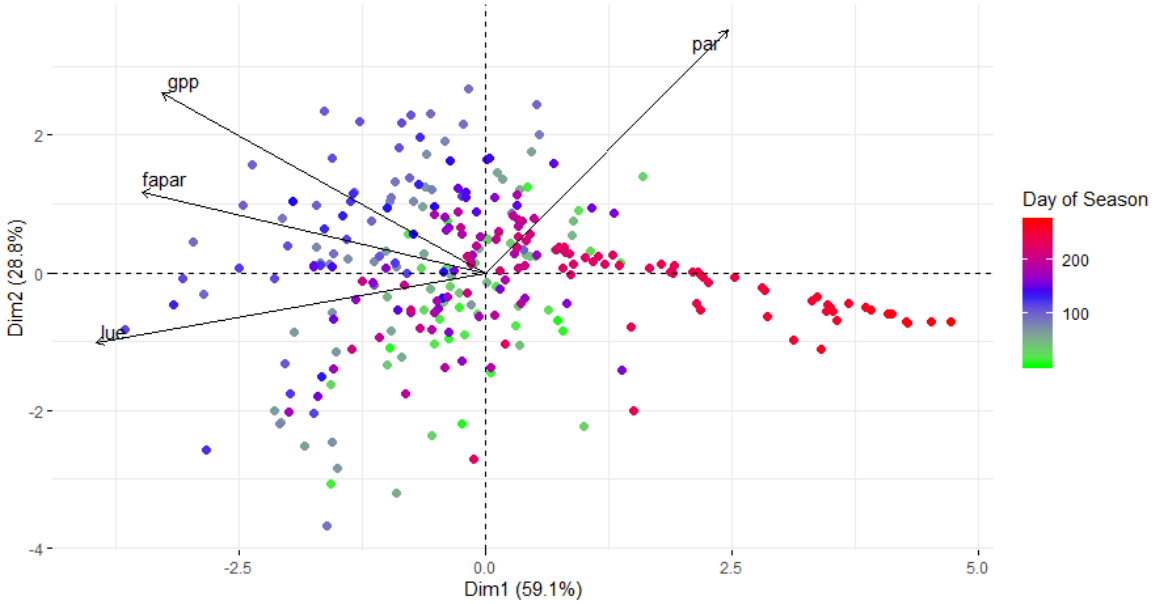
par
gpp
fapar
lue
Dim2 (28.8%)
Dim1 (59.1%)
Day of Season
200
100

b.

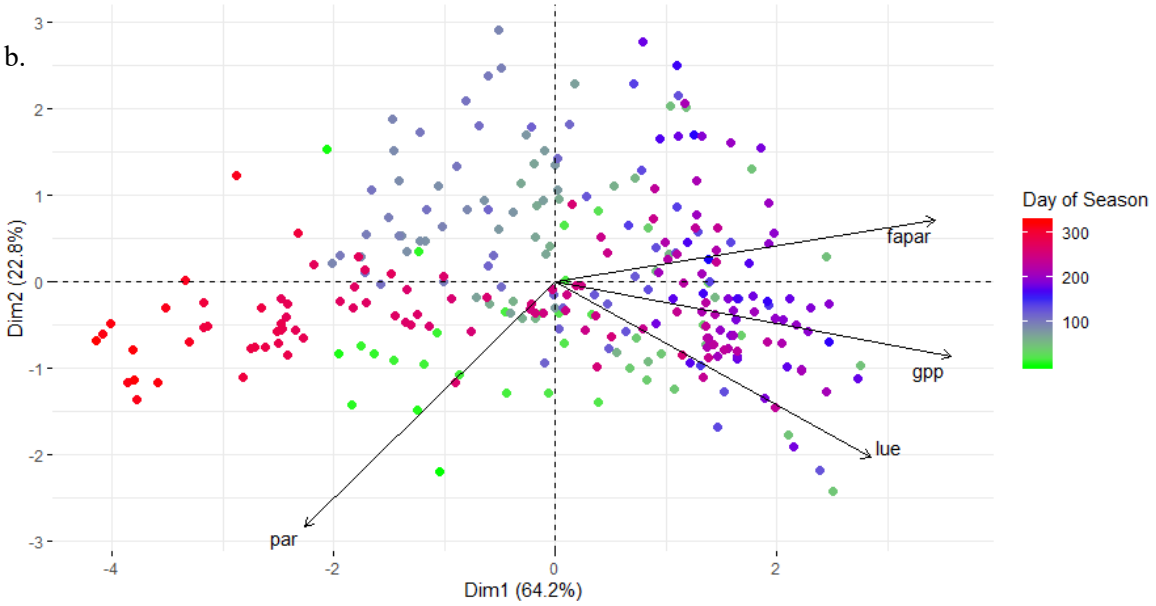
fapar
gpp
lue
par
Dim2 (22.8%)
Dim1 (64.2%)
Day of Season
300
200
100

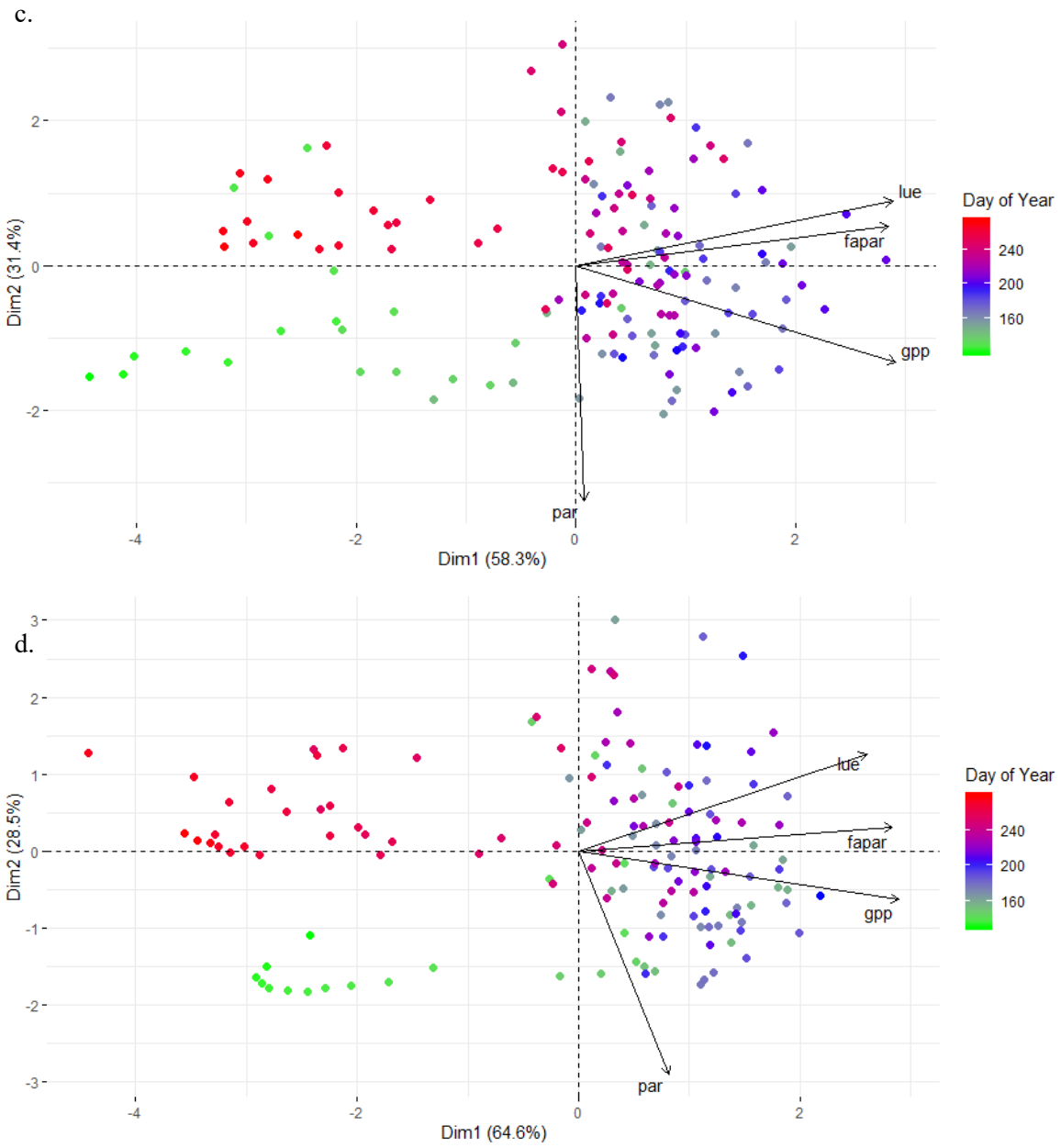

Figure 4.5 - PCA biplot displaying the two first components (Dim 1 and Dim 2) and explained variance (%) derived from PAC analysis of gross primary productivity (GPP), fraction of available photosynthetically active radiation (*fAPAR*), photosynthetically active radiation (*PAR*), and light use efficiency (*LUE*). Vectors show the contribution of single variables to the principal component. Color bar shows the day of the year (for DBF) or day of season (for TDF) for season a) 2013, b) 2014, c) 2015, and d) 2016.

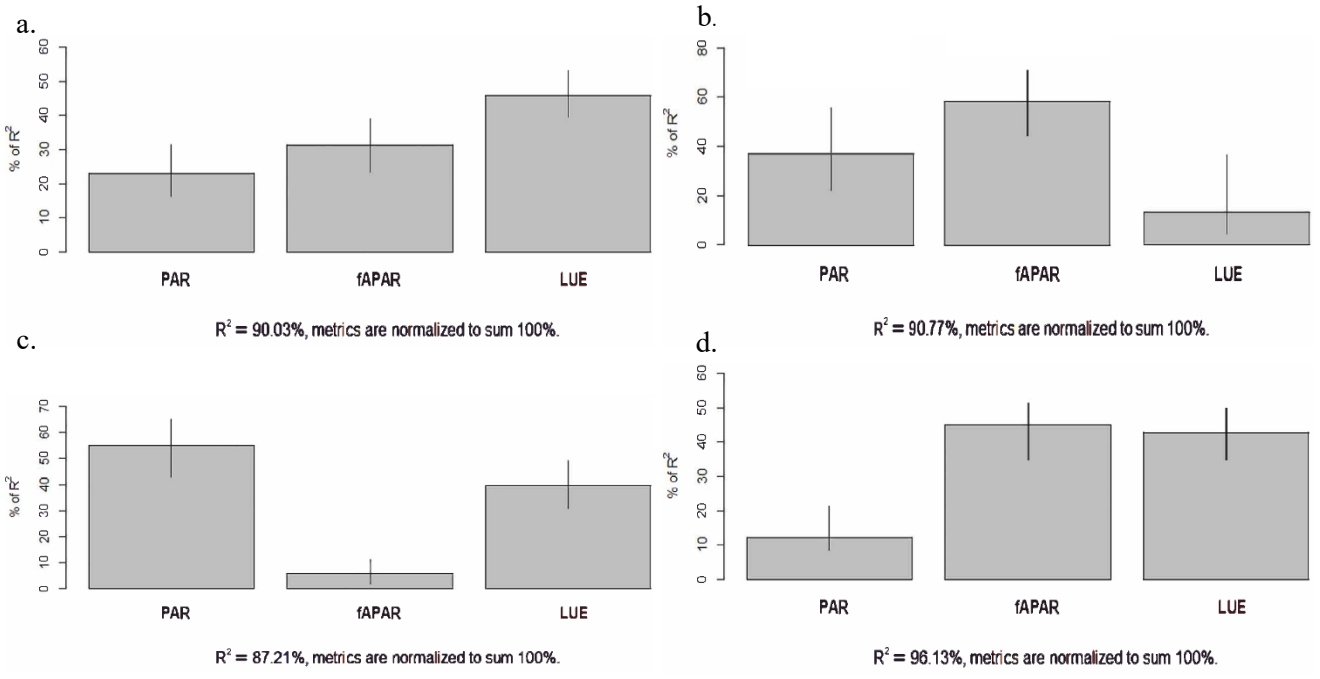

Figure 4.6 - Relative importance analysis of 2013 LUE model variables PAR, fAPAR, and LUE about GPP for (a) combined season, (b) green-up, (c) maturity, and (d) senescence. An LMG relative importance models was used. Combined variables accounted for 90.03%, 90.77%, 87.21%, and 96.13% of seasonal, green-up, maturity, and senescence GPP variability, respectively.

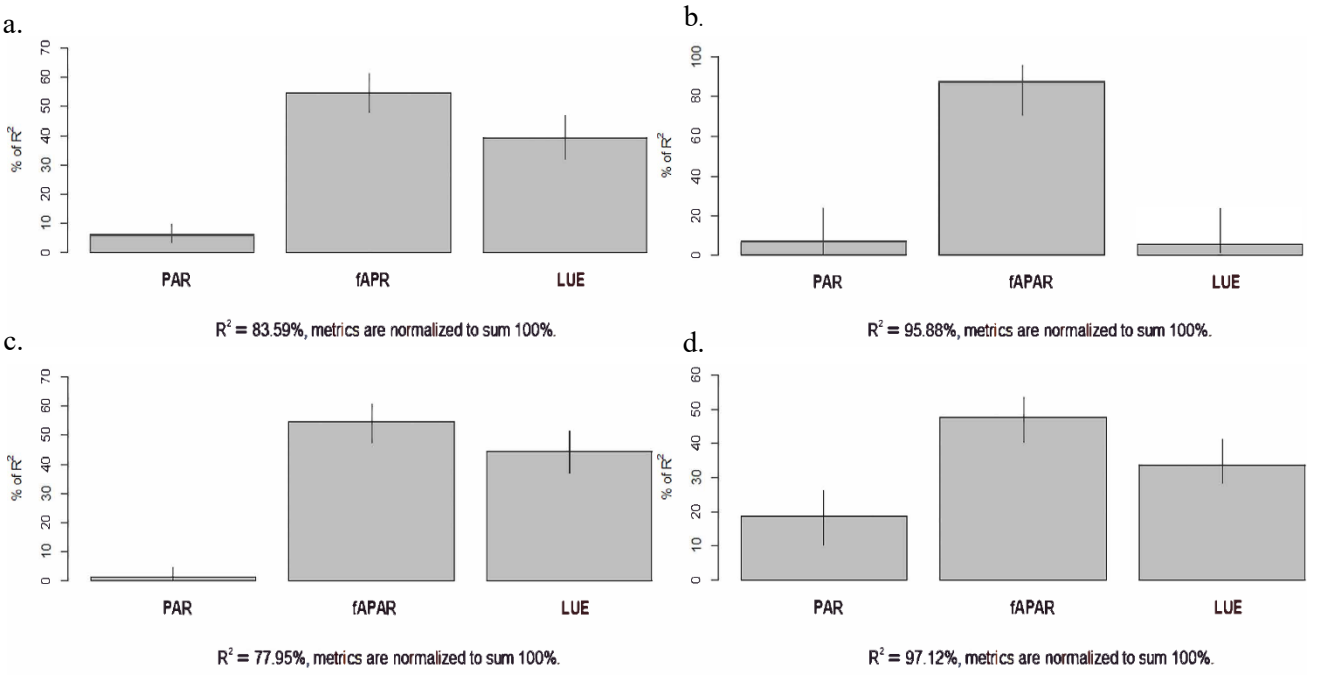

Figure 4.7 - Relative importance analysis of 2014 LUE model variables PAR, fAPAR, and LUE about GPP for (a) combined season, (b) green-up, (c) maturity, and (d) senescence. An LMG relative importance models was used. Combined variables accounted for 83.59%, 95.88%, 77.95%, and 97.12% of seasonal, green-up, maturity, and senescence GPP variability, respectively.

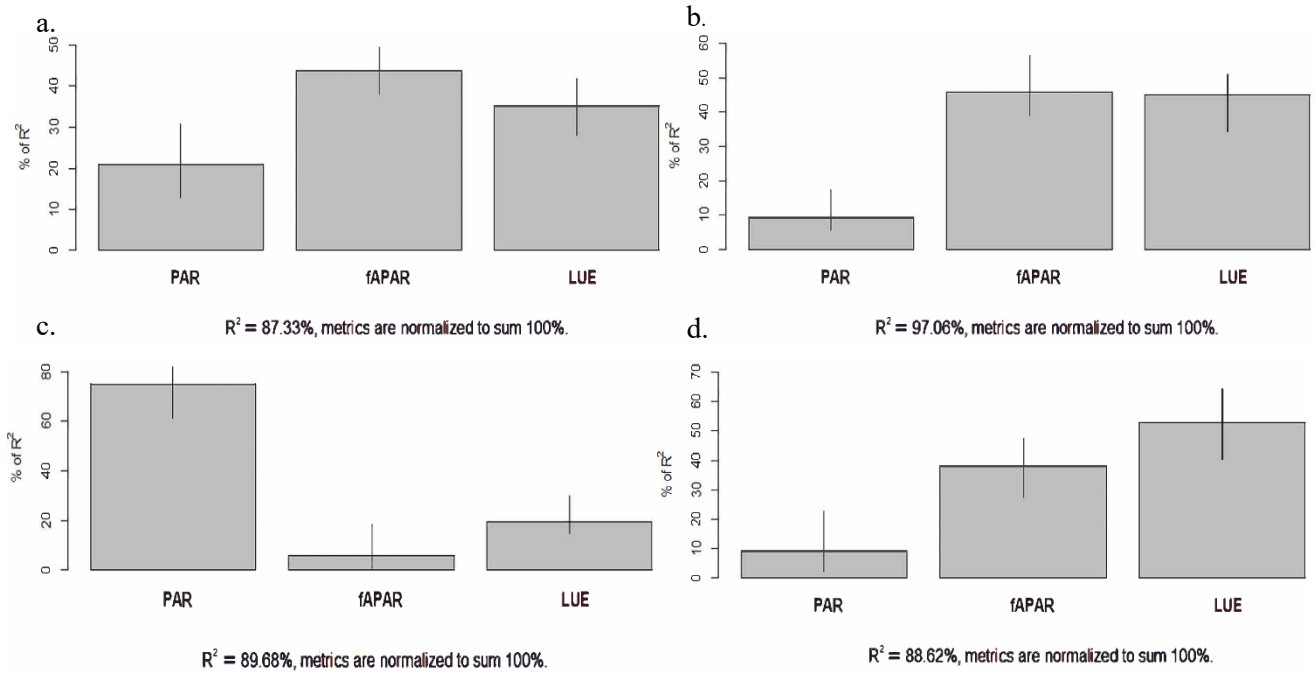

Figure 4.8 - Relative importance analysis of 2015 LUE model variables PAR, fAPAR, and LUE about GPP for (a) combined season, (b) green-up, (c) maturity, and (d) senescence. An LMG relative importance models was used. Combined variables accounted for 87.33%, 97.06%, 89.68%, and 88.62% of seasonal, green-up, maturity, and senescence GPP variability, respectively.

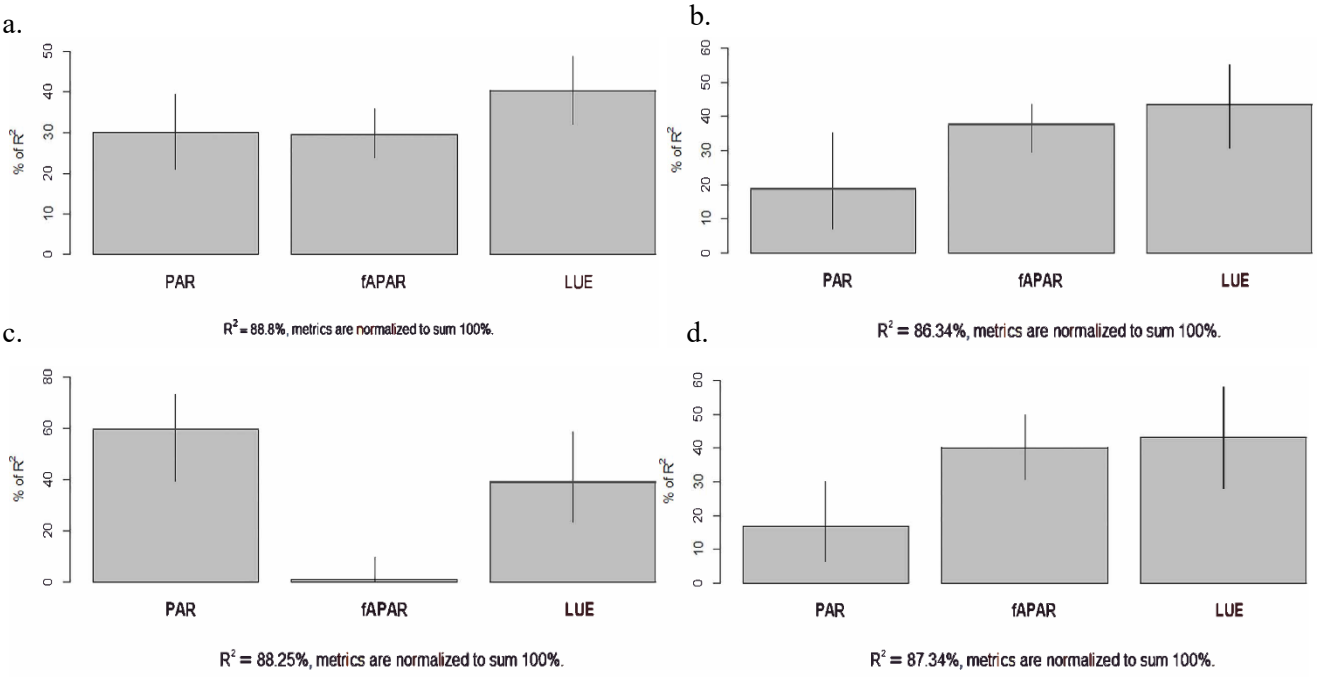

Figure 4.9 - Relative importance analysis of 2016 LUE model variables PAR, fAPAR, and LUE about GPP for (a) combined season, (b) green-up, (c) maturity, and (d) senescence. An LMG relative importance models was used. Combined variables accounted for 86.80%, 86.34%, 88.25%, and 87.34% of seasonal, green-up, maturity, and senescence GPP variability, respectively.

Table 4.1 - Instrumentation and characteristics of TDF and DBF study sites.

Site name	Peace River Ecosystem Monitoring Super Site (PR-EMSS)	Santa Rosa National Park Ecosystem Monitoring Super Site (PR-EMSS)
Counrty	Canada	Costa Rica
Coordinates	56.7441° N, 118.3439° W; 870m	10.8543° N, 85.6080° W; 305 m
Biome	Tropical Dry forest (TDF)	Deciduous Boreal Forest (DBF)
Dominant Species	Populus tremuloides (trembling aspen)	Luehea speciosa, Lonchocarpus minimiflorus, Guazuma ulmifolia (bastard cedar), Byrsonima crassifolia
Seasons	2013 & 2014	2015 & 2016
Micrometeorological instumentation	CPEC 200 (close path eddy covariance system) Campbell Scientific	CPEC 200 (close path eddy covariance system) Campbell Scientific
WSN nodes	29 ENV-Link-Mini-LXRS with SQ-110, Apogee Quantum sensors	15 ENV-Link-Mini-LXRS with SQ-110, Apogee Quantum sensors
Phenology Measurements	Yes	Yes

Table 4.2 – Aggregation results divided by phenological cycle for the 2013 TDF season.

		SRNP-EMSS 2013			
		Max r^2	Min r^2	Delta r^2	p-value
fAPAR	Greenup	0.50 (@8hrs)	0.11 (@30 min)	0.39	<0.05
	Maturity	0.16 (@10hrs)	0.11 (@30 min)	0.05	>0.05
	Senescence	0.87 (@8hrs)	0.84 (@10 hrs)	0.03	>0.05
PAR	Greenup	0.27 (@6hrs)	0.098 (@30 min)	0.17	<0.05
	Maturity	0.22 (@10hrs)	0.064 (@30 min)	0.16	<0.05
	Senescence	0.64 (@8hrs)	0.46 (@30 min)	0.18	<0.05
APAR	Greenup	0.37 (@8hrs)	0.08 (@30 min)	0.29	<0.05
	Maturity	0.41 (@11hrs)	0.20 (@30 min)	0.21	<0.05
	Senescence	0.79 (@8hrs)	0.79 (@30 min)	0.0	>0.05
LUE	Greenup	0.17 (@8hrs)	0.02 (@30 min)	0.15	<0.05
	Maturity	0.13 (@12hrs)	0.02 (@30 min)	0.11	<0.05
	Senescence	0.86 (@11hrs)	0.24 (@30 min)	0.62	<0.05

Table 4.3 – Aggregation results divided by phenological cycle for the 2014 TDF season.

		SRNP-EMSS 2014			
		Max r^2	Min r^2	Delta r^2	p-value
fAPAR	Greenup	0.88 (@11hrs)	0.54 (@30min)	0.34	<0.05
	Maturity	0.65 (@8hrs)	0.49 (@30min)	0.16	<0.05
	Senescence	0.78 (@6hrs)	0.71 (@30min)	0.06	>0.05
PAR	Greenup	0.14 (@9hrs)	0.061 (@30min)	0.08	<0.05
	Maturity	0.0083 (@6hrs)	0.0013 (@30min)	0.01	>0.05
	Senescence	0.50 (@10hrs)	0.35 (@30min)	0.15	<0.05
APAR	Greenup	0.86 (@8hrs)	0.68 (@30min)	0.18	<0.05
	Maturity	0.31 (@8hrs)	0.23 (@30min)	0.08	<0.05
	Senescence	0.68 (@11hrs)	0.61 (@30min)	0.07	>0.05
LUE	Greenup	0.19 (@7hrs)	0.10 (@30min)	0.09	<0.05
	Maturity	0.55 (@10hrs)	0.26 (@30min)	0.29	<0.05
	Senescence	0.74 (@8hrs)	0.47 (@30min)	0.27	<0.05

Table 4.4 – Aggregation results divided by phenological cycle for the 2015 DBF season.

		PR-EMSS 2015			
		Max r^2	Min r^2	Delta r^2	p-value
fAPAR	Greenup	0.86 (@7hrs)	0.79 (@1hr)	0.07	>0.05
	Maturity	0.14 (@12hrs)	0.05 (@30min)	0.09	>0.05
	Senescence	0.78 (@8hrs)	0.72 (@30min)	0.06	>0.05
PAR	Greenup	0.19 (@8hrs)	0.13 (@1hr)	0.06	>0.05
	Maturity	0.54 (@11 hrs)	0.19 (@30min)	0.35	<0.05
	Senescence	0.13 (@8hrs)	0.03 (@1hr)	0.10	<0.05
APAR	Greenup	0.61 (@7hrs)	0.42 (@1hr)	0.19	>0.05
	Maturity	0.53 (@10hrs)	0.18 (@30min)	0.35	<0.05
	Senescence	0.78 (@8hrs)	0.53 (@30min)	0.25	<0.05
LUE	Greenup	0.80 (@11hrs)	0.39 (@30min)	0.41	<0.05
	Maturity	0.18 (@12hrs)	0.004 (@30min)	0.18	<0.05
	Senescence	0.80 (@12hrs)	0.18 (@30min)	0.62	<0.05

Table 4.5 – Aggregation results divided by phenological cycle for the 2015 DBF season.

		PR-EMSS 2016			
		Max r^2	Min r^2	Delta r^2	p-value
fAPAR	Greenup	0.73 (@30min)	0.67 (@11hr)	0.06	>0.05
	Maturity	0.18 (@8hrs)	0.13 (@30min)	0.05	>0.05
	Senescence	0.62 (@30min)	0.56 (@11hrs)	0.06	>0.05
PAR	Greenup	0.12 (@12hrs)	0.09 (@1hr)	0.03	>0.05
	Maturity	0.48 (@11hrs)	0.10 (@30min)	0.38	<0.05
	Senescence	0.20 (@8hrs)	0.10 (@30min)	0.10	<0.05
APAR	Greenup	0.55 (@6hrs)	0.48 (@30min)	0.07	>0.05
	Maturity	0.41 (@12hrs)	0.13 (@30min)	0.28	<0.05
	Senescence	0.30 (@8hrs)	0.23 (@30min)	0.07	>0.05
LUE	Greenup	0.64 (@8hrs)	0.41 (@30min)	0.23	<0.05
	Maturity	0.21 (@10hrs)	0.04 (@30min)	0.17	<0.05
	Senescence	0.74 (@10hrs)	0.62 (@30min)	0.12	<0.05

CHAPTER 5 – Conclusions

The eddy covariance technique has greatly expanded our ability to monitor and understand mass and energy exchange between terrestrial ecosystems and the atmosphere (Baldocchi et al., 1988; 2001). The partitioning net carbon fluxes into gross primary productivity (GPP), defined as the carbon fixed during photosynthesis over a period of time, and respiration provides considerable insight into ecosystem functioning (Baldocchi, 2003). Despite wide acceptance of eddy covariance as a powerful tool for characterizing terrestrial ecosystems, theoretical assumptions limit flux applications to study sites under steady-state atmospheric conditions, with homogenous vegetation in flat terrain (Baldocchi et al., 1988; Aubinet et al., 2000). Eddy covariance application in non-ideal conditions requires accounting for complex effects such as atmospheric storage, wind divergence and advection, which can lead to significant errors in the ecosystem carbon budget (Baldocchi et al., 2000; Foken & Wichura, 1995; Massman & Lee; 2002).

The onset of remote sensing provided new possibilities for measuring ecosystem productivity at a variety of temporal and spatial scales. Furthermore, remote sensing offers the ability to measure locations with complex topography or previously inaccessible with other sampling techniques like eddy covariance. Early remote sensing studies on ecosystems were focused on mapping and monitoring with little focus on exploring ecosystem functions and physiological responses (Gamon, 2015). The development of net primary productivity (NPP) products from a variety of optical platforms (e.g. MODIS) provide the ability to examine vegetation dynamics and productivity from remote sensing data (Running et al., 2004). Comparisons of biome-scale productivity measurements from optical and flux measurements validate remote sensing data's ability to characterize broad-scale patterns in ecosystem-atmospheric carbon exchange (Goward et al., 1985, Frankenberg, et al. 2011). However, a comparison of fine-scale productivity driving mechanisms still requires extensive research.

As current trends move away from vegetation specific parametrization and more towards biophysical conditions of the ecosystem (Potter et al., 1993; Yuan et al., 2007, 2010, 2014), the comparison, validation, and integration of optical and flux data is essential. An interdisciplinary approach has shown the benefit of optical and flux data integration, resulting in additional ability to explore the driving mechanisms driving ecosystem photosynthesis and productivity (Sellers et al. 1992; 1997). This thesis explored various ways in which optical and flux data can be used to better understand, calculate and characterize ecosystem processes and productivity.

5.1 Synthesis and Significant Contributions

The overarching objective of this thesis was to explore mechanisms of ecosystem productivity through the integration of remote sensing and micrometeorological data. This was done throughout by (i) identifying the environmental mechanisms affecting productivity in tropical dry forest during normal and drought conditions; (ii) assessing the use of proximal PRI sensors as a proxy of photosynthetic efficiency and use towards a complete remote sensing derived measure of ecosystem productivity; and (iii) evaluating the impact of temporal aggregation and phenology on LUE model parametrization and ecosystem productivity in two deciduous forests.

In chapter 2 of this thesis, flux and optical data were used to identify key mechanisms of ecosystem productivity of tropical dry forest under normal and drought conditions. The study extended over four seasons (2013-2016), during which precipitation during the 2014 and 2015 season decreased by 30% and 63%, respectively, compared to regular precipitation regimes (2013, 2016 seasons). One of the key results includes the identification of preseason precipitation as the trigger for the initiation of the phenological cycle. Small precipitation events did not trigger green-up, suggesting the presence of a minimum threshold for budbreak to occur. These findings complement irrigation results showing stem recharge and leaf flush a week after hydration of vegetation (Borchert, 1994). Another study observed rapid girth growth but only after heavy rains (Reich and Borchert, 1984), suggesting the presence of minimum hydration threshold. Identifying the importance that precipitation regimes have on TDFs phenology and, in turn, productivity is of significance, especially as climate modelling studies projected precipitation to decrease over tropical dry forest (Magrin et al., 2014).

Analysis of seasonal fluxes showed a substantial decrease in productivity, net ecosystem exchange, and respiration due to drought, but the TDF remained a net carbon sink over the season. Our findings suggest that TDFs are sensitive to precipitation anomalies as occur during ENSO events. The onset of first precipitations was observed to correlate with sudden emissions of carbon. The wetting of dry soils and the subsequent pulse of CO2 release and nitrogen mineralization is known as the ‘Birch effect’ (Birch 1958). This effect has been observed in TDF (Waring and Powers 2016) but not at the ecosystem scale of our observations. Relative importance analysis identified latent heat as the principal controlling factor of TDF productivity. However, during drought, soil moisture became the limiting variable. The shift between evaporative demand and soil moisture demand shows TDF

adaptation to limited water resources.

This study provided a systematic analysis of drivers and limitations on productivity in tropical dry forest at ecosystem scale that is not common in scientific literature. As such, results from this study represent valuable material that has furthered our understanding of secondary TDF productivity and can be used to help parametrize and validate productivity models.

Chapter 3 of this thesis explored the use of automated PRI sensors to resolve diurnal and seasonal LUE changes over an aspen forest. One of the key findings of this study was the effect of calibration on the PRI signal. Uncalibrated PRI showed an overestimation in values and would also lead to GPP overestimation in LUE modelling exercises. A novel diurnal calibration procedure was also proposed and observed to account for variable illumination and solar elevation changes and resulted in the ability to resolve PRI diurnal patterns. Our results stand in contrast to Gamon et al. (2015), where they were unable to resolve diurnal PRI patters over an aspen stand. This difference advocate for the importance of site-specific light fields that can vary in complexity between different canopy structures and may affect the ability to resolve diurnal dynamics accurately.

Corrected PRI values were closely related to both LUE ($R2 = 0.62$, $p < 0.05$) and quantum yield, derived from eddy covariance light curves, ($R2 = 0.72$, $p < 0.05$) over the course of the season. These findings show that PRI can be used as a proxy of light use efficiency at both the diurnal and seasonal scale. As more commercial automated narrow-band sensors become available to the scientific community, it is important that calibration procedures are developed, and that sensor response is characterized and validated. Protocols described in this study can be used as a framework for calibrating and validating spectral indices from automated sensors. Additionally, my findings contribute towards a better understanding of PRI as a proxy of LUE and a deeper understanding of diurnal and seasonal changes of vegetation physiology that can be explored through continuous measurements.

Chapter 4 methods outline a procedure for exploring the effect of temporal aggregation on LUE model variables and, ultimately, productivity. These methods could be used as a framework for testing other factors that may affect LUE model parameters. We found that phenology caused diverse effects from seasonal results, especially for TDF fAPAR during green-up. Seasonal fAPAR aggregation analysis proved to be insensitive to aggregation. In contrast, green-up fAPAR was significantly affected by temporal aggregation ($\Delta r^2 \approx 0.35$). Aggregation results suggest that temporal aggregation can significantly impact LUE model accuracy and should be considered as we explore the proper protocols for optical and flux data integration.

Seasonal relative importance results were also different than those observed from the phenological analysis. For both the TDF and DBF, relative importance patterns from the different phenological stages were able to be explained in the context of the ecological processes at play during green-up, maturity, and senescence. Our findings support the theory proposed by Garbulsky et al. (2007) that suggests that the physiological component, and by extension the structural component, contributions of the *LUE* model can change between vegetation and environmental conditions. Furthermore, we can extend this concept by suggesting that *LUE* model components can change throughout phenology as environmental conditions and disturbances impact productivity.

5.2 Challenges and Future Directions

Based on the work and findings covered throughout my thesis, I have identified some remaining knowledge gaps and questions to be filled by future research. These include the following:

- Can automated PRI sensors and resulting continuous measurements resolve diurnal and seasonal LUE changes in deciduous-evergreen mixed forest and other complex ecosystems?
- What other variables affect the variability in LUE model parameters and optical and flux data integration?
- How to develop standardized procedures for optical and flux integration?
- How do we better parametrize LUE models to account for changes in LUE model contributions at the ecosystem level, seasonal level, and phenological level?

As we continue to explore the integration of optical and flux datasets, these questions will need to be resolved.

Of interest to me is the ongoing challenge of measuring photosynthetic efficiency through remote sensing. I believe that productivity modelling could greatly benefit from better parametrization of the LUE term. Commercial PRI instruments represent a significant advance toward developing continuous PRI datasets that allow more detail exploration of LUE. Yet, challenges remain in the interpretation of data, especially in complex ecosystems such as deciduous-evergreen mixed forests. A study by Gamon et al. (2015) using continuous PRI sensors over evergreen vegetation showed the ability to resolve diurnal LUE patterns. Still, the complexity of distinguishing the individual and combined response from different vegetation with significantly different photosynthetic responses and phenology would make the mixed forests a challenging ecosystem to explore.

Other remaining questions and areas of interest surround the issue of optical and flux data integration. As we explored the effect of temporal aggregation and phenology on the LUE model, there remain other variables that may affect how datasets should be processed, analyzed and integrated. For example, studies on fAPAR variability and bias (Leuchner et al., 2011; Widlowski, 2010; Putzenlechner et al., 2019) have explored some of the impacts of illumination, solar positioning, and wind. Testing of these factors in the context of the LUE model would be valuable toward better integration of optical and flux datasets as well as modelling of productivity.

On the parametrization of the LUE model, our results show that the physiological and structural component contributions to the *LUE* model can change between vegetation and environmental conditions, as Garbulsky et al. (2007) suggested. Our findings also extended this theory by adding the complexity of observed changes through the different phenological cycles and suggesting that modelling accuracy could benefit from this finer scale parametrization. However, questions remain on how to go about this process and if contribution metrics (such as relative importance metrics) should be used to scale the structural and physiological components of the LUE model according to their contributions.

5.3 References

Aubinet M.,Aubinet, M., Grelle, A., Ibrom, A., Rannik, Ü., Moncrieff, J., Foken, T., Kowalski, A.S., Martin, P.H., Berbigier, P., Bernhofer, Ch., Clement, R., Elbers, J., Granier, A., Grünwald, T., Morgenstern, K., Pilegaard, K., Rebmann, C., Snijders, W., Valentini, R., Vesala, T. (2000). Estimates of the annual net carbon and water exchange of forests: The EUROFLUX methodology. Advances in Ecological Research 30: 113-176.

Baldocchi D.D., Hicks B.B., and Meyers T.D. (1988). Measuring biosphereatmosphere exchanges of biologically related gases with micrometeorological methods. Ecology, 69: 1331-1340.

Baldocchi D.D., Finnigan J.J., Wilson K.W. et al., (2000). On measuring net ecosystem carbon exchange in complex terrain over tall vegetation. Boundary Layer Meteorology, 96: 257-291.

Baldocchi, D.D, Falge, E., Gu, L., Olson, R., Hollinger, D., Running, S., Anthoni, P., Bernhofer, Ch., Davis, K., Evans, R., Fuentes, J., Goldstein, A., Katul, G., Law, B., Lee, X., Malhi, Y., Meyers, T., Munger, W., Oechel, W., Paw, U.K.T., Pilegaard, K., Schmid., H.P., Valentini, R., Verma, S., Vesala, T., Wilson, K., and Wofsy, K. (2001). FLUXNET: A new tool to study the temporal and spatial variability of ecosystem-scale carbon dioxide, water vapor, and energy flux densities. Bulletin of the American Meteorological Society, 82: 2415-2434.

Baldocchi D.D. (2003). Assessing the eddy covariance technique for evaluating carbon dioxide exchange rates of ecosystems: past, present and future. Global Change Biology, 9: 479-492.

Birch H. F. (1958) The effect of soil drying on humus decomposition and nitrogen availability Plant Soil 10 9–31.

Borchert R. (1994) Soil and stem water storage determine phenology and distribution of tropical dry forest trees Ecology 75 1437–49.

Foken, T.H., Wichura, B., (1995). Tools for quality assessment of surface-based flux measurements. Agricultural and Forest Meteorology, 78: 83-105.

Gamon, J. A., Kovalchuck, O., Wong, C. Y. S., Harris, A., & Garrity, S. R. (2015). Monitoring seasonal and diurnal changes in photosynthetic pigments with automated PRI and NDVI sensors. Biogeosciences, 12(13), 4149-4159.

Garbulsky, M. F., Peñuelas, J., Gamon, J., Inoue, Y., & Filella, I. (2011). The photochemical reflectance index (PRI) and the remote sensing of leaf, canopy and ecosystem radiation use efficiencies: A review and meta-analysis. Remote Sensing of Environment, 115(2), 281-297.

Goward, S. N., Tucker, C. J., and Dye, D. G.: North-American vegetation patterns observed with the NOAA-7 Advanced Very High Resolution Radiometer, Vegetatio, 64, 3–14, 1985.

Frankenberg, C., Fisher, J. B., Worden, J., Badgley, G., Saatchi, S. S., Lee, J.-E., Toon, G. C., Butz, A., Jung, M., Kuze, A., and Yokota, T.: New global observations of the terrestrial carbon cycle from GOSAT: Patterns of plant fluorescence with gross primary productivity, Geophys. Res. Lett., 38, L17706, doi:10.1029/2011gl048738, 2011.

Leuchner, M., Hertel, C., Menzel, A., (2011) Spatial variability of photosynthetically active radiation in European beech and Norway spruce. Agric. For. Meteorol. 151.

Magrin GO, Marengo JA, Boulanger JP, Buckeridge MS, Castellanos E, Poveda G. (2014). Central and South America in Climate Change 2014: Impacts, Adaptation, and Vulnerability. Part B: Regional Aspects. Contribution of Working Group II to the Fifth Assessment Report of the Intergovernmental Panel on Climate Change.Barros, V.R., C.B. Field, D.J. Dokken, M.D. Mastrandrea, K.J. Mach, T.E. Bilir, M. Chatterjee, K.L. Ebi, Y.O. Estrada, R.C. Genova, B. Girma, E.S. Kissel, A.N. Levy, S. MacCracken, P.R. Mastrandrea, and L.L.White (Eds.), Cambridge University Press, Cambridge and New York,1499-1566

Massman W.J., Lee X., (2002). Eddy covariance flux correlations and uncertainties in long term studies of carbon and energy exchanges. Agricultural and Forest Meteorology, 113: 121-144.

Potter, C. S., Randerson, J. T., Field, C. B., Matson, P. A., Vitousek, P. M., Mooney, H. A., and Klooster, S. A. (2003) Terrestrial ecosystem production: a process model based on global satellite and surface data. Global Biogeochem., 7: 811–841.

Putzenlechner, B., Castro, S., Kiese, R., Ludwig, R., Marzahn, P., Sharp, I., & Sanchez-Azofeifa, A. (2019). Validation of Sentinel-2 fAPAR products using ground observations across three forest ecosystems. Remote Sensing of Environment, 232, 111310.

Reich P. B. and Borchert R., (1984)Water stress and tree phenology in a tropical dry forest in the lowlands of Costa Rica J. Ecol. 72 61–74.

Running, S. W., Nemani, R. R., Heinsch, F. A., Zhao, M. S., Reeves, M., and Hashimoto, H.: A continuous satellite-derived measure of global terrestrial primary production, BioScience, 54, 547– 560, 2004.

Sellers, P. J., Hall, F. G., Asrar, G., Strebel, D. E., & Murphy, R. E. (1992). An overview of the first international satellite land surface climatology project (ISLSCP) field experiment (FIFE). Journal of Geophysical Research: Atmospheres, 97(D17), 18345-18371.

Sellers, Piers J., et al. "BOREAS in 1997 (1997). Experiment overview, scientific results, and future directions." Journal of Geophysical Research: Atmospheres 102.D24: 28731-28769.

Waring, B. G. and Powers J. S., (2016) Unraveling the mechanisms underlying pulse dynamics of soil respiration in tropical dry forests Environ. Res. Lett. 11 105005.

Widlowski, J. L. (2010). On the bias of instantaneous FAPAR estimates in open-canopy forest. Agricultural and Forest Meteorology, 150(12), 1501-1522.

Yuan, W. P., Liu, S. G., Zhou, G. S., Zhou, G. Y., Tieszen, L. L., Baldocchi, D., Bernhofer, C., Gholz, H., Goldstein, A. H., Goulden, M. L., Hollinger, D. Y., Hu, Y., Law, B. E., Stoy, P. C., Vesal, T., Wofsy, S. C., and other AmeriFlux collaborators (2007) Deriving a light use

efficiency 10 model from eddy covariance flux data for predicting daily gross primary production across biomes. Agr. Forest Meteorol., 143: 189–207.

Yuan, W. P., Liu, S. G., Yu, G. R., Bonnefond, J., Chen, J., Davis, K., Desai, A. R., Goldstein, A. H., Gianelle, D., Rossi, F., Suyker, A. E., and Verma, S. B. (2010) Global estimates of evapotranspiration and gross primary production based on MODIS and global meteorology 15 data. Remote Sens. Environ., 114: 1416–1431.

Yuan, W., Cai, W., Liu, S., Dong, W., Chen, J., Arain, M. A., ... & Genesio, L. (2014). Vegetation-specific model parameters are not required for estimating gross primary production. *Ecological modelling*, *292*, 1-10.

Works Cited

Adkinson, A.C.; Syed, K.H.; Flanagan, L.B. Contrasting responses of growing season ecosystem CO2 exchange to variation in temperature and water table depth in two peatlands in northern Alberta, Canada. J. Geophys. Res. Biogeosci. 2011, 116, doi:1029/2010JG001512.

Alberta Environmental Protection. Natural Regions and Subregions of Alberta: A Summary; Publ. I/531 and Map, 1 Sheet; Alberta Environmental Protection: Edmonton, AB, Canada, 1994.

Allen, K., Dupuy, J.M., Gei, M.G., Hulshof, C., Medvigy, D., Pizano, C., Salgado-Negret, B., Smith, C.M., Trierweiler, A., Van Bloem, S.J. and Waring, B.G., 2017. Will seasonally dry tropical forests be sensitive or resistant to future changes in rainfall regimes?. Environmental Research Letters, 12(2), p.023001.

Alton, P. B. (2008). Reduced carbon sequestration in terrestrial ecosystems under overcast skies compared to clear skies. Agricultural and Forest Meteorology, 148(10), 1641-1653.

Asrar, G., Fuchus, M., Kanemasu, E. T., and Hatfield, J. L. (1984). Estimating absorbed photosynthetic radiation and leaf area index from spectral reflectance in wheat. Agronomy Journal 76:300-306.

Asrar, G.M.; Myneni, R.B.; Choudhury, B.J. Choudhury. Spatial heterogeneity in vegetation canopies and remote sensing of absorbed photosynthetically active radiation: A modeling study. Remote Sens. Environ. 1992, 41, 85–103.

Atmospheric Environment Service. Canadian Climate Normals (19511980); Precipitation Environment Canada: Downsview, ON, Canada, 1982; Volume 3, p. 602

Aubinet, M., Grelle, A., Ibrom, A., Rannik, Ü., Moncrieff, J., Foken, T., Kowalski, A.S., Martin, P.H., Berbigier, P., Bernhofer, C. and Clement, R., 1999. Estimates of the annual net carbon and water exchange of forests: the EUROFLUX methodology. Advances in ecological

research, 30, pp.113-175.

Baldocchi, D.D., Hincks, B.B. and Meyers, T.P., 1988. Measuring biosphere-atmosphere exchanges of biologically related gases with micrometeorological methods. Ecology, 69(5), pp.1331-1340.

Baldocchi, D., 1997. Measuring and modelling carbon dioxide and water vapour exchange over a temperate broad-leaved forest during the 1995 summer drought. Plant, Cell & Environment, 20(9), pp.1108-1122.

Baldocchi D.D., Finnigan J.J., Wilson K.W. et al., (2000). On measuring net ecosystem carbon exchange in complex terrain over tall vegetation. Boundary Layer Meteorology, 96: 257-291.

Baldocchi, D.D, Falge, E., Gu, L., Olson, R., Hollinger, D., Running, S., Anthoni, P., Bernhofer, Ch., Davis, K., Evans, R., Fuentes, J., Goldstein, A., Katul, G., Law, B., Lee, X., Malhi, Y., Meyers, T., Munger, W., Oechel, W., Paw, U.K.T., Pilegaard, K., Schmid., H.P., Valentini, R., Verma, S., Vesala, T., Wilson, K., and Wofsy, K. (2001). FLUXNET: A new tool to study the temporal and spatial variability of ecosystem-scale carbon dioxide, water vapor, and energy flux densities. Bulletin of the American Meteorological Society, 82: 2415-2434.

Baldocchi D.D. (2003). Assessing the eddy covariance technique for evaluating carbon dioxide exchange rates of ecosystems: past, present and future. Global Change Biology, 9: 479-492.

Balvanera, P., Castillo, A. and MartÍnez-Harms, M.J., 2011. Ecosystem services in seasonally dry tropical forests. In Seasonally Dry Tropical Forests (pp. 259-277). Island Press/Center for Resource Economics.

Balzarolo, M.; Anderson, K.; Nichol, C.; Rossini, M.; Vescovo, L.; Arriga, N.; Wohlfahrt, G.; Calvet, J.C.; Carrara, A.; Cerasoli, S.; et al. Ground-based optical measurements at European flux sites: A review of methods, instruments and current controversies. Sensors 2011, 11, 7954–7981.

Barton, C. V. M., & North, P. R. J. (2001). Remote Sensing of canopy light use efficiency using the Photochemical Reflectance Index. Model and analysis. Remote Sensing of Environment, 78(264), 273.

Becknell, J.M., Kucek, L.K. and Powers, J.S., 2012. Aboveground biomass in mature and secondary seasonally dry tropical forests: A literature review and global synthesis. Forest Ecology and Management, 276, pp.88-95.

Birch, H.F., 1958. The effect of soil drying on humus decomposition and nitrogen availability. Plant and soil, 10(1), pp.9-31.

Björkman, O.; Demmig-Adams, B. Regulation of photosynthetic light energy capture, conversion, and dissipation in leaves of higher plants. In Ecophysiology of Photosynthesis; Springer: Berlin/Heidelberg, Germany, 1995; pp. 17–47.

Bloom, A.J., Chapin III, F.S. and Mooney, H.A., 1985. Resource limitation in plants-an economic analogy. Annual review of Ecology and Systematics, 16(1), pp.363-392.

Bonal, D., Burban, B., Stahl, C., Wagner, F., & Hérault, B. 2016. The response of tropical rainforests to drought—lessons from recent research and future prospects. Annals of forest science, 73(1), pp.27-44.

Borchert, R., 1994. Soil and stem water storage determine phenology and distribution of tropical dry forest trees. Ecology, 75(5), pp.1437-1449.

Becknell, J.M., Kucek, L.K. and Powers, J.S., 2012. Aboveground biomass in mature and secondary seasonally dry tropical forests: A literature review and global synthesis. Forest Ecology and Management, 276, pp.88-95.

Braswell, B.H., Schimel, D.S., Linder, E., and Moore III, B. (1997). The response of global terrestrial ecosystems to interannual temperature variability. Science 278:870-873.

Brock, W., & Xepapadeas, A. (2017). Climate change policy under polar amplification. European Economic Review 99: 91–112.

Balzter, H., Gerard, F.F., George, C.T., Rowland, C.S., Jupp, T.E., McCallum, I., Shvidenko, A., Nilsson, S., Sukhinin, A., Onuchin, A. and Schmullius, C., (2005). Impact of the Arctic Oscillation pattern on interannual forest fire variability in Central Siberia. Geophysical Research Letters. 32(14).

Cao, S. and Sanchez-Azofeifa, A., 2017. Modeling seasonal surface temperature variations in secondary tropical dry forests. International Journal of Applied Earth Observation and Geoinformation, 62, pp.122-134.

Castillo, A., Magaña, A., Pujadas, A., Martínez, L. and Godínez, C., 2005. Understanding the interaction of rural people with ecosystems: a case study in a tropical dry forest of Mexico. Ecosystems, 8(6), pp.630-643.

Castro, S., & Sanchez-Azofeifa, A. (2018). Testing of Automated Photochemical Reflectance Index Sensors as Proxy Measurements of Light Use Efficiency in an Aspen Forest. Sensors, 18(10), 3302.

Castro, S. M., G. A. Sanchez-Azofeifa, and H. Sato. 2018. “Effect of Drought on Productivity in a Costa Rican Tropical Dry Forest.” Environmental Research Letters 13(4).

Chen, J.M., Chen, W., Liu, J. & Cihlar, J. (2000) Annual carbon balance of Canada’s forests during 1895–1996. Global Biogeochemical Cycles, 14, 839–850.

Chen, J., Shen, M., & Kato, T. (2009). Diurnal and seasonal variations in light-use efficiency in an alpine meadow ecosystem: causes and implications for remote sensing. Journal of Plant Ecology, 2(4), 173-185.

Chadwick, R., Good, P., Martin, G. and Rowell, D.P., 2016. Large rainfall changes consistently projected over substantial areas of tropical land. Nature Climate Change, 6(2), p.177.

Cheng, Y.B.; Middleton, E.M.; Zhang, Q.; Corp, L.A.; Dandois, J.; Kustas, W.P. The photochemical reflectance index from directional cornfield reflectances: Observations and simulations. Remote Sens. Environ. 2012, 124, 444–453.

Chevan, A. and Sutherland, M., 1991. Hierarchical partitioning. The American Statistician, 45(2), pp.90-96.

Choudhury, B.J. 2001. Estimating gross photosynthesis using satellite and ancillary data: approach and preliminary results. Remote Sensing Environ. 75:1–25.

Coursolle, C., Margolis, H.A., Barr, A.G., Black, T.A., Amiro, B.D., McCaughey, J.H., Flanagan, L.B., Lafleur, P.M., Roulet, N.T., Bourque, C.P.A., Arain, M.A., Wofsy, S.C., Dunn, A., Morgenstern, K., Orchansky, A.L., Bernier, P.Y., Chen, J.M., Kidston, J., Saigusa, N. & Hedstrom, N. (2006) Late-summer carbon fluxes from Canadian forests and peatlands along an east-west continental transect. Canadian Journal of Forest Research, 36, 783–800.

Coops, N. C., Waring, R. H., & Law, B. E. (2005). Assessing the past and future distribution and productivity of ponderosa pine in the Pacific Northwest using a process model, 3-PG. Ecological Modelling, 183(1), 107-124.

Coops, C., Hilker, T., Hall, F.G., Nichol, C.J., Drolet G.G. (2010). Estimation of light-use efficiency of terrestrial ecosystems from space: a status report. Bioscience, 60: 788-797

Cramer, W., Kicklighter, D. W., Bondeau, A., Iii, B. M., Churkina, G., Nemry, B., ... & Intercomparison, T. P. O. T. P. N. M. (1999). Comparing global models of terrestrial net primary productivity (NPP): overview and key results. Global change biology, 5(S1), 1-15.

Dale, V.H., Joyce, L.A., McNulty, S., Neilson, R.P., Ayres, M.P., Flannigan, M.D., Hanson, P.J., Irland, L.C., Lugo, A.E., Peterson, C.J., Simberloff, D., Swanson, F.J., Stocks, B.J. and Wotton, B.M., (2001). Climate change and forest disturbances. Bioscience. 51(9), 723- 734.

Daubenmire, R., 1972. Phenology and other characteristics of tropical semi-deciduous forest in north-western Costa Rica. The Journal of Ecology, pp.147-170.

Deering, D.W.; Leone, P. A sphere-scanning radiometer for rapid directional measurements of sky and ground radiance. Remote Sens. Environ. 1986, 19, 1–24.

Demmig-Adams, B.; Adams, W.W., III; Logan, B.A.; Verhoeven, A.S. Xanthophyll cycle-dependent energy dissipation and flexible photosystem II efficiency in plants acclimated to light stress. Funct. Plant Biol. 1995, 22, 249–260.

Demmig-Adams, B.; Adams, W.W., III. The role of xanthophyll cycle carotenoids in the protection of photosynthesis. Trends Plant Sci. 1996, 1, 21–26.

Doi, H. & Takahashi, M. (2008) Latitudinal patterns in the phenological responses of leaf colouring and leaf fall to climate change in Japan. Global Ecology and Biogeography, 17, 556– 561.

Drolet, G.G.; Huemmrich, K.F.; Hall, F.G.; Middleton, E.M.; Black, T.A.; Barr, A.G.; Margolis, H.A. A MODIS-derived photochemical reflectance index to detect inter-annual variations in the photosynthetic light-use efficiency of a boreal deciduous forest. Remote Sens. Environ. 2005, 98, 212–224

Drolet, G.; Wade, T.; Nichol, C.J.; MacLellan, C.; Levula, J.; Porcar-Castell, A.; Nikinmaa, E.; Vesala, T.A temperature-controlled spectrometer system for continuous and unattended measurements of canopy spectral radiance and reflectance. Int. J. Remote Sens. 2014, 35, 1769–1785.

Enquist, C.A.F., (2002). Predicted regional impacts of climate change on the geographical distribution and diversity of tropical forests in Costa Rica. Journal of Biogeography, 29:519-534.

Eamus, D. and Prior, L., 2001. Ecophysiology of trees of seasonally dry tropics: comparisons among phenologies. Advances in Ecological Research, 32, pp.113-197.

Fajardo, L., Gonzalez, V., Nassar, J.M., Lacabana, P., Portillo, Q., Carlos, A., Carrasquel, F. and Rodriguez, J.P., 2005. Tropical dry forests of Venezuela: characterization and current conservation status. Biotropica, 37(4), pp.531-546.

Falge, E., Baldocchi. D., Tenhunen, J., Aubinet, M., Bakwin, P., Berbigier, P., Bernhofer, C., Burba, G., Clement, R., Davis, K.J. (2002). Seasonality of ecosystem respiration and gross primary production as derived from FLUXNET measurements. Agricultural and Forest Meteorology, 113: 53-74.

Feng, X., Porporato, A., & Rodriguez-Iturbe, I. (2013). Changes in rainfall seasonality in the tropics. Nature Climate Change, 3(9), 811.

Field, C.B., 1991. Ecological scaling of carbon gain to stress and resource. In Response of plants to multiple stresses (pp. 35-65). Academic Press San Diego.

Field, C.B.; Gamon, J.A.; Peñuelas, J. Remote sensing of photosynthesis. In Ecophysiology of Photosynthesis; Schulze, E.-D., Caldwell, M.M., Eds.; Ecological Studies; Springer: Berlin/Heidelberg, Germany; New York, NY, USA, 1994; Volume 100, pp. 511−527.

Field C.B., Randerson J.T., and Malmastrom C.M. (1995) Global net primary production: combining ecology and remote sensing. Remote Sensing of Environment, 51:74-88.

Filella. I., Amaro, T., Araus, J., L., and Peñuelas, J. (1996) Relationship between photosynthetic radiation-use efficiency of barley canopies and the photochemical reflectance index (PRI). Physiol Plant 96: 211–216.

Filella, I., Porcar-Castell, A., Munné-Bosch, S., Bäck, J., Garbulsky, M. F., & Peñuelas, J. (2009). PRI assessment of long-term changes in carotenoids/chlorophyll ratio and short-term changes in de-epoxidation state of the xanthophyll cycle. International Journal of Remote Sensing, 30(17), 4443-4455.

Finnigan, J.J. A re-evaluation of long-term flux measurement techniques part II: Coordinate systems. Bound.-Layer Meteorol. 2004, 113, 1–41.

Flanagan, L.B.; Johnson, B.G. Interacting effects of temperature, soil moisture and plant biomass production on ecosystem respiration in a northern temperate grassland. Agric. For. Meteorol. 2005, 130, 237–253.

Foken, T.H., Wichura, B., (1995). Tools for quality assessment of surface-based flux measurements. Agricultural and Forest Meteorology, 78: 83-105.

Frankenberg, C., Fisher, J. B., Worden, J., Badgley, G., Saatchi, S. S., Lee, J.-E., Toon, G. C., Butz, A., Jung, M., Kuze, A., and Yokota, T.: New global observations of the terrestrial carbon cycle from GOSAT: Patterns of plant fluorescence with gross primary productivity, Geophys. Res. Lett., 38, L17706, doi:10.1029/2011gl048738, 2011.

French, N.N.F., (2002). The Impact of Fire Disturbance on Carbon and Energy Exchange in the Alaskan Boreal Region: A Geospatial Data Analysis. Ph.D. dissertation Thesis, University of Michigan, Ann Arbor, 105.

Galvão, L.S.; Breunig, F.M.; dos Santos, J.R.; de Moura, Y.M. View-illumination effects on hyperspectral vegetation indices in the Amazonian tropical forest. Int. J. Appl. Earth Obs. Geoinf. 2013, 21, 291–300.

Gamon, J.A., Field, C.B., Bilger, W., Björkman, O., Fredeen, A.L., and Peñuelas, J. (1990) Remote sensing of the xanthophyll cycle and chlorophyll fluorescence in sunflower leaves and canopies. Oecologia 85: 1–7.

Gamon, J.A., Peñuelas J., and Field C.B. (1992). A narrow-waveband spectral index that tracks diurnal changes in photosynthetic efficiency. Remote Sensing of Environment 41: 35–44.

Gamon, J.A., Filella, I., Peñuelas, J. (1993) The dynamic 531-nanometer Δ reflectance signal: a

survey of twenty angiosperm species. Yamamoto HY , Smith CM (Eds). Photosynthetic Responses to the Environment. American Society of Plant Physiologists, Rockville. pp. 172-177.

Gamon, J. A.,Field, C.B., Goulden, M., Griffin, K., Hartley, A., Joel, G., Peñuelas, J., Valentini, R. (1995). Relationship between NDVI, canopy structure, and photosynthesis in three Californian vegetation types. Ecological Applications, 5: 28-41.

Gamon, J.A.; Serrano, L.; Surfus, J. The photochemical reflectance index: An optical indicator of photosynthetic radiation use efficiency across species, functional types, and nutrient levels. Oecologia 1997, 112, 492–501.

Gamon, J.A.; Surfus, J.S. Assessing leaf pigment content and activity with a reflectometer. New Phytol. 1999, 143, 105–117.

Gamon, J.A.; Rahman, A.F.; Dungan, J.L.; Schildhauer, M.; Huemmrich, K.F. Spectral Network (SpecNet)—What is it and why do we need it? Remote Sens. Environ. 2006, 103, 227–235.

Gamon, J. A., & Berry, J. A. (2012). Facultative and constitutive pigment effects on the Photochemical Reflectance Index (PRI) in sun and shade conifer needles. Israel Journal of Plant Sciences, 60(1-2), 85-95.

Gamon, J. A. (2015). Reviews and syntheses: Optical sampling of the flux tower footprint.

Gamon, J.A.; Kovalchuck, O.; Wong, C.Y.; Harris, A.; Garrity, S.R. Monitoring seasonal and diurnal changes in photosynthetic pigments with automated PRI and NDVI sensors. Biogeosciences 2015, 12, 4149–4159.

Gamon, J.A.; Huemmrich, K.F.; Wong, C.Y.; Ensminger, I.; Garrity, S.; Hollinger, D.Y.; Noormets, A.; Peñuelas, J. A remotely sensed pigment index reveals photosynthetic phenology in evergreen conifers. Proc. Natl. Acad. Sci. USA 2016, 113, 13087–13092.

Garbulsky, M.F.; Peñuelas, J.; Papale, D.; Ardö, J.; Goulden, M.L.; Kiely, G.; Richardson, A.D.; Rotenberg, E.; Veenendaal, E.M.; Filella, I. Patterns and controls of the variability of radiation use efficiency and primary productivity across terrestrial ecosystems. Glob. Ecol. Biogeogr. 2010, 19, 253–267.

Garbulsky, M. F., Peñuelas, J., Gamon, J., Inoue, Y., & Filella, I. (2011). The photochemical reflectance index (PRI) and the remote sensing of leaf, canopy and ecosystem radiation use efficiencies: A review and meta-analysis. Remote Sensing of Environment, 115(2), 281-297.

Garrity, S.R.; Vierling, L.A.; Bickford, K. A simple filtered photodiode instrument for continuous measurement of narrowband NDVI and PRI over vegetated canopies. Agric. For. Meteorol. 2010, 150, 489–496.

Garrity, S. R., Eitel, J. U., & Vierling, L. A. (2011). Disentangling the relationships between plant pigments and the photochemical reflectance index reveals a new approach for remote estimation of carotenoid content. Remote Sensing of Environment, 115(2), 628-635.

Genizi, A., 1993. Decomposition of R 2 in multiple regression with correlated regressors. Statistica Sinica, pp.407-420.

Gillespie, T.W., Grijalva, A. and Farris, C.N., 2000. Diversity, composition, and structure of tropical dry forests in Central America. Plant ecology, 147(1), pp.37-47.

Gitelson, A.A.; Gamon, J.A. The need for a common basis for defining light-use efficiency: Implications for productivity estimation. Remote Sens. Environ. 2015, 156, 196–201.

Gitelson, A.A.; Gamon, J.A.; Solovchenko, A. Multiple drivers of seasonal change in PRI: Implications for photosynthesis 1. Leaf level. Remote Sens. Environ. 2017, 190, 110–116.

Gitelson, A.A.; Gamon, J.A.; Solovchenko, A. Multiple drivers of seasonal change in PRI: Implications for photosynthesis 2. Stand level. Remote Sens. Environ. 2017, 190, 198–206.

Glenn, A.J.; Flanagan, L.B.; Syed, K.H.; Carlson, P.J. Comparison of net ecosystem CO2 exchange in two peatlands in western Canada with contrasting dominant vegetation, Sphagnum and Carex. Agric. For. Meteorol. 2006, 140, 115–135.

Gobron, N.; Pinty, B.; Aussedat, O.; Chen, J.M.; Cohen, W.B.; Fensholt, R.; Gond, V.; Huemmrich, K.F.; Lavergne, T.; Mélin, F.; et al. Evaluation of fraction of absorbed photosynthetically active radiation products for different canopy radiation transfer regimes: Methodology and results using Joint Research Center products derived from SeaWiFS against ground-based estimations. J. Geophys. Res. Atmos. 2006, 111, doi:10.1029/2005JD006511.

Goerner, A.; Reichstein, M.; Tomelleri, E.; Hanan, N.; Rambal, S.; Papale, D.; Dragoni, D.; Schmullius, C. Remote sensing of ecosystem light use efficiency with MODIS-based PRI. Biogeosciences 2011, 8, 189– 202.

Goulden, M. L., Miller, S. D., Da Rocha, H. R., Menton, M. C., de Freitas, H. C., & de Sousa, C. A. D. 2004. Diel and seasonal patterns of tropical forest CO2 exchange. Ecological Applications, 14(sp4), pp42-54.

Goward, S. N., Tucker, C. J., and Dye, D. G.: North-American vegetation patterns observed with the NOAA-7 Advanced Very High Resolution Radiometer, Vegetatio, 64, 3–14, 1985.

Grace J., Nichol, C., Disney, M., Lewis, P., Quaife, T., Bowyer, P. (2007). Can we measure terrestrial photosynthesis from space directly, using spectral reflectance and fluorescence? Global Change Biology, 13:1487-1497.

Gromping U., 2006. relaimpo: Relative Importance of Regressors in Linear Models. R package version 1.1-1.

Gu, L., Baldocchi, D., Verma, S. B., Black, T. A., Vesala, T., Falge, E. M., & Dowty, P. R. (2002). Advantages of diffuse radiation for terrestrial ecosystem productivity. Journal of

Geophysical Research: Atmospheres, 107(D6), ACL-2.

Hanan, N.P., Burba, G., Verma, S.B., Berry, J.A., Suyker, A. and Walter-Shea, E.A., 2002. Inversion of net ecosystem CO_2 flux measurements for estimation of canopy PAR absorption. Global Change Biology, 8(6), pp.563-574.

Hanson, P.J., Amthor, J.S., Wullschleger, S.D., Wilson, K.B., Grant, R.F., Hartley, A., Hui, D., Hunt Jr, E.R., Johnson, D.W., Kimball, J.S. and King, A.W., 2004. Carbon and water cycle simulations for an upland oak forest using 13 stand-level models: intermodel comparisons and evaluations against independent measurements. Ecol. Monogr, 74, pp.443-489.

Harris, A.; Gamon, J.A.; Pastorello, G.Z.; Wong, C.Y.S. Retrieval of the photochemical reflectance index for assessing xanthophyll cycle activity: A comparison of near-surface optical sensors. Biogeosciences.2014, 11, 6277–6292.

Hilker, T.; Coops, N.C.; Hall, F.G.; Black, T.A.; Wulder, M.A.; Nesic, Z.; Krishnan, P. Separating physiologically and directionally induced changes in PRI using BRDF models. Remote Sens. Environ. 2008, 112, 2777–2788.

Hilker, T.; Coops, N.C.; Nesic, Z.; Wulder, M.A.; Black, A.T. Instrumentation and approach for unattended year round tower based measurements of spectral reflectance. Comput. Electron. Agric. 2007, 56, 72–84.

Huemmrich, K.F., Black, T.A., Jarvis, P.G., McCaughey, J.H. and Hall, F.G., 1999. High temporal resolution NDVI phenology from micrometeorological radiation sensors. Journal of Geophysical Research: Atmospheres, 104(D22), pp.27935-27944.

Huemmrich, K. F., Campbell, P., Landis, D., & Middleton, E. (2019). Developing a common globally applicable method for optical remote sensing of ecosystem light use efficiency. Remote Sensing of Environment, 230, 111190.

Huete, A. R., Didan, K., Shimabukuro, Y. E., Ratana, P., Saleska, S. R., Hutyra, L. R., ... & Myneni, R. 2006. Amazon rainforests green-up with sunlight in dry season. Geophysical research letters, 33(6).

Huete, A.; Ponce-Campos, G.; Zhang, Y.; Restrepo-Coupe, N.; Ma, X.; Moran, M. Monitoring photosynthesis from space. In Land Resources Monitoring, Modeling, and Mapping with Remote Sensing; Remote Sensing Handbook; CRC Press: Boca Raton, FL, USA, 2015; pp. 3–22.

Hutyra, L.R., Munger, J.W., Saleska, S.R., Gottlieb, E., Daube, B.C., Dunn, A.L., Amaral, D.F., De Camargo, P.B. and Wofsy, S.C., 2007. Seasonal controls on the exchange of carbon and water in an Amazonian rain forest. Journal of Geophysical Research: Biogeosciences, 112(G3).

Hutyra, L.R., Munger, J.W., Hammond-Pyle, E., Saleska, S.R., Restrepo-Coupe, N., Daube, B.C., de Camargo, P.B. and Wofsy, S.C., 2008. Resolving systematic errors in estimates of net ecosystem exchange of CO 2 and ecosystem respiration in a tropical forest biome. agricultural and forest meteorology, 148(8), pp.1266-1279.

IPCC (2013). Climate Change 2013: The Physical Scientific Basis. Contribution of Working Group I to the Fifth Assessment Report of the Intergovernmental Panel on Climate Change. Cambridge University Press, New York, USA.

Janzen, D.H., 1988. Tropical dry forests. Biodiversity, p.538.

Janzen, D.H., 2000. Costa Rica's Area de Conservación Guanacaste: a long march to survival through non-damaging biodevelopment. Biodiversity, 1(2), pp.7-20.

Jarvis PG, Leverenz JW. Productivity of temperate, deciduous and evergreen forests. InPhysiological plant ecology IV 1983 (pp. 233-280). Springer, Berlin, Heidelberg.

Jarvis, P., Rey, A., Petsikos, C., Wingate, L., Rayment, M., Pereira, J., Banza, J., David, J., Miglietta, F., Borghetti, M. and Manca, G., 2007. Drying and wetting of Mediterranean soils stimulates decomposition and carbon dioxide emission: the "Birch effect". Tree physiology, 27(7), pp.929-940.

Jenkins, J.P.; Richardson, A.D.; Braswell, B.H.; Ollinger, S.V.; Hollinger, D.Y.; Smith, M.L. Refining light-use efficiency calculations for a deciduous forest canopy using simultaneous tower-based carbon fluxand radiometric measurements. Agric. For. Meteorol. 2007, 143, 64–79.

Johnson, J.W., Lebreton J.M. 2004. History and Use of Relative Importance Indices in Organizational Research. Organizational Research Methods, 7, pp.238–257.

Jung, M., Reichstein, M. and Bondeau, A., 2009. Towards global empirical upscaling of FLUXNET eddy covariance observations: validation of a model tree ensemble approach using a biosphere model. Biogeosciences, 6(10), pp.2001-2013.

Kasischke, E.S. and Stocks, B.J., (2000). Fire, Climate Change, and Carbon Cycling in the Boreal Forest. Ecological Studies 138. Springer-Verlag, New York, pp. 461.

Kimes, D.S. Dynamics of directional reflectance factor distributions for vegetation canopies. Appl. Opt.
1983, 22, 1364–1372.

Kljun, N.; Calanca, P.; Rotach, M.W.; Schmid, H.P. A simple parameterisation for flux footprint
predictions. Bound.-Layer Meteorol. 2004, 112, 503–523.

Knyazikhin, Y.; Schull, M.A.; Stenberg, P.; Mottus, M.; Rautiainen, M.; Yang, Y.; Marshak, A.; Latorre Carmona, P.; Kaufmann, R.K.; Lewis, P.; et al. Hyperspectral remote sensing of foliar nitrogen content. Proc. Natl. Acad. Sci. USA 2013, 110, E185–E192, doi:10.1073/pnas.1210196109.

Kumar, J., Hoffman, F.M., Hargrove, W.W. and Collier, N., 2016. Understanding the representativeness of FLUXNET for upscaling carbon flux from eddy covariance measurements. Earth Syst. Sci. Data Discuss, pp.1-25.

Kutsch, W. L., Hanan, N., Scholes, R. J., McHugh, I., Kubheka, W., Eckhardt, H., & Williams, C. 2008. Response of carbon fluxes to water relations in a savanna ecosystem in South Africa. Biogeosciences Discussions, 5(3), pp.2197-2235.

Landsberg L. L., Waring R. H., (1997). A generalized model of forest productivity using simplified concepts of radiation-use efficiency, carbon balance and partitioning. Forest Ecology and Management, 95:209-228.

Law, B. E., Waring, R., Anthoni, P. M., & Aber, J. D. (2000). Measurements of gross and net ecosystem productivity and water vapour exchange of a Pinus ponderosa ecosystem, and an evaluation of two generalized models. Global Change Biology, 6(2), 155-168.

Law, B.E., Falge, E., Gu, L., Baldocchi, D.D., Bakwin, P., Berbigier, P., Davis, K., Dolman, A.J., Falk, M., Fuentes, J.D. (2002). Environmental controls over carbon dioxide and water vapor exchange of terrestrial vegetation. Agricultural and Forest Meteorology, 113: 97-120.

Leuchner, M., Hertel, C., Menzel, A., 2011. Spatial variability of photosynthetically active radiation in European beech and Norway spruce. Agric. For. Meteorol. 151, 1226–1232.

Li, W., Cao, S., Campos-Vargas, C. and Sanchez-Azofeifa, A., 2017. Identifying tropical dry forests extent and succession via the use of machine learning techniques. International Journal of Applied Earth Observation and Geoinformation, 63, pp.196-205.

Liu, L.; Zhang, Y.; Jiao, Q.; Peng, D. Assessing photosynthetic light-use efficiency using a solar-inducedchlorophyll fluorescence and photochemical reflectance index. Int. J. Remote Sens. 2013, 34, 4264–4280.

Lieberman, D., 1982. Seasonality and phenology in a dry tropical forest in Ghana. The Journal of Ecology, pp.791-806.

Lindeman, R.H. and Lindeman, R.H., 1980. Introduction to bivariate and multivariate analysis (No. 04; QA278, L553.).

Maass, J.M., Balvanera, P., Castillo, A., Daily, G.C., Mooney, H.A., Ehrlich, P., Quesada, M., Miranda, A., Jaramillo, V.J., García-Oliva, F. and Martínez-Yrizar, A., 2005. Ecosystem services of tropical dry forests: insights from longterm ecological and social research on the Pacific Coast of Mexico. Ecology and society: a journal of integrative science for resilience and sustainability, 10(1), pp.1-23.

Malhi, Y., Roberts, J.T., Betts, R.A., Killeen, T.J., Li, W. and Nobre, C.A., 2008. Climate change, deforestation, and the fate of the Amazon. science, 319(5860), pp.169-172.

Malhi, Y., 2012. The productivity, metabolism and carbon cycle of tropical forest vegetation. Journal of Ecology, 100(1), pp.65-75.

Magrin GO, Marengo JA, Boulanger JP, Buckeridge MS, Castellanos E, Poveda G. (2014). Central and South America in Climate Change 2014: Impacts, Adaptation, and Vulnerability. Part B: Regional Aspects. Contribution of Working Group II to the Fifth Assessment Report of the Intergovernmental Panel on Climate Change.Barros, V.R., C.B. Field, D.J. Dokken, M.D. Mastrandrea, K.J. Mach, T.E. Bilir, M. Chatterjee, K.L. Ebi, Y.O. Estrada, R.C. Genova, B. Girma, E.S. Kissel, A.N. Levy, S. MacCracken, P.R. Mastrandrea, and L.L.White (Eds.), Cambridge University Press, Cambridge and New York,1499-1566

Massman W.J., Lee X., (2002). Eddy covariance flux correlations and uncertainties in long term studies of carbon and energy exchanges. Agricultural and Forest Meteorology, 113: 121-144.

Moncrieff, J.B., Massheder, J.M., De Bruin, H., Elbers, J., Friborg, T., Heusinkveld, B., Kabat, P., Scott, S., Soegaard, H. and Verhoef, A., 1997. A system to measure surface fluxes of momentum, sensible heat, water vapour and carbon dioxide. Journal of Hydrology, 188,

pp.589-611.

Moncrieff, J.; Clement, R.; Finnigan, J.; Meyers, T. Averaging, detrending, and filtering of eddy covariance time series. In Handbook of Micrometeorology; Springer: Dordrecht, The Netherlands, 2004; pp. 7–31.

Montgomery, R.A., Chazdon, R.L., 2001. Forest structure, canopy architecture, and light forest structure, canopy architecture, and light transmittance in tropical wet forests. Ecology 82, 2707–2718.

Monteith, J.L. Solar radiation and productivity in tropical ecosystems. J. Appl. Ecol. 1972, 9, 747–766.

Monteith, J.L. Principles of Environmental Physics; Elsevier: New York, NY, USA, 1973.

Monteith, J.L. (1977). Climate and the efficiency of cop production in Britain. Phil. Trans. R. Soc. Lond. B. 281: 277-294.

Mooney, H.A. and Gulmon, S.L., 1979. Environmental and evolutionary constraints on the photosynthetic characteristics of higher plants. In Topics in plant population biology (pp. 316-337). Macmillan Education UK.

Mooney, H.A. and Gulmon, S.L., 1982. Constraints on leaf structure and function in reference to herbivory. BioScience, 32(3), pp.198-206.

Mortazavi, S.H., Salehe, M., MacGregor, M.H., 2014. Maximum WSN coverage in environments of heterogeneous path loss. International Journal of Sensor Networks 16, 185–198.

Moore, C.J. (1986). Frequency response corrections for eddy correlation systems. Boundary-Layer Meteorol, 37: 17-35.

Murphy, P.G. and Lugo, A.E., 1986. Ecology of tropical dry forest. Annual review of ecology and

systematics, 17(1), pp.67-88.

Myneni, R.B., & Williams, D.L., (1994). On the relationship between FAPAR and NDVI. Remote Sensing of Environment, 49:200-211.

Natural Regions Committee 2006. Natural Regions and Subregions of Alberta. Compiled by D.J. Downing and W.W. Pettapiece. Government of Alberta. Pub. No. T/852.

Nichol, C.J.; Lloyd, J.O.; Shibistova, O.; Arneth, A.; Röser, C.; Knohl, A.; Matsubara, S.; Grace, J. Remote sensing of photosynthetic-light-use efficiency of a Siberian boreal forest. Tellus B Chem. Phys. Meteorol. 2002, 54, 677–687.

Norman, J.M.; Arkebauer, T.J. Predicting canopy light-use efficiency from leaf characteristics. Model. Plant Soil Syst. 1991, 31, 125–143.

Pacheco-Labrador, J.; Martín, M.P. Nonlinear response in a field portable spectroradiometer:
Characterization and effects on output reflectance. IEEE Trans. Geosci. Remote Sens. 2014, 52, 920–928.

Papale, D. and Valentini, R., 2003. A new assessment of European forests carbon exchanges by eddy fluxes and artificial neural network spatialization. Global Change Biology, 9(4), pp.525-535.

Pan, Y., Birdsey, R.A., Fang, J., Houghton, R., Kauppi, P.E., Kurz, W.A., Phillips, O.L., Shvidenko, A., Lewis, S.L., Canadell, J.G. and Ciais, P. (2011). A large and persistent carbon sink in the world's forests. Science, 333(6045), 988-993.

Penuelas, J., Filella, I., & Gamon, J. A. (1995). Assessment of photosynthetic radiation-use efficiency with spectral reflectance. New Phytologist, 131(3), 291-296.

Prince, S.D. and Goward, S.N. (1995). Global primary production: a remote sensing approach. Journal of Biogeography 22: 815–835.

Potter, C. S., Randerson, J. T., Field, C. B., Matson, P. A., Vitousek, P. M., Mooney, H. A., & Klooster, S. A. (1993). Terrestrial ecosystem production: a process model based on global satellite and surface data. Global Biogeochemical Cycles, 7(4), 811-841.

Putzenlechner, B., Castro, S., Kiese, R., Ludwig, R., Marzahn, P., Sharp, I., & Sanchez-Azofeifa, A. (2019). Validation of Sentinel-2 fAPAR products using ground observations across three forest ecosystems. Remote Sensing of Environment, 232, 111310.

Quesada, M., Sanchez-Azofeifa, G.A., Alvarez-Anorve, M., Stoner, K.E., Avila-Cabadilla, L., Calvo-Alvarado, J., Castillo, A., Espírito-Santo, M.M., Fagundes, M., Fernandes, G.W. and Gamon, J., 2009. Succession and management of tropical dry forests in the Americas: Review and new perspectives. Forest Ecology and Management, 258(6), pp.1014-1024.

Rahman, A.F.; Cordova, V.D.; Gamon, J.A.; Schmid, H.P.; Sims, D.A. Potential of MODIS ocean bands
for estimating CO_2 flux from terrestrial vegetation: A novel approach. Geophys. Res. Lett. 2004, 31, doi:10.1029/2004GL019778.

Rankine, C.J.; Sanchez-Azofeifa, G.A.; MacGregor, M.H. Seasonal wireless sensor network link performance in boreal forest phenology monitoring. In Proceedings of the 2014 Eleventh Annual IEEE International Conference on Sensing, Communication, and Networking (SECON), Singapore, 30 June–3 July 2014; pp. 302–310.

Reichstein, M., Tenhunen, J.D., Roupsard, O., Ourcival, J.M., Rambal, S., Dore, S. and Valentini, R., 2002. Ecosystem respiration in two Mediterranean evergreen Holm Oak forests: drought effects and decomposition dynamics. Functional Ecology, 16(1), pp.27-39.

Reichstein, M., Tenhunen, J., Roupsard, O., Ourcival, J.M., Rambal, S., Miglietta, F., Peressotti, A., Pecchiari, M., Tirone, G. and Valentini, R., 2003. Inverse modeling of seasonal drought effects on canopy CO_2/H_2O exchange in three Mediterranean ecosystems. Journal of Geophysical Research: Atmospheres, 108(D23).

Reichstein, M., Falge, E., Baldocchi, D., Papale, D., Aubinet, M., Berbigier, P., Bernhofer, C., Buchmann, N., Gilmanov, T., Granier, A. and Grünwald, T., 2005. On the separation of net ecosystem exchange into assimilation and ecosystem respiration: review and improved algorithm. Global Change Biology, 11(9), pp.1424-1439.

Reich, P.B. and Borchert, R., 1982. Phenology and ecophysiology of the tropical tree, Tabebuia neochrysantha (Bignoniaceae). Ecology, 63(2), pp.294-299.

Reich, P.B. and Borchert, R., 1984. Water stress and tree phenology in a tropical dry forest in the lowlands of Costa Rica. The Journal of Ecology, pp.61-74.

Reich, P.B. and Borchert, R., 1988. Changes with leaf age in stomatal function and water status of several tropical tree species. Biotropica, pp.60-69.

Reich, P.B., 1995. Phenology of tropical forests: patterns, causes, and consequences. Canadian Journal of Botany, 73(2), pp.164-174.

Reich, P.B., Turner, D.P., Bolstad, P. (1999). An approach to spatially distributed modeling of net primary production (NPP) at the landscape scale and its application in validation of EOS NPP products. Remote Sensing of Environment, 70: 69−81.

Ruimy, A.L.; Jarvis, P.G.; Baldocchi, D.D.; Saugier, B. CO_2 fluxes over plant canopies and solar radiation:A review. Adv. Ecol. Res. 1995, 26, 1–68.

Ryan, P.J.; Stolzenbach, K.D. Engineering Aspects of Heat Disposal from Power Generation; Harleman,
D.R.F., Ed.; RM Parson Laboratory for Water Resources and Hydrodynamics, Department of Civil Engineering, Massachusetts Institute of Technology: Cambridge, MA, USA, 1972.

Running S.W. et al. (2004). A continuous satellite-derived measure of global terrestrial primary production. Bioscience, 54(6): 547-560.

Sims, D. A., & Gamon, J. A. (2002). Relationships between leaf pigment content and spectral reflectance across a wide range of species, leaf structures and developmental stages. Remote sensing of environment, 81(2-3), 337-354.

Sánchez-Azofeifa, G.A., Quesada, M., Rodriguez, J.P., Nassar, J.M., Stoner, K.E., Castillo, A., Garvin, T., Zent, E.L., Calvo-Alvarado, J.C., Kalacska, M.E. and Fajardo, L., 2005. Research priorities for neotropical dry forests. Biotropica, 37(4), pp.477-485.

Schimel D.S. (1995). Terrestrial biogeochemical cycles: global estimates with remote sensing. Remote Sensing of Environment, 51: 49−56.

Schimel, D.S., House, J.I., Hibbard, K.A., Bousquet, P., Ciais, P., Peylin, P., Braswell, B.H., Apps, M.J., Baker, D., Bondeau, A. and Canadell, J., (2001). Recent patterns and mechanisms of carbon exchange by terrestrial ecosystems. Nature, 414:169-172.

Schimel, D.; Pavlick, R.; Fisher, J.B.; Asner, G.P.; Saatchi, S.; Townsend, P.; Miller, C.; Frankenberg, C.; Hibbard, K.; Cox, P. Observing terrestrial ecosystems and the carbon cycle from space. Glob. Chang. Biol.2015, 21, 1762–1776.

Sellers, P.J. (1985). Canopy reflectance, photosynthesis, and transpiration. International Journal of Remote Sensing, 6(8):1335-1372.

Sellers, P.J. (1987). Canopy reflectance, photosynthesis, and transpiration II. The role of biophysics in the linearity of their interdependence. Remote Sensing of Environment, 21: 143−183.

Sellers, P. J., Hall, F. G., Asrar, G., Strebel, D. E., & Murphy, R. E. (1992). An overview of the first international satellite land surface climatology project (ISLSCP) field experiment (FIFE). Journal of Geophysical Research: Atmospheres, 97(D17), 18345-18371.

Sellers, Piers J., et al. "BOREAS in 1997 (1997). Experiment overview, scientific results, and future directions." Journal of Geophysical Research: Atmospheres 102.D24: 28731-28769.

Sims, D.A.; Gamon, J.A. Relationships between leaf pigment content and spectral reflectance across a wide range of species, leaf structures and developmental stages. Remote Sens. Environ. 2002, 81, 337–354.

Sims, D.A., Rahman, A.F., Cordova, V.D., Baldocchi, D.D., et al. (2005). Midday values of gross CO2 flux and light use efficiency during satellite overpasses can used to directly estimate eight-day mean flux. Remote Sensing of Environment, 101: 1-12.

Sobrado, M.A., 1997. Embolism vulnerability in drought-deciduous and evergreen species of a tropical dry forest. Acta Oecologica, 18(4), pp.383-391.

Soil Classification Working Group. The Canadian System of Soil Classification; Publication 1646
(Revised); Agriculture and Agri-Food Canada: Ottawa, ON, Canada, 1998; p. 187.

Stylinski, C., Gamon, J., & Oechel, W. (2002). Seasonal patterns of reflectance indices, carotenoid pigments and photosynthesis of evergreen chaparral species. Oecologia, 131(3), 366-374.

Syed, K.H.; Flanagan, L.B.; Carlson, P.J.; Glenn, A.J.; Van Gaalen, K.E. Environmental control of net ecosystem CO_2 exchange in a treed, moderately rich fen in northern Alberta. Agric. For. Meteorol. 2006,
140, 97–114.

Townsend, P.A.; Serbin, S.P.; Kruger, E.L.; Gamon, J.A. Disentangling the contribution of biological and physical properties of leaves and canopies in imaging spectroscopy data. Proc. Natl. Acad. Sci. USA 2013, 110, E1074, doi:10.1073/pnas.1300952110.

Turner, D. P., et al., (2005). Site-level evaluation of satellite-based global terrestrial GPP and NPP monitoring, Global Change Biol., 11(4), 666–684.

Van Leeuwen, M.; Kremens, R.L.; van Aardt, J. Tracking diurnal variation in photosynthetic

down-regulation using low cost spectroscopic instrumentation. Sensors 2015, 15, 10616–10630.

Verduzco, V. S., Garatuza-Payán, J., Yépez, E. A., Watts, C. J., Rodríguez, J. C., Robles-Morua, A., & Vivoni, E. R. 2015. Variations of net ecosystem production due to seasonal precipitation differences in a tropical dry forest of northwest Mexico. Journal of Geophysical Research: Biogeosciences, 120(10), pp2081-2094.

Vickers, D.; Mahrt, L. Quality control and flux sampling problems for tower and aircraft data. J. Atmos.
Ocean. Technol. 1997, 14, 512–526.

Walter, H., (1979). Vegetation of the Earth and Ecological Systems of the Geo-biosphere. Springer-Verlag, New York, pp. 274.

Waring, B.G. and Powers, J.S., 2016. Unraveling the mechanisms underlying pulse dynamics of soil respiration in tropical dry forests. Environmental Research Letters, 11(10), p.105005.

Webb, E.K.; Pearman, G.I.; Leuning, R. Correction of flux measurements for density effects due to heat
and water vapour transfer. Q. J. R. Meteorol. Soc. 1980, 106, 85–100.

Whigham, D.F., Zugasty, T., Cabrera, C., O'neill, J. and Ley, E., 1990. The effect of annual variation in precipitation on growth and litter production in a tropical dry forest in the Yucatan of Mexico. Tropical Ecology, 31(2), pp.23-34.

Widlowski, J. L. (2010). On the bias of instantaneous FAPAR estimates in open-canopy forest. Agricultural and Forest Meteorology, 150(12), 1501-1522.

Winton, M. (2006). Amplified Arctic climate change: What does surface albedo feedback have to do with it? Geophysical Research Letters, 33(3).

Yang, G.-Y., Slingo, J., 2001. The diurnal cycle in the tropics. Mon. Weather Rev. 129, 784–801

Younis, M., Akkaya, K., 2008. Strategies and techniques for node placement in wireless sensor networks: a survey. Ad Hoc Netw. 6, 621–655

Yuan, W. P., Liu, S. G., Zhou, G. S., Zhou, G. Y., Tieszen, L. L., Baldocchi, D., Bernhofer, C., Gholz, H., Goldstein, A. H., Goulden, M. L., Hollinger, D. Y., Hu, Y., Law, B. E., Stoy, P. C., Vesal, T., Wofsy, S. C., and other AmeriFlux collaborators (2007) Deriving a light use efficiency 10 model from eddy covariance flux data for predicting daily gross primary production across biomes. Agr. Forest Meteorol., 143: 189–207.

Yuan, W. P., Liu, S. G., Yu, G. R., Bonnefond, J., Chen, J., Davis, K., Desai, A. R., Goldstein, A. H., Gianelle, D., Rossi, F., Suyker, A. E., and Verma, S. B. (2010) Global estimates of evapotranspiration and gross primary production based on MODIS and global meteorology 15 data. Remote Sens. Environ., 114: 1416–1431.

Yuan, W., Cai, W., Liu, S., Dong, W., Chen, J., Arain, M. A., ... & Genesio, L. (2014). Vegetation-specific model parameters are not required for estimating gross primary production. Ecological modelling, 292, 1-10.

Zelazowski, P., Malhi, Y., Huntingford, C., Sitch, S. and Fisher, J.B., 2011. Changes in the potential distribution of humid tropical forests on a warmer planet. Philosophical Transactions of the Royal Society of London A: Mathematical, Physical and Engineering Sciences, 369(1934), pp.137-160.

Zhang, C.; Filella, I.; Garbulsky, M.; Peñuelas, J. Affecting factors and recent improvements of thephotochemical reflectance index (PRI) for remotely sensing foliar, canopy and ecosystemic radiation-use efficiencies. Remote Sens. 2016, 8, 677.

Zhang, C.; Filella, I.; Liu, D.; Ogaya, R.; Llusià, J.; Asensio, D.; Peñuelas, J. Photochemical reflectance
index (PRI) for detecting responses of diurnal and seasonal photosynthetic activity to

experimental drought and warming in a mediterranean shrubland. Remote Sens. 2017, 9, 1189.

Zuber, V. and Strimmer, K., 2010. High-dimensional regression and variable selection using CAR scores. arXiv preprint arXiv:1007.5516.

Appendix A1

A1.1 Meteorology and Phenology Instrumentation

Broadband optical measurements from two-band radiometers provided fully automated continuous measurements of both the target reflectance and the sky conditions. The phenology tower allowed near-continuous measurements since first installed in February 2013. Measurements included light conditions, through upward looking photosynthetic active radiation (PAR) and pyranometer (PYR) spot radiometers (Apogee Instruments Inc., Logan, Utah, USA), and canopy reflectance, through paired upward and downward-looking PAR and PYR sensors (Apogee Instruments Inc., Logan, Utah, USA). Ancillary meteorological data included temperature (T) and relative humidity (RH) measurements (Apogee Instruments Inc., Logan, Utah, USA) from which vapor pressure deficit was calculated. Three pairs of volumetric soil water content (VWC) sensors (EC5, Decagon Devices Inc., Pullman, Washington, USA) were installed within the flux footprint and logged continuously at 30-minute intervals. Continuous optical measurements were logged at an interval of 10 minutes throughout the 2013, 2014, 2015, and 2016 growing seasons. Data was logged onto a MicroStrain ENV-Link Mini Data Logger Node (Onset Computer Corporation, Bourne, Massachusetts, USA, Massachusetts).

A broadband NDVI was derived from the two-band spot radiometers following a revised method of the Huemmrich et al. (1999) method. The index was constructed as follows:

$$NDVI = (\rho_{PYR} - \rho_{PAR})/ (\rho_{PYR} + \rho_{PAR}) \quad (1)$$

where ρ_{PYR} is the solar radiation reflectance calculated from the ratio of upwelling to downwelling radiation using the pyranometers; and ρ_{PAR} is the total reflectance of photosynthetically active radiation (PAR) calculated from the ratio of upwelling to downwelling PPFD.

A1.1.2 Eddy Covariance Instrumentation:

Flux equipment was installed on horizontal boom oriented NE, the prevailing wind direction, at a height of 35m above the forest floor. Additional meteorological equipment integrated into the flux tower including a 4-component net radiometer (model NR01, Hukseflux Thermal Sensors B.V., Delft, Netherland) and complete weather station (model HOBO U-30-NRC Weather station, Onset Computer Corp., Bourne, MA, USA) with Iridium satellite communications (Upward Innovations

Inc., East Falmouth, MA, USA).

High-frequency eddy covariance data was processed using the post-acquisition software EdiRe (http://www.geos.ed.ac.uk/abs/research/micromet/EdiRe). Flux of CO_2 was expressed as the product of mean air density and the covariance between instantaneous vertical wind velocity and concentration fluctuations.

$$F_c = - \rho_a \overline{w' s'} \quad (2)$$

where F_c represents the vertical CO_2 (μmol m^{-2} s^{-1}), ρ_a is the dry air density (mol m^{-3}), w is the instantaneous vertical wind speed (m s^{-1}), and s is the molar mixing ratio (mol mol^{-1} dry air). Overbars over the wind speed and mixing ratio terms indicate time averaging, while primes indicate fluctuations about the mean (over a 30-minute time aggregate), following Reynolds decomposition. The negative notation in the expression was added since a meteorological notation was adopted for representation of NEE, where negative NEE values represented net CO2 uptake into an ecosystem and a positive values represent net CO2 release into the atmosphere.

Time lag correction was applied to the 10Hz eddy covariance data to compensate for IRGA and SAT instrument separation (Moore, 1986). High-frequency losses due to attenuation associated with the close path system were corrected following the method described Moncrieff et al. (1997). Spikes were detected as three or less outliers falling outside a plausibility range for each variable, defined in standard deviation units as outlined by Vickers and Mahrt (1997). A double rotation coordinate correction (Finnigan et al., 2003), allowed the proper alignment of the mean vertical wind direction to a position exactly perpendicular to the mean wind streamlines. To correct for the effect of changes in temperature and water vapor on air density (and CO2 mixing ratio) (Webb et al. 1980), the Webb-Pearman-Leuning correction was applied. After all corrections were applied, fluxes (CO2, H2O, momentum and energy) were calculated as 30-minute block averages. Cospectral and ogive analyses of CO2, H2O, and heat flux measurements allowed the verification of appropriate instrument sampling frequency and averaging intervals to capture all flux eddies (Kaimal et al., 1972; Lee at al. 2004). For this site, 30-minute averaging intervals at 10 Hz indicated adequate capture of low-frequency fluxes. Precipitation events were not explicitly removed from the dataset. However, diagnostic/error flags associate with IRGA and SAT instrument failure, including during heavy rainfall, were used as a filter. A requirement of 80% data coverage was applied for each 30-minute averaging interval.

Additional processing products included calculations of H and LE. H is computed as the

covariance between instantaneous vertical wind and temperature, expressed in energy units (W m-2). LE is the product of the latent heat of vaporization and the water vapor flux, expressed in energy units (W m-2). LE represents the plant evapotranspiration process, where negative values indicate condensation and positive values indicate evaporation plus transpiration.

Wind regime changes associated with seasonal changes made it necessary to characterize the footprint during wet and dry season independently. Flux-footprint analysis' were performed following the Kljun et al. (2004) parametrization (A simple parameterization for flux footprint predictions, online footprint, available at http://footprint.kljun.net/, 2004). The model products provided an estimate of the horizontal distance associated with the maximum contribution of measured fluxes (Xmax) and distances within which 90% of fluxes originate (X90%). During the wet season, Xmax was 357 m, and X90% was 704 m. Footprint direction was to the northeast (Fig. 2). High wind speeds are common during the dry season leading to increases in Xmax and X90% ranges. 453 m and 872 m, respectively. Also, wind direction variability changed as more components were seen from the west direction. Due to the large plateau where the tower is located, fetch limitations were not of concern.

A1.1.3 Eddy Covariance Partitioning:

Measurements of NEE was partitioned into its two components as,

$$NEE = -GPP + R_{eco} \quad (3)$$

where GPP is the gross primary production (µmol m^{-2} s^{-1}) and R_{eco} is the total ecosystem respiration (µmol m^{-2} s^{-1}). Reco was estimated using night-time fluxes based approach, using the Reichstein et al. (2005) partitioning algorithm. This model is based on the exponential regression response between temperature and respiration (Lloyd and Taylor, 1994) expressed by the equation,

$$R_{eco}\,(T) = R_{ref}\, e^{E_o\left(\frac{1}{T_{ref}-T_o} - \frac{1}{T-T_o}\right)} \quad (4)$$

where R_{ref} is the respiration at reference temperature 15°C, the T_{ref} is the reference temperature at 15°C, E_o is the activation-energy parameter, T is the observed air or soil temperature, and T_o is kept constant at -46.02°C. For nighttime results to be properly extrapolated to daytime fluxes, nighttime periods need to represent well mixed periods. Observed relationship between NEE and fictional velocity (u*, m s^{-1}) allowed us to determine the u* threshold (< 0.21 m s^{-1}) where NEE measurements

were likely to be unreliable as a result of calm conditions. Tropical ecosystems have been suggested as being susceptible to decupling between traditional temperature-respiration relationships as temperature shows little seasonal variability (Hutyra et al., 2007, 2008). A light-response curve model, independent of respiration by relying solely on characterizing carbon assimilation as a function of light, was used as an independent method to estimating R_{eco} and GPP. This method uses typically a hyperbolic function that resembles the response of photosynthesis to radiation. There are a variety of light response curve models available, but The specific function used for this study (eq. 5) was utilized by Hutyra et al. (2007) for eddy covariance data in a tropical forest and expressed as,

$$NEE(PAR) = \frac{a \times PAR}{b+PAR} + c = GPP + Reco \quad (5)$$

In eq. 5, net ecosystem exchange is a function of photosynthetically active radiation (PAR) with three parameters *a*, *b*, and *c*. T he first term represents the GPP (eq. 6) estimates over intervals after first fitting eq. 5 to flux data, while the second term, the constant *c*, represents ecosystem respiration for that interval and emerges from eq. 5 as PAR → 0.

$$GPP\ (PAR) = \frac{a \times PAR}{b+PAR} \quad (6)$$

A1.1.4 Regression and Relative Importance Modeling:

Relative importance modeling was used using the 'relaimpo' library (Gromping, 2006) within R statistical software. As described by Gromping (2006), relative importance metrics provide a quantification of a regressor's contribution to multiple regression models (i.e. amount of explained variance of a regression model). A number of relative importance models have been proposed in literature, each calculating importance metrics by different methods. We used four different models including the Linderman, Merenda, and Gold (LGM) model, First model, Genezi model, and CAR model, to increase the reliability of results. Details on each model can be found in the 'relaimpo' documentation, as well as in source material (Genezi, 1993; Johnson and Lebreton, 2004; Linderman et al., 1980; Zuber and Strimmer, 2010).

A1.2 Supplementary Results

A1.2.1 Interseasonal Precipitation Variability

Variability in rainfall patterns can be seen in the percent monthly accumulation contribution to total quantities (Fig. 2). During the "normal" 2013 and 2016 seasons, precipitation events occurred continuously throughout the wet season. Monthly rainfall contributions remained stable during May-August and peaked during September-October. By contrast, the 2014 and 2015 droughts initiated their seasons (May and June, respectively) with precipitation events that were then quickly followed with low rainfall periods. The 2014 drought was most severe during July, which saw only 21.8mm (+2.8mm SD) of rain and accounted for 1.9 % of the total seasonal precipitation (Fig. 3). The 2015 season saw a severe drought extending from July to September. August 2015 was particularly dry, with only 6.2mm (+0.5mm SD) of rainfall. Still, in both drought seasons, precipitation peaked during September and October.

A1.2.2 Relative Importance Analysis on Phenology

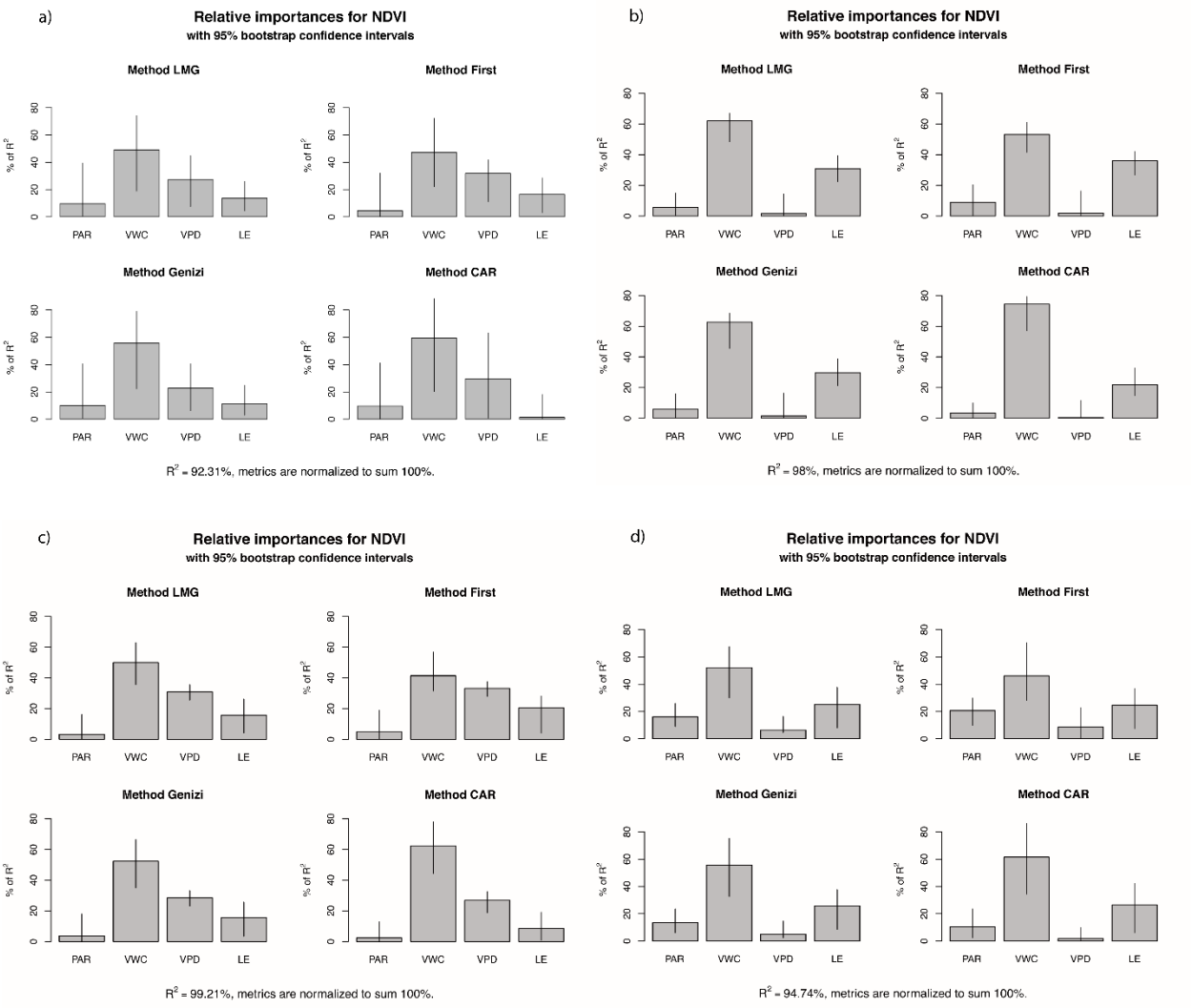

Figure A1.1 Relative importance analysis of GLM NDVI = PAR + VWC + VPD + LE during green-up of the (a) 2013, (b) 2014, (c) 2015, and (d) 2016 seasons. Four relative importance models were used including LMG, First, Genizi, and CAR. GLM accounted for 16.12%, 22.92%, 66.96%, and 36.81% of 2013, 2014, 2015 and 2016 GPP variability, respectively.

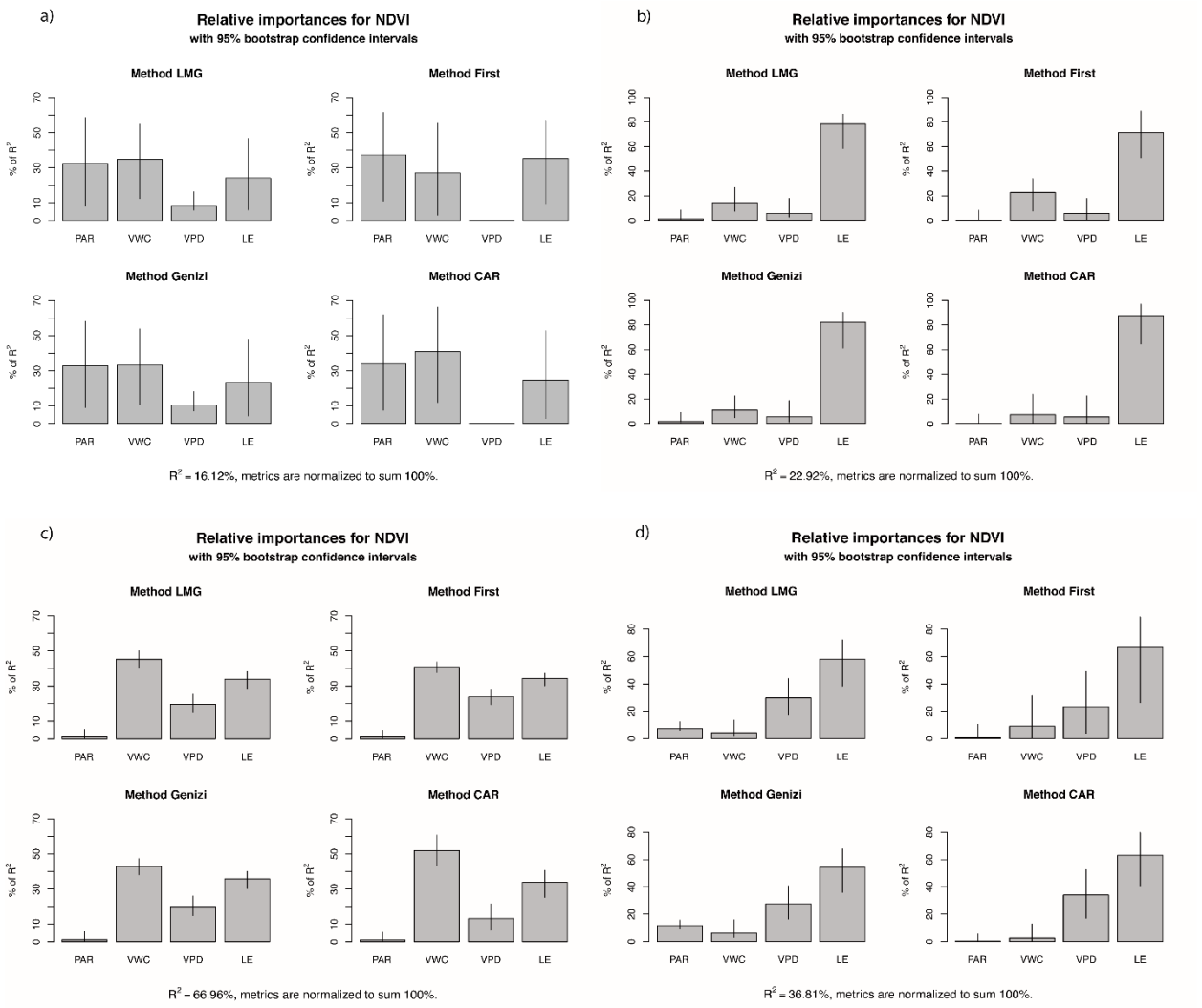

Figure A1.2 Relative importance analysis of GLM NDVI = PAR + VWC + VPD + LE during senescence of the (a) 2013, (b) 2014, (c) 2015, and (d) 2016 seasons. Four relative importance models were used including LMG, First, Genizi, and CAR. GLM accounted for 16.12%, 22.92%, 66.96%, and 36.81% of 2013, 2014, 2015 and 2016 GPP variability, respectively.

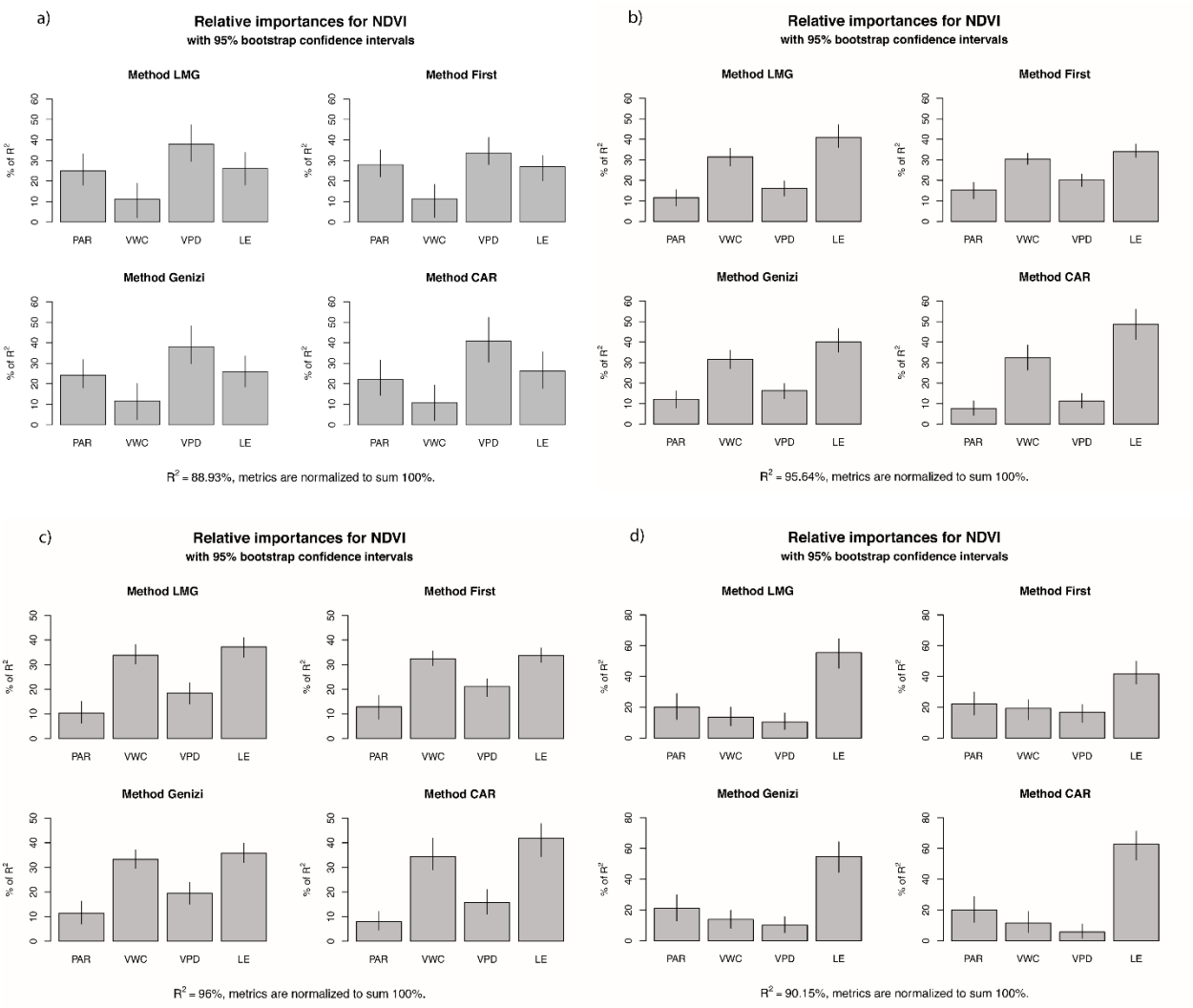

Figure A1.3: Relative importance analysis of GLM NDVI = PAR + VWC + VPD + LE during senescence of the (a) 2013, (b) 2014, (c) 2015, and (d) 2016 seasons. Four relative importance models were used including LMG, First, Genizi, and CAR. GLM accounted for 89.93%, 95.64%, 96.00%, and 90.15% of 2013, 2014, 2015 and 2016 GPP variability, respectively.

Table A1.1 Relative importance metrics for 2013, 2014, 2015 and 2016 green-up. Model accounts for 92.31%, 98%, 99.21%, 94.74%, respectively.

	2013				2014			
	lmg	**first**	**genizi**	**car**	**lmg**	**first**	**genizi**	**car**
PAR	0.098	0.044	0.101	0.096	0.056	0.089	0.059	0.034
VWC	0.491	0.472	0.558	0.595	0.619	0.532	0.628	0.743
VPD	0.274	0.318	0.227	0.296	0.016	0.020	0.015	0.005
LE	0.137	0.166	0.114	0.013	0.309	0.360	0.297	0.218

	2015				2016			
	lmg	**first**	**genizi**	**car**	**lmg**	**first**	**genizi**	**car**
PAR	0.032	0.050	0.037	0.023	0.162	0.206	0.134	0.103
VWC	0.501	0.414	0.523	0.624	0.522	0.462	0.557	0.615
VPD	0.309	0.332	0.285	0.268	0.065	0.085	0.050	0.017
LE	0.158	0.204	0.156	0.084	0.252	0.246	0.258	0.265

Table A1.2 Relative importance metrics for 2013, 2014, 2015 and 2016 maturity. Model accounts for 16.12%, 22.92%, 66.96%, 36.81%, respectively.

	2013				2014			
	lmg	**first**	**genizi**	**car**	**lmg**	**first**	**genizi**	**car**
PAR	0.325	0.375	0.328	0.340	0.011	0.002	0.017	0.000
VWC	0.348	0.271	0.332	0.410	0.145	0.227	0.107	0.072
VPD	0.086	0.000	0.106	0.001	0.058	0.055	0.056	0.053
LE	0.242	0.354	0.234	0.248	0.785	0.715	0.820	0.875

	2015				2016			
	lmg	**first**	**genizi**	**car**	**lmg**	**first**	**genizi**	**car**
PAR	0.012	0.011	0.012	0.011	0.075	0.007	0.118	0.003
VWC	0.452	0.408	0.429	0.519	0.045	0.091	0.062	0.026
VPD	0.196	0.238	0.200	0.132	0.297	0.235	0.277	0.339
LE	0.340	0.343	0.359	0.338	0.582	0.667	0.543	0.632

Table A1.3 Relative importance metrics for 2013, 2014, 2015 and 2016 senescence. Model accounts for 88.93%, 95.64%, 96%, 90.15%, respectively.

	2013				2014			
	lmg	**first**	**genizi**	**car**	**lmg**	**first**	**genizi**	**car**
PAR	0.249	0.280	0.242	0.220	0.115	0.153	0.122	0.076
VWC	0.110	0.113	0.117	0.109	0.314	0.303	0.316	0.324
VPD	0.110	0.337	0.382	0.408	0.161	0.203	0.163	0.113
LE	0.110	0.269	0.259	0.263	0.410	0.341	0.400	0.487

	2015				2016			
	lmg	**first**	**genizi**	**car**	**lmg**	**first**	**genizi**	**car**
PAR	0.104	0.129	0.114	0.080	0.202	0.222	0.213	0.200
VWC	0.338	0.323	0.333	0.344	0.137	0.193	0.138	0.116
VPD	0.185	0.210	0.196	0.157	0.105	0.168	0.101	0.057
LE	0.373	0.337	0.358	0.419	0.556	0.417	0.548	0.628

A1.3 Supplementary References:

Huemmrich, K.F., Black, T.A., Jarvis, P.G., McCaughey, J.H. and Hall, F.G., 1999. High temporal resolution NDVI phenology from micrometeorological radiation sensors. Journal of Geophysical Research: Atmospheres, 104(D22), pp.27935-27944.

Hutyra, L.R., Munger, J.W., Saleska, S.R., Gottlieb, E., Daube, B.C., Dunn, A.L., Amaral, D.F., De Camargo, P.B. and Wofsy, S.C., 2007. Seasonal controls on the exchange of carbon and water in an Amazonian rain forest. Journal of Geophysical Research: Biogeosciences, 112(G3).

Finnigan, J.J., R. Clement, Y. Mahli, R. Leuning, H.A. Cleugh. 2003. A re-evaluation of long-term flux measurement techniques. Part I: averaging and coordinate rotation, Boundary-Layer Meteorology, 107, pp.1-48

Genizi, A., 1993. Decomposition of R 2 in multiple regression with correlated regressors. Statistica Sinica, pp.407-420.

Gromping U., 2006. relaimpo: Relative Importance of Regressors in Linear Models. R package

version 1.1-1.

Kaimal, J.C., Wyngaard, J., Izumi, Y. and Coté, O.R., 1972. Spectral characteristics of surface-layer turbulence. Quarterly Journal of the Royal Meteorological Society, 98(417), pp.563-589.

Kljun, N., Calanca, P., Rotach, M.W. and Schmid, H.P., 2004. A simple parameterisation for flux footprint predictions. Boundary-Layer Meteorology, 112(3), pp.503-523.

Lee, X. and Finnigan, J., 2004. Coordinate systems and flux bias error. In Handbook of Micrometeorology (pp. 33-66). Springer Netherlands.

Lindeman, R.H. and Lindeman, R.H., 1980. Introduction to bivariate and multivariate analysis (No. 04; QA278, L553.).

Lloyd, J. and Taylor, J.A., 1994. On the temperature dependence of soil respiration. Functional ecology, pp.315-323.

Moore, C.J., 1986. Frequency response corrections for eddy correlation systems. Boundary-Layer Meteorology, 37(1-2), pp.17-35.

Moncrieff, J.B., Massheder, J.M., De Bruin, H., Elbers, J., Friborg, T., Heusinkveld, B., Kabat, P., Scott, S., Soegaard, H. and Verhoef, A., 1997. A system to measure surface fluxes of momentum, sensible heat, water vapour and carbon dioxide. Journal of Hydrology, 188, pp.589-611.

Reichstein, M., Falge, E., Baldocchi, D., Papale, D., Aubinet, M., Berbigier, P., Bernhofer, C., Buchmann, N., Gilmanov, T., Granier, A. and Grünwald, T., 2005. On the separation of net ecosystem exchange into assimilation and ecosystem respiration: review and improved algorithm. Global Change Biology, 11(9), pp.1424-1439

Vickers, D. and Mahrt, L., 1997. Quality control and flux sampling problems for tower and aircraft data. Journal of Atmospheric and Oceanic Technology, 14(3), pp.512-526.

Webb, E.K., Pearman, G.I. and Leuning, R., 1980. Correction of flux measurements for density effects due to heat and water vapour transfer. Quarterly Journal of the Royal Meteorological Society, 106(447), pp.85-100.

Zuber, V. and Strimmer, K., 2010. High-dimensional regression and variable selection using CAR scores. arXiv preprint arXiv:1007.5516.

Appendix A2

The seasonal time series of NEE, GPP, R_{eco}, and key meteorological variables are shown in Figure A2.1. Seasonal patterns of NEE (Figure A2.1a) are similar to those usually observed in northern deciduous forests, resulting from the known phenologic cycle. During spring and fall dormancy, NEE values are in the positive range, suggesting a higher proportion of respiration than photosynthesis that leads to a net carbon source. As leaf flush occurred, the opposite happens with productivity outpacing respiration, leading to increasingly negative NEE and net carbon sequestration. NEE and GPP progressively increased throughout the season (Figure A2.1a), reaching peak productivity during July (1.4 ± 0.02 mg m^{-2} s^{-1} and 1.8 ± 0.03 mg m^{-2} s^{-1}, respectively). Peak respiration (0.80 ± 0.03 mg m^{-2} s^{-1}) also occurred during July but slightly offset from peak productivity. NEE, GPP, and R_{eco} showed a gradual decline into leaf senescence. The length of the growing season was approximately 170 days (± 7 days), spanning from 15 April to 1, October 2015.

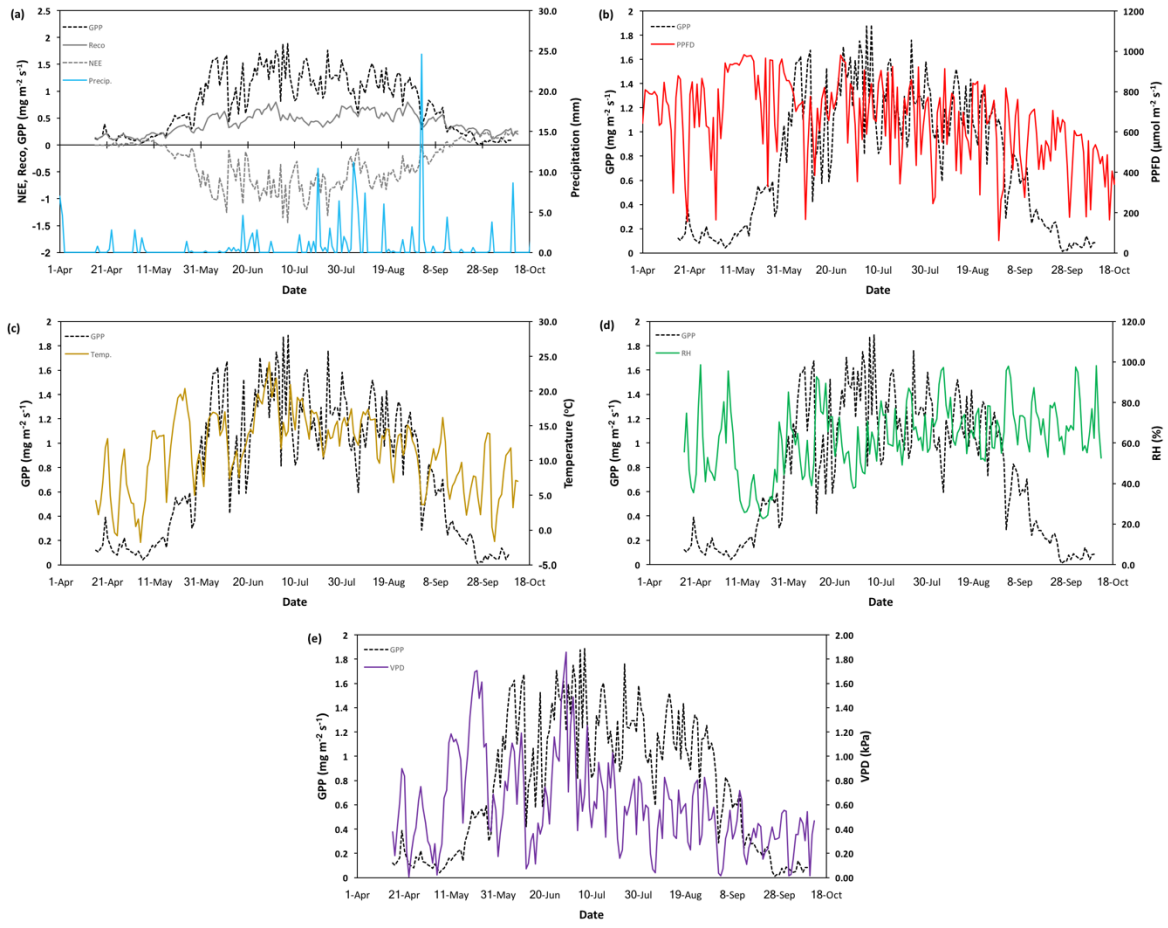

Figure A2.1. Gross primary productivity (GPP) and seasonal meteorological parameters for the 2015 growing season at the Peace River Environmental Monitoring Super Site. From top to bottom: (**a**) daily average net ecosystem exchange and ecosystem respiration, (**b**) photosynthetic photon flux density (PPFD), (**c**) temperature, (**d**) relative humidity (RH), and (**e**) vapor pressure deficit (VPD).

Seasonal trends in temperature (Figure A2.1c) show a continuous increase from the beginning of the season to late June, after which temperature progressively decreases until the end of the season (October). Overall, relative humidity (Figure A2.1d) increases until mid-June and then remains stable during the remainder of the growing season. VPD seasonal changes (Figure A2.1e) showed an initial increase during the start of the season, followed by a sharp decrease during mid-June and then remaining low and stable from July until end of the season. Beyond these general seasonal changes, short-term changes in climatic status directed intra-seasonal variability in productivity. Throughout the season productivity was linked to air temperature (Figure A2.1c), particularly during spring and fall warming/cooling events, where warming was associated with increased GPP and cooling with seasonal decreases. The largest drops in GPP and R_{eco} values occurred during periods were temperature reached approached <5 °C. VPD (Figure A2.1e) was principally influenced by temperature and shared similar patterns and associations to GPP. PPFD appeared to be the principal driver of productivity throughout large parts of the season (Figures A2.1b and 5).

A combination of factors appears to affect apparent quantum yield (α) over the course of the growing season. Periods of low quantum yield occurred during high temperatures (Figure A2.2a), which we would expect from a heat-stressed ecosystem. The opposite relationship is observed when comparing RH and α (Figure A2.2b). In general, high α values coincide with periods of high relative humidity, which represent low evaporative demand. Peak α values correspond closely with soil water moisture (Figure A2.2b). An exception to this connection was observed during 31 August when a soil moisture peak is observed but α seems to decrease slightly. This decrease in α is associated with low PPFD (61.49 μmol m^{-2} s^{-1}) and T_{air} (3.7 °C), indicating that these variables are limiting during this period.

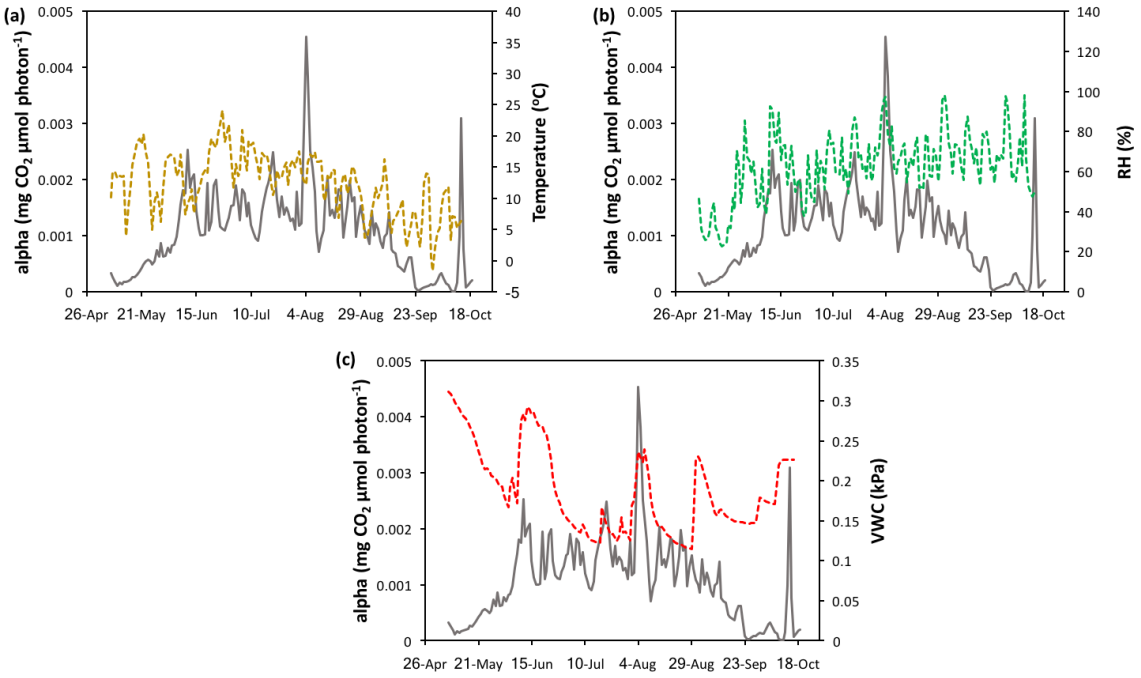

Figure A2.2. Time series of apparent quantum yield and (**a**) temperature, (**b**) relative humidity (RH), and (**c**) soil volumetric water moisture (VWC). Apparent quantum yield values were derived from eddy covariance measurements.

Appendix A3

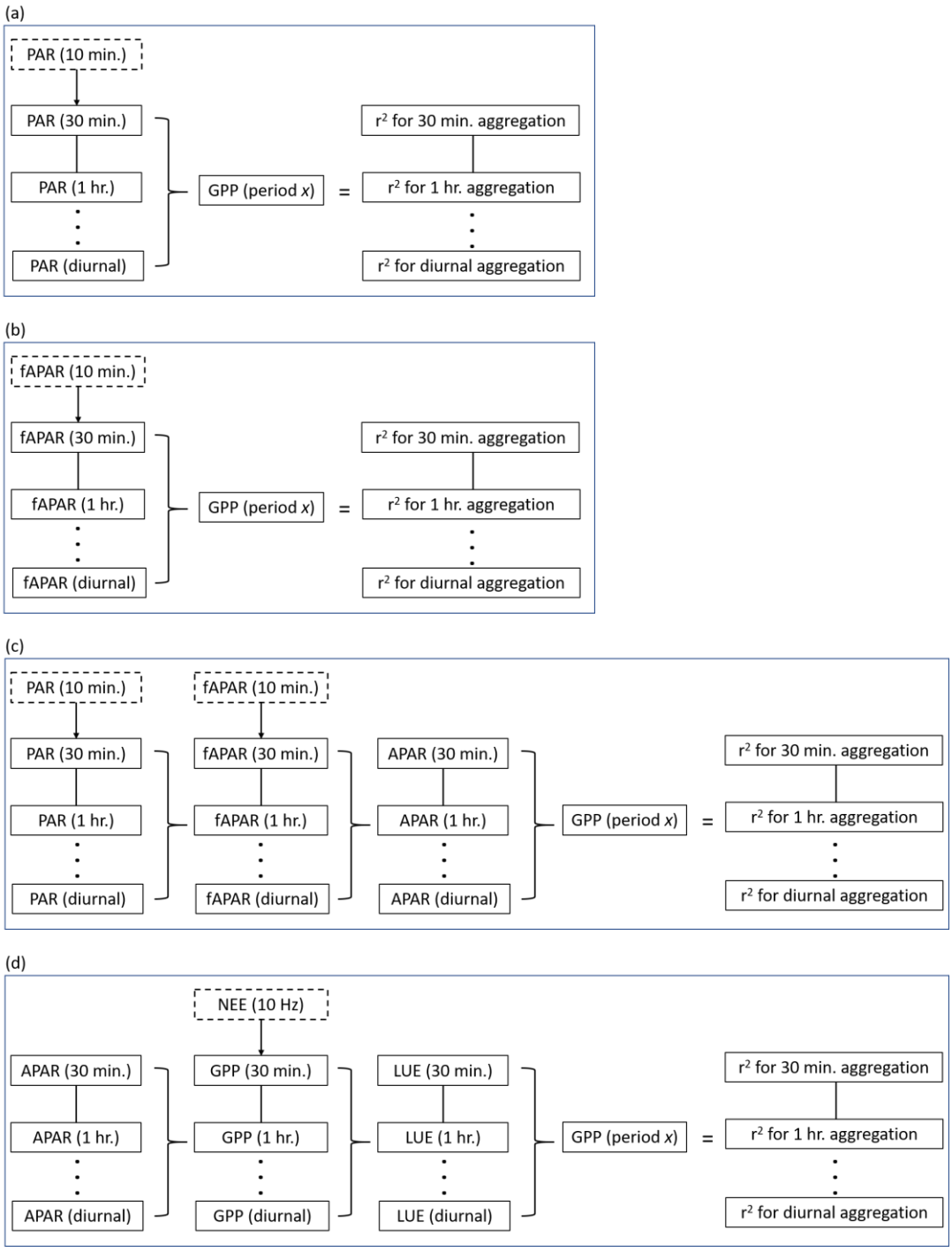

Figure A3.1 Conceptual diagram of temporal aggregation workflows for each of the LUE model variables: (a) PAR, (b) fAPAR, (c) APAR, and (d) LUE. Aggregation was done sequentially increasing the period by 1 hour, centered on midday, until the maximum diurnal hours were reached. This procedure was applied for datasets from both TDF and DBF sites.